STAFF VICE PRESIDENT
MDRL

1630 24 APR 1981

NASA CONTRACTOR
REPORT

DO NOT DESTROY
RETURN TO LIBRARY
DEPT. 022

NASA CR-161665

NASA-CR-161665 (1)

LASER-HEATED THRUSTER - INTERIM REPORT

By N. H. Kemp and P. F. Lewis
Physical Sciences, Inc.
30 Commerce Way
Woburn, Massachusetts 01801

Interim Report

February 1980

19 JAN 1989
McDONNELL AIRCRAFT COMPANY
[illegible]
[illegible] MO.

Prepared for

NASA - George C. Marshall Space Flight Center
Marshall Space Flight Center, Alabama 35812

LM135534E

BRN 48852

TECHNICAL REPORT STANDARD TITLE PAGE

1 REPORT NO.	2. GOVERNMENT ACCESSION NO.	3 RECIPIENT'S CATALOG NO.
NASA CR-161665		

4. TITLE AND SUBTITLE	5. REPORT DATE
Laser-Heated Thruster - Interim Report	February 1980
	6. PERFORMING ORGANIZATION CODE
7. AUTHOR(S)	8. PERFORMING ORGANIZATION REPORT #
N. H. Kemp and P. F. Lewis	PSI TR-205
9. PERFORMING ORGANIZATION NAME AND ADDRESS	10. WORK UNIT NO.
Physical Sciences, Inc. 30 Commerce Way Woburn, Massachusetts 01801	11. CONTRACT OR GRANT NO. NAS8-33097
	13. TYPE OF REPORT & PERIOD COVERED Contractor 1 Sep 78 - 31 Aug 79
12. SPONSORING AGENCY NAME AND ADDRESS National Aeronautics and Space Administration Washington, DC 20546	14. SPONSORING AGENCY CODE

15. SUPPLEMENTARY NOTES

Technical Monitor: Lee W. Jones, MSFC.

16. ABSTRACT The objective of this research is to develop a computer program useful for the design of the thrust chamber for a CW laser-heated thruster. Interest is focussed on hydrogen as the propellant gas and high temperature absorber. For low temperature absorption, seeds of Cs or H_2O and Cs are considered for 10.6μm laser radiation, and seeds of NO and CO or H_2O and CO are considered for 5.3μm radiation. The laser absorption coefficient of these mixture/laser radiation combinations is given in terms of temperature and species densities. The radiative and absorptive properties are also given, so that radiation from such gas mixtures can be determined. The thermodynamic and transport properties of cesium-seeded hydrogen are modeled up to 30 000 K and 100 atm. A computer code is described for calculating the axisymmetric channel flow of a gas mixture in chemical equilibrium, including laser energy absorption and convective and radiative heating. A radiative heating model for use in this code is described for a 30 atm mixture of $H_2/H_2O/Cs$ = 0.945/0.05/0.005, and the results of one calculation are presented. The conclusions are as follows: (1) Small amounts of cesium seed substantially increase the 10.6μm absorption coefficient of hydrogen at temperatures of a few thousand degrees K; (2) cesium is a strong radiator and contributes greatly to radiation of cesium-seeded hydrogen; (3) water vapor appears to be a poor absorber of 10.6μm in the range 500-1500 K, but existing experimental measurements are uncertain, and good experiments are needed; and (4) for 5.3μm radiation, both H_2O/CO and NO/CO seeded hydrogen mixtures are good absorbers. In an extension of the present program, PSI will measure absorption of 10.6μm radiation by water vapor in a shock tube.

17. KEY WORDS	18. DISTRIBUTION STATEMENT
	Unclassified-Unlimited A. A. McCool, Director Structures & Propulsion Laboratory

19. SECURITY CLASSIF. (of this report)	20. SECURITY CLASSIF. (of this page)	21. NO. OF PAGES	22. PRICE
Uncl	Uncl	178	NTIS

For sale by National Technical Information Service, Springfield, Virginia 22151

ACKNOWLEDGEMENT

A number of the authors' colleagues provided valuable encouragement and assistance. Among them were Mr. George Caledonia, Dr. Anthony Pirri and Dr. Robert Root. Valuable programming assistance was given by Mr. John Cronin, Mr. Richard Conti and Miss Mary Staniewicz. The understanding and encouragement of Mr. Lee Jones of NASA/Marshall Spaceflight Center was also most helpful. In the early stages of the work, Mr. Dale Blount, also of NASA/MSFC, was the program monitor.

TABLE OF CONTENTS

SECTION		PAGE
	ABSTRACT	i
	ACKNOWLEDGEMENT	ii
I	INTRODUCTION	1
II	LASER ABSORPTION COEFFICIENTS	9
	2.1 Inverse Bremsstrahlung Absorption	11
	2.2 Molecular Absorption	22
III	RADIATIVE AND ABSORPTIVE PROPERTIES MODELING	41
	3.1 Molecular Vibrational Radiation	43
	3.2 Electronic Radiation Processes	64
IV	THERMODYNAMIC AND TRANSPORT PROPERTIES OF EQUILIBRIUM SEEDED HYDROGEN	81
	4.1 Equilibrium Composition	82
	4.2 Thermodynamic Properties	89
	4.3 Equilibrium Constants	100
	4.4 Transport Properties	106
V	DEVELOPMENT OF THRUST CHAMBER DESIGN COMPUTER PROGRAM	121
	5.1 Equations of Motion	122
	5.2 Transformation of Equations of Motion	126
	5.3 Wall Shape	129
	5.4 Laser Beam Shape	130
	5.5 Radiation Model	134
	5.6 Heat Flux to the Wall	151
	5.7 Numerical Method	153
	5.8 Numerical Example	154
	5.9 Further Development	166
VI	CONCLUSIONS	167
	REFERENCES	169
	DISTRIBUTION LIST	173

Page intentionally left blank

Page intentionally left blank

LIST OF ILLUSTRATIONS

FIGURE		PAGE
1-1	Thruster Performance	7
2-1	Electron-Ion Bremsstrahlung Absorption Coefficient at 10.6 μm.	17
2-2	Electron-Neutral Bremsstrahlung Coefficient for H_2 at 10.6 μm	18
2-3	Electron-Neutral Bremsstrahlung Absorption Coefficient for Cs at 10.6 μm	19
2-4	Absorption Coefficient for H_2/Cs Mixture and Pure H_2 at 10.6 μm	21
2-5	Absorption Coefficient of H_2O at 10.6 μm	24
2-6	Absorption Coefficient of H_2O at 5.3 μm	28
2-7	Absorption Coefficient of NO at 5.3 μm	29
2-8	Absorption Coefficient of CO at 5.3 μm	30
2-9	Absorption Coefficient at 10.6 μm for 3 atm	32
2-10	Absorption Coefficient at 10.6 μm at 30 and 100 atm	33
2-11	Absorption Coefficient at 5.3 μm at 3 atm	37
2-12	Absorption Coefficient at 5.3 μm at 100 atm	38
3-1	Calculated Emissivity of OH	51
3-2	Calculated Emissivity of CO	52
3-3	Calculated Emissivity of CO_2	54
3-4	Calculated Emissivity of H_2O	57
3-5	Emissivity of CO	60
3-6	Emissivity of CO_2	62
3-7	Emissivity of H_2O	63
3-8	Emissivity of Hydrogen for p=100 atm, ℓ=30 cm	75
3-9	Normalized Blackbody Spectral Function	76
3-10	Transparent Spectral Emissivity of Cesium for p = 1 atm, ℓ = 1 cm	77
3-11	Emissivity of Cesium	80
4-1	Thermal Conductivity of Equilibrium Hydrogen	118
5-1	Profiles of Intensity and Power for the Incoming Laser Beam	133

LIST OF ILLUSTRATIONS (Cont.)

FIGURE		PAGE
5-2a	Absorption Coefficient as a Function of Wavenumber for $H_2/H_2O/Cs$ = 0.945/0.05/0.005. T = 2000 K, p = 30 atm.	139
5-2b	Absorption Coefficient as a Function of Wavenumber for $H_2/H_2O/Cs$ = 0.945/0.05/0.005. T = 4000 K, p = 30 atm.	140
5-2c	Absorption Coefficient as a Function of Wavenumber for $H_2/H_2O/Cs$ = 0.945/0.05/0.005. T = 6000 K, p = 30 atm.	141
5-3a	Component Absorption Coefficients as a Function of Wavenumber for $H_2/H_2O/Cs$ = 0.945/0.05/0.005. T = 2000 K, p = 30 atm.	142
5-3b	Component Absorption Coefficients as a Function of Wavenumber for $H_2/H_2O/Cs$ = 0.945/0.05/0.005. T = 4000 K, p = 30 atm	143
5-3c	Component Absorption Coefficients as a Function of Wavenumber for $H_2/H_2O/Cs$ = 0.945/0.05/0.005. T = 6000 K, p = 30 atm	144
5-4a	Normalized Blackbody Function $B_\omega/\sigma T^4$. T = 2000 K	145
5-4b	Normalized Blackbody Function $B_\omega/\sigma T^4$. T = 4000 K	146
5-4c	Normalized Blackbody Function $B_\omega/\sigma T^4$. T = 6000 K	147
5-5a	Laser Intensity Profiles at Various Axial Stations $0 \leq \xi \leq 1.326$ cm	157
5-5b	Laser Intensity Profiles at Various Axial Stations $1.538 \leq \xi \leq 96.529$	158
5-6a	Temperature Profiles at Various Axial Stations $0 \leq \xi \leq 1.326$ cm	160
5-6b	Temperature Profiles at VArious Axial Stations $1.538 \leq \xi \leq 96.529$ cm	161
5-7	Axial Distribution of Wall Radius	162
5-8	Axial Distribution of Power in the Laser Beam P_L and Power in the Gas, P_G	163
5-9	Axial Distribution of Local Convective Wall Heat Flux q_C and Local Total Wall Heat Flux q_w	165

LIST OF TABLES

TABLE		PAGE
2-1	TA(T) x 10^{34} (From Ref. 6)	16
3-1	Parameters for OH and CO	50
3-2	Parameters for CO_2	50
3-3	Parameters for H_2O	56
3-4	Vibrational Emissivity of Molecular Hydrogen at a Total Pressure of 100 atm and Path Length of 30 cm	56
3-5	Quantum Defect Parameters for Cs (Ref. 29)	71
3-6	Cross-Section for Photo-Detachment of H^- (Ref. 31)	73
4-1	Statistical Weights and Energies for Cesium	105
4-2	Source of Collision Integrals	116

I. INTRODUCTION

This is an Interim Report on a research study being conducted for NASA/Marshall Spaceflight Center by Physical Sciences Inc. on the subject of laser-heated thrusters. The objective of this study is the development of a computer program useful for the design of the thrust chamber for a CW laser-heated thruster.

Physical Sciences has been studying the physics and fluid mechanics of laser-heated CW thrusters under NASA sponsorship for about six years. The first study, as reported in Ref. 1, considered methods of absorbing laser energy into gases, a simple fluid-mechanical model of a laser-heated gas flowing in a nozzle, and the stability of the flow. The second study, Ref. 2, concentrated on a CO_2 10.6 μm laser heating a pure hydrogen propellant gas. A detailed model was constructed for laser absorption, the flow of dissociating and ionizing hydrogen, and the radiation from the hot hydrogen. Methods of initiating the absorption of laser energy in time were also investigated, and some study was made of the use of particles to absorb radiation from the hot hydrogen.

An important element of a pure hydrogen CW laser-heated thruster is the method of initiating the absorption of laser energy in space. For pure hydrogen, the only absorption mechanism is inverse Bremsstrahlung, which requires the presence of electrons. But electrons are only produced in hydrogen by ionization which occurs at temperatures above 7000 to 11000 K, depending on the pressure. Thus, only after the hydrogen gets hot can the laser energy be absorbed. Some other mechanism must operate to heat the gas from its inlet temperature to these high temperatures where electrons are produced.

Such a mechanism has been observed to exist in air and a few other gases. It has become known as a laser-supported combustion (LSC) wave. Such a wave is a region of rapidly increasing temperature in a laser-heated gas. The laser energy is absorbed in the hot gas near the rear of the wave. This hot gas radiates and conducts energy forward

down the temperature gradient to the cooler part of the wave and the incoming cool gas. This radiation and conduction then provides the mechanism for heating the cold gas up to the temperature where electrons are produced and inverse Bremsstrahlung can act to absorb energy and heat the gas. Such an LSC wave is the laser-heated analogy of an ordinary deflagration wave heated by chemical combustion. It is a low-speed, nearly constant pressure wave in which the temperature increases, and the density decreases. In order to conserve mass, the velocity increases to keep the mass flow per unit area constant.

This LSC wave provides a possible mechanism for initiating the absorption of laser energy in space in a pure hydrogen thruster. The wave is stationary at the beginning of the heating region, and as the hydrogen flows through it, it heats and absorbs the laser energy. Although no hydrogen LSC waves have been studied experimentally, they have been observed in air (Ref. 3).* They are found to have a characteristic propagation speed, which depends on the pressure level and laser beam intensity. If they are to remain stationary in a flowing gas, the incoming gas must flow at this LSC wave speed.

In the hydrogen 10.6 μm laser-heated thruster concept studied in Ref. 2 an LSC wave was postulated as the mechanism for initiating the absorption in space. However, no detailed study of the wave was performed. A wave speed for a given intensity was assumed based on a simple modification of a theory previously presented for air. It was important, however, to examine LSC waves in hydrogen to determine their speed vs. intensity relation. Therefore, in Ref. 4, a detailed model of hydrogen LSC waves was constructed, and their speed-intensity characteristics were calculated as a function of pressure. The subsequent acceleration of the hot hydrogen emerging from the wave was also considered for one particular case.

The studies described in Refs. 2 and 4 show the main features of laser-heated thrusters using pure hydrogen. Because the absorption mechanism is a high temperature one, these thrusters operate at peak temperatures

* Since the present work was performed, LSC waves have been observed in hydrogen by Conrad at the Army High Energy Laser Laboratory

of about 20000 K. Even after acceleration to a throat, the gas is nearly 16000 K. These high temperatures lead to the possibility of very high specific impulses, perhaps near 4000 s, but they also lead to very large convective and radiative heat fluxes to the containing walls, and therefore, large energy transfer out of the gas. The case calculated to the throat in Ref. 4 had only 58% of the laser energy still in the gas when it reached the throat. It was also found that the LSC wave in hydrogen had a threshold intensity, below which a wave could not exist. This is in agreement with results for air LSC waves. If losses due to radiation and sideways convection are included, the threshold intensity increases. Threshold intensities are quite high, above 3 E4 W/cm^2 at 10 atm, so that for laser power in the kilowatt range the size of the laser spot is quite small, leading to a small thruster cross-section. For example, a 10 kW laser and a pressure of 10 atm would require a spot no larger than 0.65 cm in diameter.

In view of the high temperature and small size associated with pure hydrogen rockets at moderate laser powers, a study of other alternatives seems warranted, to determine how thrusters can operate with lower temperature and specific impulse. One idea is to seed the hydrogen with an easily ionizable gas, such as an alkali metal vapor. This seed will yield electrons at much lower temperatures than pure hydrogen, and so permit inverse Bremsstrahlung absorption to start at lower temperature. This lowers the whole temperature level of the thruster, and reduces radiation and convection out of the gas. An LSC wave mechanism will still be needed, however, to heat the gas from the inlet temperature up to the temperature at which sufficient ionization has occurred to permit absorption of laser energy. But this will be an LSC wave in seeded hydrogen, and will have a different wave speed vs. intensity characteristic than in pure hydrogen. Such an LSC wave is being studied under the present program.

A second alternative to the pure hydrogen thruster is to seek an absorber which operates at the inlet gas temperature, and continues absorbing until the alkali metal seed produces electrons to continue absorption. Such a low temperature absorber operates by molecular absorption,

and must be chosen so as to be "tuned" to the particular laser radiation being used. Based on the absorption studies of Ref. 1, a likely candidate for 10.6 μm radiation is water vapor, which will absorb this radiation until it dissociates at around 4000 K. By that temperature, the alkali metal seed will have produced enough electrons to let inverse Bremsstrahlung take over as the absorber. With both a low temperature absorber, H_2O, and a medium temperature absorber, alkali metal vapor (and a high temperature absorber, hydrogen, if needed) there is no need for the use of the LSC wave mechanism to heat the gas. It is possible for the absorption to proceed continuously from the inlet temperature to the temperature at which all the laser energy in the beam is absorbed. We will refer to this as the continuous heating case, in contrast to the LSC wave case, where only medium and high temperature absorbers are used.

If one is interested in radiation from CO lasers, around 5.3 μm, then Ref. 1 suggests that either NO or H_2O can function as the low temperature absorber. In this case, there is also a molecular absorber, CO, which survives to medium temperature (at least 6000 K), and could be used instead of the alkali metal vapor seed. It is advantageous not to use the latter seed, if possible, because its large molecular weight reduces the specific impulse.

In any of these thruster concepts it is very important to consider the radiative and convective heat flux to the walls, since it may prove difficult to cool the walls if these fluxes are too high. The objective of high specific impulse requires heating the gas to rather high temperatures (4000 to 5000 K, or higher) and the resulting heat fluxes will be substantial. One of the purposes of the present work is to develop a computer model which will calculate these fluxes, so the difficulty of handling them may be evaluated.

The objective of the present work, as stated above, is to develop a computer program useful for the design of a thrust chamber for a CW laser-heated thruster. The discussion above indicates that there are

two basic modes of gas heating. One is the LSC wave, seeded hydrogen mode. The other is the molecular absorber, seeded hydrogen, continuous heating mode. These two modes will require two different computer programs. The first will be an extension of the pure hydrogen LSC wave code developed in Ref. 4, and the other will be an axisymmetric channel flow code including laser energy absorption, and convective and radiative heating.

The particular laser wavelength/propellant gas mixture combinations we have considered are:

1. CO_2 (10.6 μm) radiation/H_2 - Cs
2. CO_2 (10.6 μm) radiation/ H_2 - H_2O - Cs
3. CO (5.3 μm) radiation/ H_2-NO-CO or H_2-H_2O-CO.

The first is the LSC wave heating mode and the second and third are in the continuous heating mode.

To develop the computer model a number of physical properties of the gas mixture must be modeled:

1. Laser absorption properties.
2. Radiative and absorptive properties.
3. Thermodynamic and transport properties.

These properties must be incorporated in a flow model which includes the relevant effects of heating by laser absorption, gas radiation emission and absorption, as well as the usual fluid flow effects of convection and heat transfer.

In this interim report we will describe the progress we have made in each of these areas. Section II deals with absorption of 10.6 and 5.3 μm radiation by inverse Bremsstrahlung, and by the molecules H_2O, CO, and NO. Section III develops a model for the absorption coefficients of the important radiative species contained in the gas mixtures

listed above, from which their radiative and absorptive properties can be obtained. Section IV develops a model for the thermodynamic and transport properties of a mixture of hydrogen and cesium up to temperatures of 20,000 K, for use in the LSC wave heating mode. For the other mixtures, in the continuous heating mode, standard chemical equilibrium codes can be used up to the temperatures of interest for continuous heating, which are approximately 6000 K. In Section V, the continuous heating flow model is described. As yet, the extension of the hydrogen LSC wave code to hydrogen-cesium mixtures has not been completed, so its description is reserved for the final report at the completion of the present work. The final section of this report, Section VI, sets forth the conclusions which can be drawn so far from the work completed.

Before proceeding to the details of the modeling, it is of interest to consider the over-all energy, thrust, specific impulse and mass flow relations for a laser-heated thruster, or indeed any thruster. This will give us some idea of the parameters needed for a desired level of performance. There are simple relations between thrust Th, mass flow rate $\dot{m}$, vacuum specific impulse I_{sp}, and power in the gas converted to exhaust velocity, P_G. The exhaust velocity is gI_{sp}, so that

$$Th = \dot{m} g I_{sp} \quad , \quad P_G = \dot{m} \, (gI_{sp})^2/2$$

$$\dot{m} = 2P_G/g^2 I_{sp}^2 \quad , \quad Th = 2P_G/gI_{sp} \quad .$$

Plots of $\dot{m}$ and Th vs I_{sp} are shown in Fig. 1-1, with an auxiliary scale of $P_G/\dot{m} = (gI_{sp})^2/2$. The dimensions of $P_G/\dot{m}$ are energy per unit mass, the same as enthalpy, so for a given gas at a given pressure, a temperature scale can be drawn on the $P_G/\dot{m}$ axis. The parameter on the curves is the power in the gas.

We see, for example, that at I_{sp} = 2000 s, for a power in the gas of 10 MW, the thrust is 1 kN, and the mass flow about 0.05 kg/s. For 10 kW in the gas, the thrust is 1 N and the mass flow is 5 E-5 kg/s, or

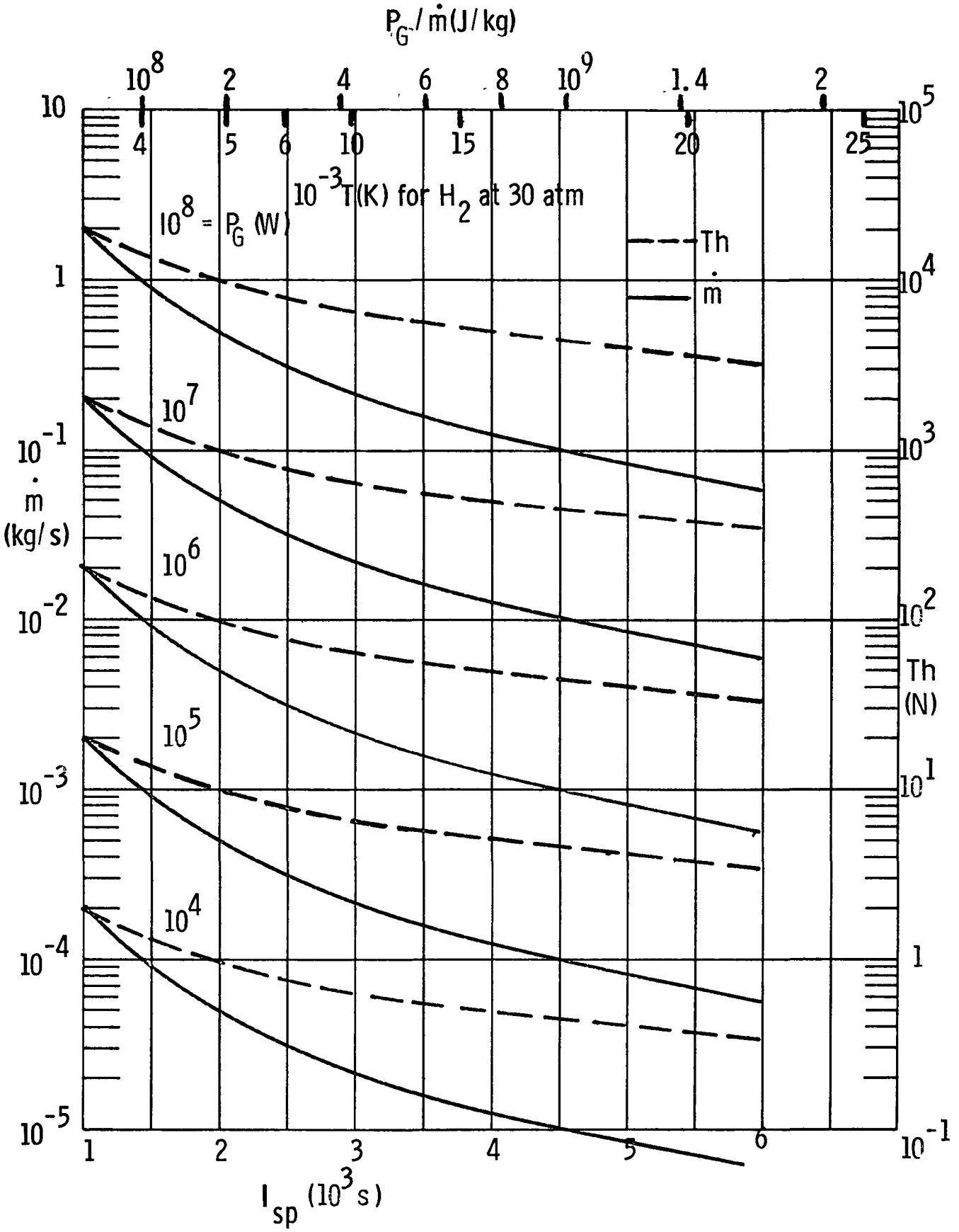

Fig. 1-1 Thruster Performance.

0.05 g/s. The enthalpy $P_G/\dot{m}$ of this gas is 2 E8 J/kg, which corresponds to a temperature of 5000 K in hydrogen at a pressure of 30 atm.

This simplistic calculation does not account for energy lost from the gas by convection and radiation; the laser power must certainly be larger than P_G, and the enthalpy in the heating region must be larger than $P_G/\dot{m}$. However, it does give us an idea of how hot the gas must be to attain a desired I_{sp}. It would appear that reaching 6000 K in hydrogen will put enough energy into the gas to reach values of I_{sp} in the interesting range of 1000 to 2000 s. To reach 4000 s requires temperatures of the order of 16000 K.

II. LASER ABSORPTION COEFFICIENTS

In a laser-heated thruster, the gas is heated by energy which it absorbs from the incoming laser beam. This energy transfer must be accomplished by some mechanism which permits the coupling of the monochromatic energy in the laser beam into the gas. There are a number of such mechanisms. A common one is inverse Bremsstrahlung, which involves the interaction of electrons with either ions or neutral particles to absorb the laser energy. This mechanism can work for any type of particle and any laser beam wavelength, since it does not require a resonance between the laser and the gas particles.

A second possible absorption mechanism is molecular absorption, in which the laser energy is absorbed by means of a resonance with some transition in the internal state of a particular molecule. This does require matching the absorber to the laser energy wavelength.

Since the inverse Bremsstrahlung mechanism requires electrons, it can only operate at temperatures where they are present. In a propellant gas like hydrogen, electrons are made only at high temperatures, since the hydrogen must first dissociate before it ionizes. Therefore, inverse Bremsstrahlung will become an effective absorber only at around 10,000K or higher. One can reduce the temperature where electrons appear by introducing small amounts of an easily ionized gas, like the alkali metals, which can ionize at a few thousand degrees. Such a seed gas will permit absorption by inverse Bremsstrahlung at much lower temperatures than pure hydrogen. But even with a seed, absorption cannot occur at low temperatures if electrons are needed. If one starts with cold gas ($T < 1000$ K), some other heating mechanism will be required to heat the gas up to temperatures where electrons are made so that inverse Bremsstrahlung can take over.

One possible low temperature heating mechanism is conduction and radiative heating. This is the mechanism used in laser-supported combustion (LSC) waves, and its application to pure hydrogen is described in Ref. 4. It leads to temperatures on the order of 20,000K in the hottest region of the gas, and makes the thruster difficult to design because of the necessity of handling such hot gases with their attendant high rate of loss by radiation and convection. In the present work, the effect of seeding with cesium on the hydrogen LSC wave is to be explored to see how that moderates the temperature level at which these waves operate.

In addition to the LSC wave mechanism of radiation and conduction, another possible low temperature mechanism is molecular absorption. This can operate from room temperature up to the temperature at which the molecules dissociate, and if the latter is high enough so that seed electrons are present, the high temperature inverse Bremsstrahlung mechanism can take over. This gives the possibility of continuously heating the gas by absorption from the inlet temperature until the laser energy is completely absorbed, without the need for an LSC wave to form. This continuous heating mode is also to be explored in the present work.

The laser wavelengths of interest here are 10.6μm and 5.3μm. The molecular absorbers considered have been based on the study described in Ref. 1. For 10.6μm we have considered H_2O, and for 5.3μm, NO, H_2O and CO.

The absorption of a gas to a laser beam of intensity I is described by an absorption coefficient k_L defined by the equation

$$dI/dx = -k_L I \qquad (2\text{-}1)$$

describing the rate the beam intensity decays along the direction of propagation. In this section we shall describe the absorption coefficients for the various absorbers and absorption mechanisms considered.

2.1 Inverse Bremsstrahlung Absorption ($e + X + h\nu \rightarrow e + X$)

The inverse Bremsstrahlung mechanism involves interactions between electrons, and either ions or neutrals. For ions, the interaction is by Coulomb forces, and is independent of the type of ion. For neutrals, it depends on the particular neutral particle involved.

Electron-Ion Inverse Bremsstrahlung ($e + I^+ + h\nu \rightarrow e + I^+$)

Ref. 1 gives the electron-ion absorption coefficient in terms of electron and ion number densities n_E, n_I as

$$k_{LEI} = \sigma_{EI}\, n_E\, n_I \left(\exp\,(h_p\, c/\lambda kT) - 1\right) \qquad (2\text{-}2)$$

where λ is the laser wavelength, and σ_{EI} is the electron-ion absorption cross-section, given in Ref. (2-2) as

$$\sigma_{EI} = \frac{4}{3} \left(\frac{2\pi}{3m_E kT}\right)^{\frac{1}{2}} \frac{Z^2\, e^6\, \lambda^3}{h_p c^4\, m_E}$$

Here Ze is the ion charge, e the electron charge, c the speed of light, h_p Planck's constant, and m_E the electron mass. For singly charged ions, the expression for σ_{EI} becomes

$$\sigma_{EI} = 1.37\ \text{E-23}\quad \lambda^3 / \ T^{\frac{1}{2}} \quad (\text{cm}^5 \text{ in cgs}) \tag{2.3a}$$

$$= 1.37\ \text{E-27}\quad \lambda^3 / \ T^{\frac{1}{2}} \quad (\text{m}^5 \text{ in mks}) \tag{2.3b}$$

The expression given so far is a semi-classical one. To account for quantum-mechanical effects, Eq. (2.2) is multiplied by a Gaunt factor G, which depends on temperature. We have gotten this factor from Ref. 5, where we fitted a parabola to Fig. 5. For $\lambda = 10.6\mu$m the parameters of the figure are $\gamma^2 = 157{,}900/T$, $u = h_p c/\lambda kT = 1357/T$. Then we read the following table from the Figure:

γ^2	T	u	$\overline{g}_{ff} = G$
3	52633	.0258	2.1
10	15790	.0859	1.55
10^2	1579	.859	1.1

We fitted a quadratic to this table to get a Gaunt factor

$$G = 1.04 + 3.74\text{E-5}T \quad - 3.28\text{E-10}T^2 \tag{2-4}$$

The expression for k_{LEI} is then

$$k_{LEI} = 1.37\text{E-23}\ G\ \lambda^3\ T^{-\frac{1}{2}}\ n_E\ n_I\ (e^{1.4388/\lambda T} - 1) \quad (\text{cm}^{-1} \text{ in cgs}) \tag{2.5a}$$

$$= 1.37\text{E-27}\ G\ \lambda^3\ T^{-\frac{1}{2}}\ n_E\ n_I\ (e^{0.014388/\lambda T} - 1) \quad (\text{m}^{-1} \text{ in mks}) \tag{2.5b}$$

Electron-H Inverse Bremsstrahlung ($e + H + h\nu \rightarrow e + H$)

For the electron-hydrogen atom absorption coefficient, Ref. 1 suggests using the results of Stallcop, which are given in terms of the electron and hydrogen number densities n_E and n_H as

$$k_{LEH} = Q_{EH}\, n_E\, n_H \left[1 - \exp\left(-h_p\, c/\lambda kT\right)\right]$$

$$Q_{EH} = \frac{2.96\ \text{E-45}\,T}{1 - \exp\left(-h_p c/\lambda kT\right)} \left(\frac{\theta_I k\lambda}{h_p c}\right)^2 \sqrt{\frac{\theta_I}{T}}\ e^{-\xi}\ (\text{cm}^5)$$

$$\xi = 4.862 \sqrt{\frac{T}{\theta_I}} \left[1 - 0.2096 \sqrt{\frac{T}{\theta_I}} + 0.0170 \left(\frac{T}{\theta_I}\right) - 0.00968 \left(\frac{T}{\theta_I}\right)^{3/2}\right] \quad (2\text{-}6)$$

where $\theta_I = h_I^o\, m_H/k$, with h_I^o the ionization energy per unit mass of hydrogen and m_H the mass of the hydrogen atom. If we put Q_{EH} into k_{LEH} we find

$$k_{LEH} = 1.43\text{E-45}\ \theta_I^{5/2}\ T^{1/2}\ \lambda^2\ e^{-\xi}\ n_E\, n_H\ (\text{cm}^{-1}\ \text{in cgs}) \quad (2.7a)$$

$$= 1.43\text{E-51}\ \theta_I^{5/2}\ T^{1/2}\ \lambda^2\ e^{-\xi}\ n_E\, n_H\ (\text{m}^{-1}\ \text{in mks}) \quad (2.7b)$$

Electron-Neutral Inverse Bremsstrahlung ($e + N + h\nu \rightarrow e + N$)

For other electron-neutral interactions, we use the results of John in Ref. 6. He has provided an expression for the absorption coefficient for a large number of neutrals in the form $A(T)\ \lambda^2$ per unit electron pressure, per neutral particle, including stimulated emission. He tabulates $A(T)$ for each neutral. To convert his expression to our k_L we multiply by the electron pressure $n_E\ kT$ and the number density n_N of the neutral particle of interest. We also restore the more familiar form of the stimulated emission factor by noting that for $h_p c/\lambda kT$ small

$$\lambda^3 \left[1 - \exp\ (-h_p c/\lambda kT)\right] = h_p c\lambda^2/kT$$

which explains the λ^2 factor in John's formula. Then we find, since John's λ is in $\overset{o}{A}$,

$$k_{LEN} = \frac{k\ T^2 A(T)\ \lambda^2(A)\ (1 - e^{-h_p c/\lambda kT}) n_E\ n_N}{h_p\ c/k\lambda}$$

Use of cgs or mks units for λ and the physical constants enables us to write

$$k_{LEN} = 9.60\ E\text{-}1\ T^2 A(T)\ \lambda^3\ (1 - e^{-1.4388/\lambda T}) n_E\ n_N\ (cm^{-1}\ \text{in cgs}) \qquad (2.8a)$$

$$= 9.60\ E\text{-}5\ T^2 A(T)\ \lambda^3\ (1 - e^{-0.014388/\lambda T}) n_E n_N\ (m^{-1}\ \text{in mks}) \qquad (2.8b)$$

The factor A(T) is taken from Table I of Ref. 6. Since it is a function of T, we must interpolate. In fact, TA(T) is a smoother function of T, so we choose to interpolate in that function. John tabulates many neutrals, including Cs, Na, Li, the noble gases, H_2, O_2, N_2, H, O, N, CO, CO_2, H_2O. In Table 2-1 we give TA(T) for species of present interest.

Results for 10.6μm Radiation

Fig. 2-1 gives a plot of the electron-ion Bremsstrahlung 10.6μm absorption coefficient per electron-ion pair, $k_{LEI}/n_E n_I$ in cm^5, from Eqs. (2-5a) and (2-4), vs T. This shows a decrease with T, per electron-ion pair. However, the number of pairs increases with T, and this dominates k_{LEI}, as will be seen later.

Fig. 2-2 shows the electron-neutral 10.6μm Bremsstrahlung for H and H_2 per electron-neutral pair, $k_{LEN}/n_E n_N$ in cm^5, from Eqs. (2-7a, 2-6) and Eqs. (4-8a) with Table 2-1. These increase with T, but again, their behavior will change when the dependence of n_E and n_N is included.

Fig. 2-3 gives the electron-neutral 10.6μm Bremsstrahlung for Cs per electron - Cs pair, $k_{LEN}/n_E n_N$ in cm^5, from Eqs. (4-8a) with Table 2-1. The minimum reflects the minimum in TA(T) of Table 2-1. The increase of electrons with T will change that shape.

TABLE 2-1

$TA(T) \times 10^{34}$ (From Ref. 6)

Species	1000K	5000K	10,000K	25,000K
H_2	703.	2145.	2900.	2800.
N	120.	500.	904.	1748.
O	103.	372.	654.	1280.
CO	605.	2250.	2800.	3750.
N_2	459.	1665.	2930.	3500.
O_2	261.	855.	1140.	1900.
CO_2	1750.	960.	1600.	3250.
Cs	57.E3	24.E3	28.E3	30.E3

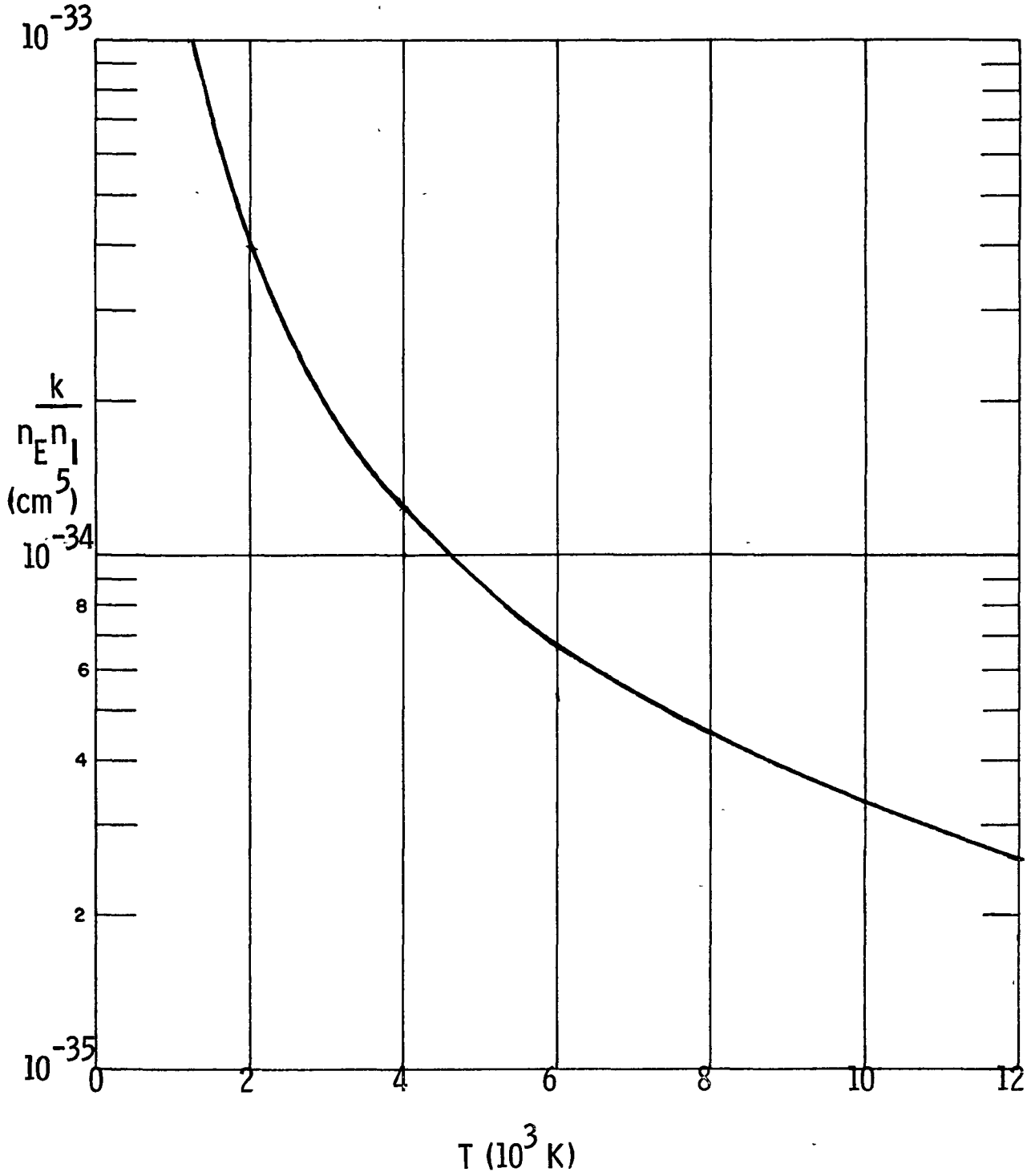

Fig. 2-1 Electron-Ion Bremsstrahlung Absorption Coefficient at 10.6 μm.

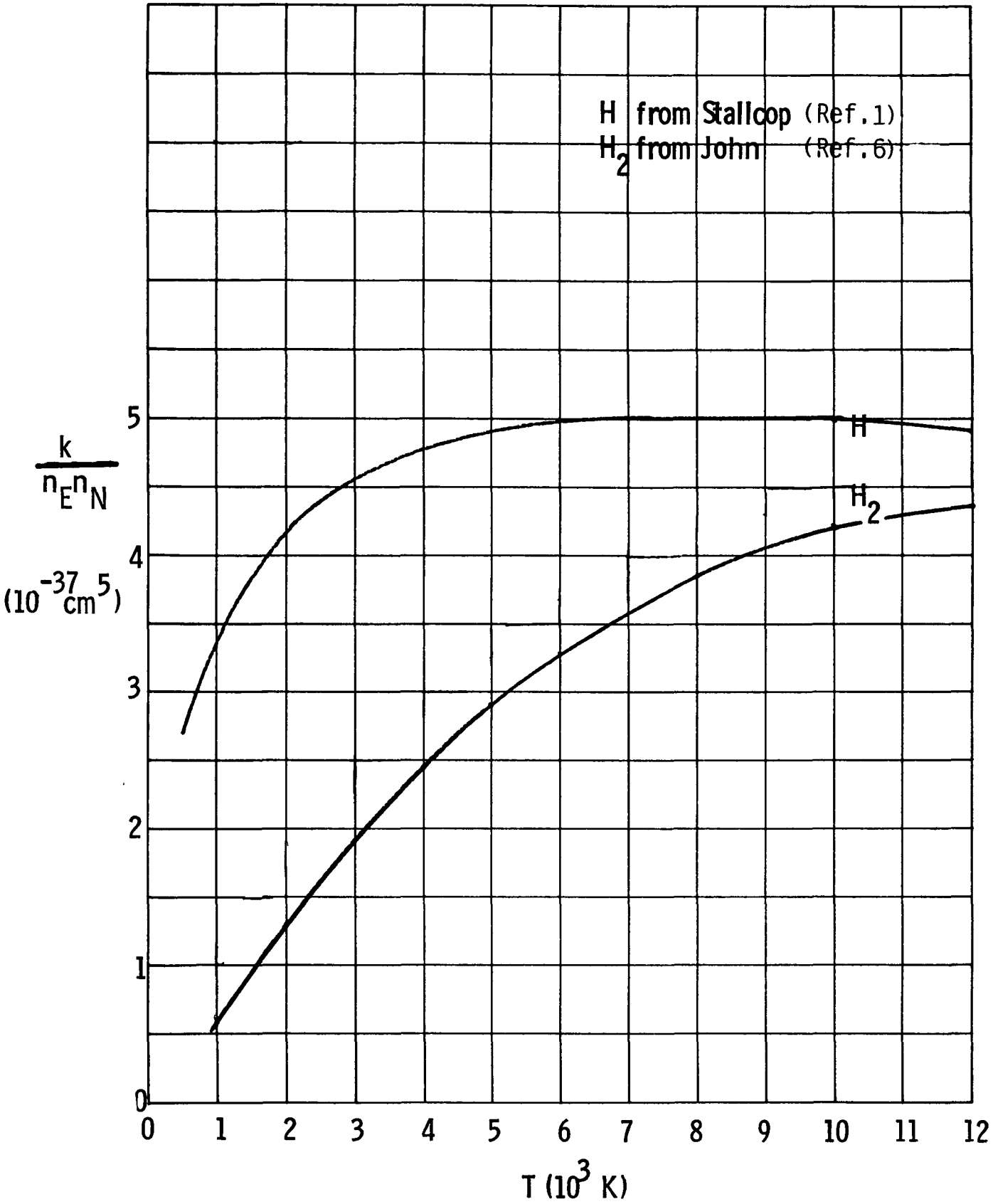

Fig. 2-2 Electron-Neutral Bremsstrahlung Coefficient for H_2 at 10.6 μm.

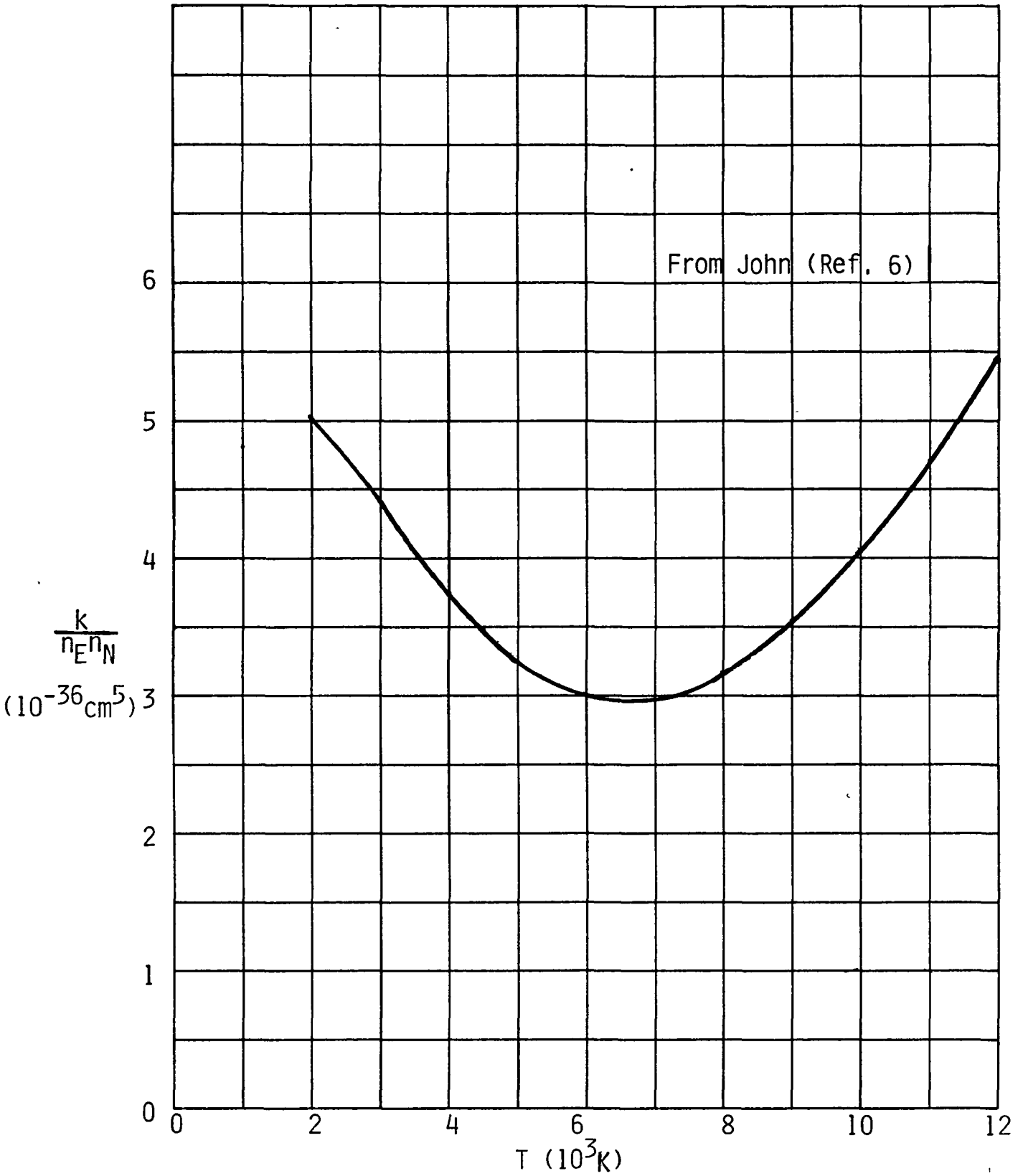

Fig. 2-3 Electron-Neutral Bremsstrahlung Absorption Coefficient for Cs at 10.6 μm.

Finally, we may obtain the actual 10.6μm absorption coefficient k_L by combining the k_L per pair with the equilibrium composition for a H_2/Cs mixture as calculated by the method described in Section IV of this report. The values from Figs. 2-1, 2-2 and 2-3 are multiplied by the appropriate number densities from the equilibrium calculation and the four contributions to k_L are added to get the total absorption coefficient. The result will depend on pressure as well as temperature, because the composition depends on pressure.

When this is done, the results shown in Fig. 2-4 are obtained. The solid curves are for a mixture H/Cs = 0.99/0.01, that is, one Cs atom for each 99 hydrogen atoms. For comparison, the dashed curves are for pure hydrogen. At low temperatures, the large increase in k_L when cesium is added is clearly shown, caused by the presence of electrons from the easily ionized cesium. The solid curves flatten when the cesium is fully ionized, and even dip slightly as the increasing temperature reduces the density. They rise again when hydrogen ionization begins to supply additional electrons. The pure hydrogen absorption coefficient is far below that of the seeded mixture until near 12,000 K at the highest pressures, and near 9,000 K at the lowest pressure. If one consideres 10^{-1} cm as a reasonable absorption coefficient, then the mixture is absorbing well at temperatures as low as 2,000 K for 100 atm, 3,000 K for 10 atm, but not until 12,000 K for 1 atm. The advantage of higher pressure is evident.

It is important to note that even the seeded mixture does not absorb well below 2,000 to 3,000 K. Heating the gas to this temperature must be accomplished by some other means, such as introducing a low temperature molecular absorber, or by the LSC wave mechanism of conduction and forward radiative heating. The cesium is a good absorber of 10.6μm radiation in the middle temperature range, and extends the absorption capabilities of pure hydrogen down to 2,000 to 3,000 K.

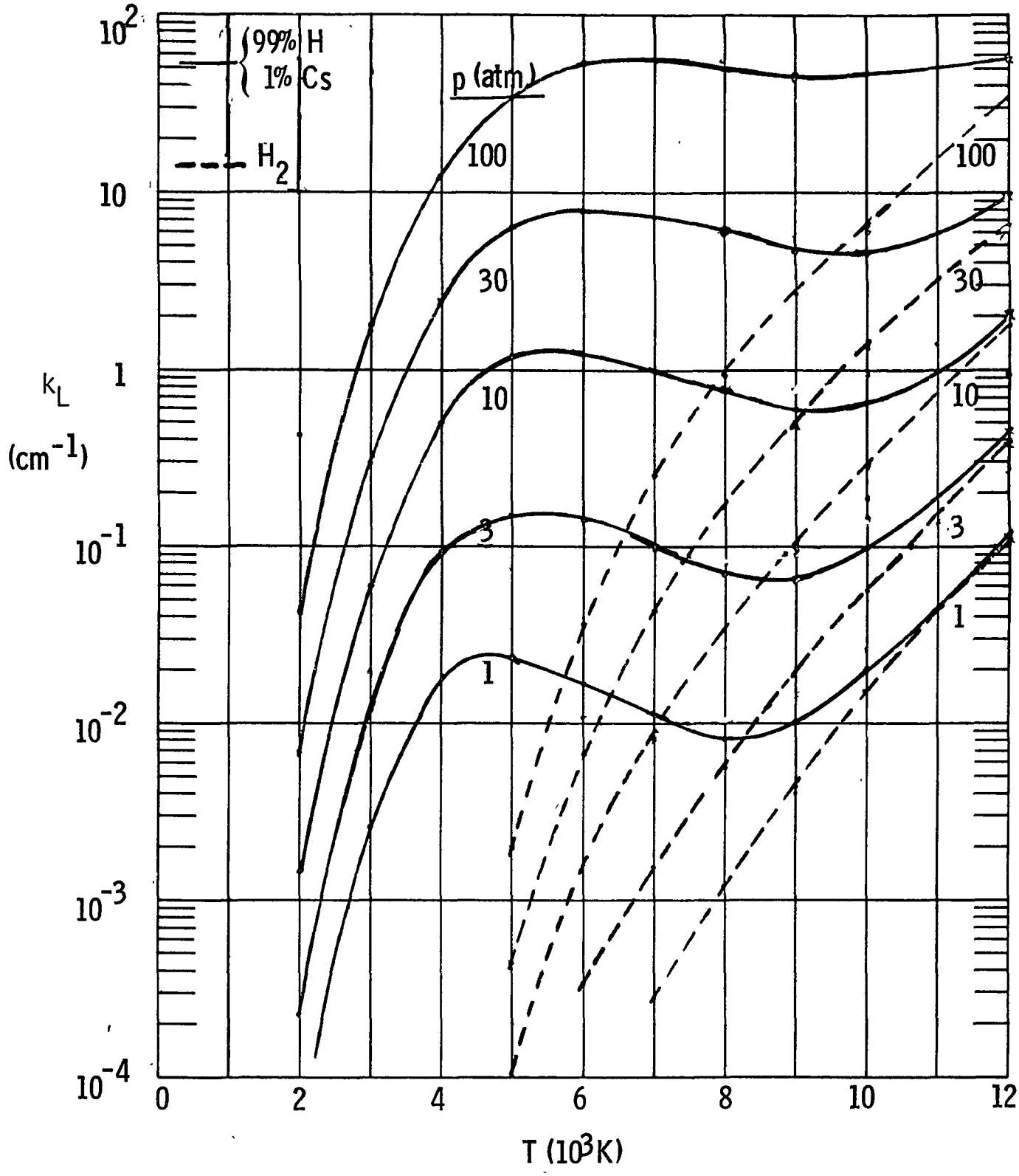

Fig. 2-4. Absorption Coefficient for H_2/Cs Mixtures and pure H_2 at 10.6 μm.

2.2 Molecular Absorption

Laser energy absorption by molecules for the wavelengths of 10.6μm and 5.3μm has also been examined by a study of the available literature. Since this absorption depends on resonance between an internal molecular transition and the laser wavelength of interest, one must match the absorber to the laser. Another characteristic of molecular absorption is a rapid cut-off with temperature as the molecule dissociates. Most molecular absorbers work only at low temperatures, their temperature limit depending on the dissociation energy of the molecule.

We will first consider the absorption coefficients for several molecular absorbers, normalized by a fixed number density of molecules. This will display the intrinsic temperature dependence. Later we will combine this with calculations of the actual number densities in gas mixtures, to obtain the total absorption coefficient of the mixture.

It is important to realize that the molecular absorption coefficients discussed below are calculated or measured for conditions of vibrational and rotational equilibrium and that they represent averages over a finite frequency range (the lines are assumed to overlap or the measurements have a relatively coarse resolution). This could lead to significant errors because of the very narrow linewidth of the laser line, particularly for absorption by H_2O where line broadening parameters for broadening by H_2 are not known, and the line spacing can be very large because of the large rotational spacing which can occur. The present work will include experimental measurements of absorption of selected 10.6μm laser lines by water vapor, made in H_2O/H_2 mixtures at elevated temperatures and pressures. The results should help resolve these questions.

Absorption by H_2O at 10.6μm

Water absorbs 10.6μm radiation, and may be a good low temperature absorber, since it doesn't dissociate until about 4,000 K, by which time cesium can provide enough electrons for Bremsstrahlung to take over. A survey of the literature on this absorption coefficient is shown in Fig. 2-5, which gives k vs 1000/T, with T in K and k in cm^{-1} per amagat, where an amagat is 2.69E19 particles per cm^3.

The lines on the right (at low temperature) arise from continuum absorption, and are derived from Ref. 7. At 10.6μm, this reference presents an absorption coefficient for 296K as 2.25 E-22 cm^2 atm^{-1} $molecule^{-1}$, and gives a temperature correction factor as exp [1800 (1/T - 1/296)]. For an amagat of particles, this becomes

$$k = 1.38\ E\text{-}5\ e^{1800/T}\ p_{H_2O}\ (atm)\ (cm^{-1}\ ama^{-1})$$

which shows a pressure dependence, unlike the line absorption mechanisms, whose only pressure dependence is in the particle density. If one converts to cm^{-1} by using a water number density of n_{H_2O}, then the absorption coefficient becomes

$$k = 5.14\ E\text{-}25\ e^{1800/T}\ p_{H_2O}\ n_{H_2O}\ (cm^{-1})$$

$$= 3.77\ E\text{-}3\ e^{1800/T} \left(p_{H_2O}\right)^2 / T\ (cm^{-1})$$

$$= 7.00\ E\text{-}47\ e^{1800/T} \left(n_{H_2O}\right)^2 T\ (cm^{-1})$$

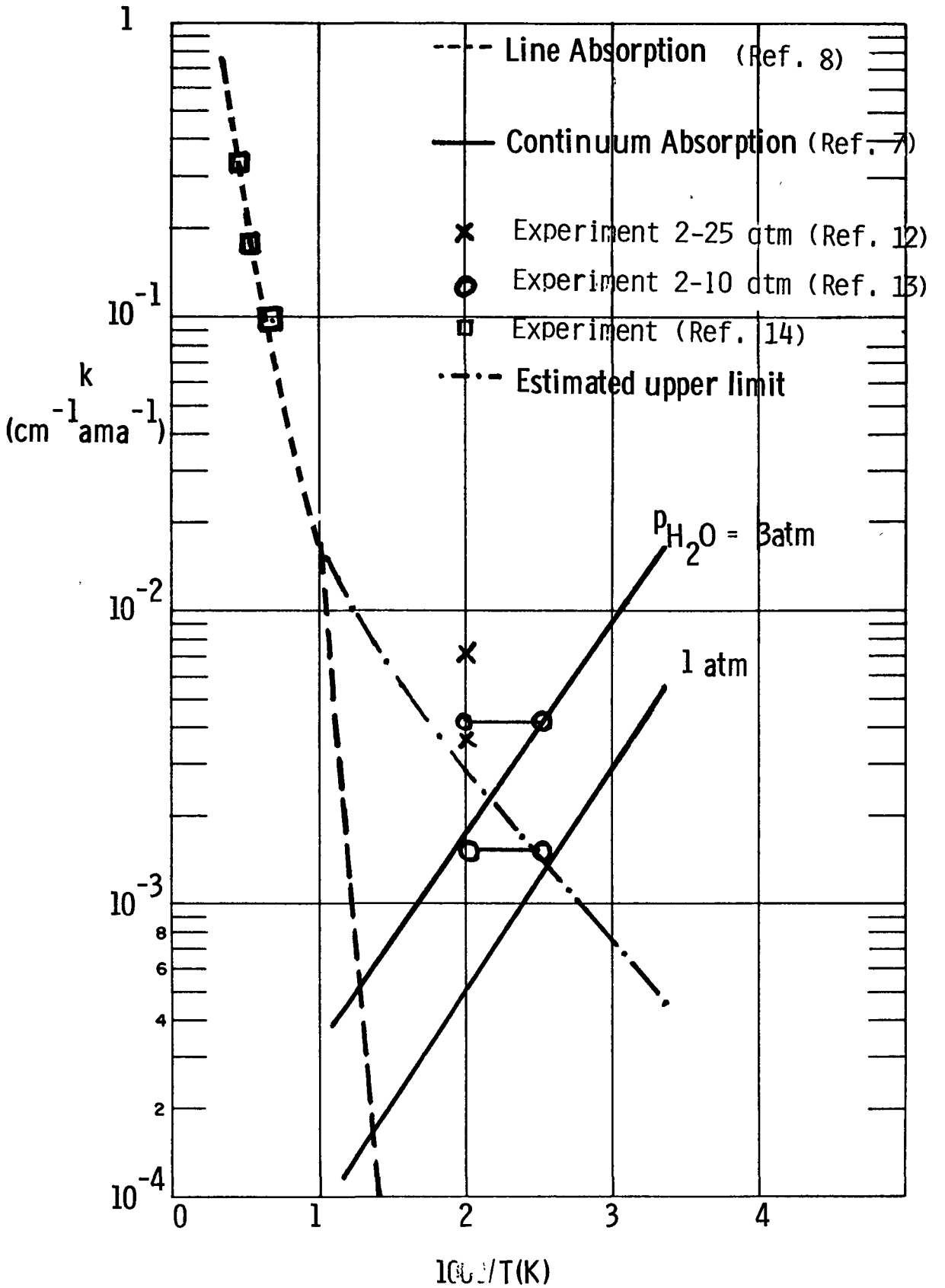

Fig. 2-5 Absorption Coefficient of H_2O at 10.6 μm.

The square dependence on pressure or number density for this absorption mechanism indicates an advantage in going to higher pressure for low temperature absorption of 10.6μm radiation by water.

The left-hand (high temperature) dashed curve is from Ref. 8, and is due to vibration-rotation line absorption. This curve is identical to that of Ref. 9, which was probably calculated the same way. Recently Fowler, Newman and Smith, in Ref. 10, have also calculated this contribution for water, and the $\bar{k}$ curve in their Fig. 23 is quite close to the dashed curve of Fig. 2-5. In fact, the points in their Fig. 23 referenced as Ludwig's data are actually calculations from the same source as the dashed curve in Fig. 2-5.

There are also rotational lines whose wings make a contribution at 10.6μm. They have been calculated in Ref. 11, but give very low values near 600K.

The few measurements of water vapor absorption in the literature are also plotted in Fig. 2-5. There is a group at low temperature between 400 and 500K from Refs. 12 and 13, and a group between 1535 and 2200K. These latter are calculated from spectral emissivities measured in Ref. 14. They fall very close to the dashed curve. All these measurements have coarse resolution in frequency.

The results of a calculation based on the "McClatchy tape" are given in Ref. 15, and they have higher values of k at low temperature. However, not enough details are given there to inspire confidence in the results. At PSI, a preliminary analysis performed by B. David Green, also using the line-by-line information in the McClatchy tape, indicated low absorption coefficients near 600K.

Based on all this information, we have drawn an upper-bound estimate for the line absorption, shown as the chain-dashed curve in Fig. 2-5, which was the curve used for our calculations, when added to the continuum absorption.

From this study, we conclude that water vapor absorption of 10.6μm radiation has a minimum around 500K, and is not as high as would be desirable below 1000K. However, the measurements are sparse and scattered, have coarse frequency resolution, and none have been made between 1500K and 500K, where the minimum is indicated in Fig. 2-5. It is clear that some careful, high resolution measurements would be very valuable in determining whether water vapor is a useful low temperature absorber for 10.6μm radiation.

If water vapor proves to be an unsatisfactory absorber at low temperatures, there are a number of other molecules which can be considered. Several have been studied theoretically in Ref. 10, and experimentally with results not yet reported. But in addition to the absorption coefficient, one must know the chemical stability of these molecules before their true potential as absorbers can be evaluated. This requires knowledge of their kinetics as well as their equilibrium properties with hydrogen. Study of these other 10.6μm abosrbers is beyond the scope of the present work.

Absorption by H_2O at 5.3μm

The absorption coefficient of H_2O for 5.3μm radiation is shown in Fig. 2-6, where k in cm^{-1} $amagat^{-1}$ is plotted against 1000/T. This curve is taken from Ref. 16, up to 3000K (1000/T = 1/3). For higher values of T, the curve is extrapolated horizontally. It is seen that water is a good absorber over the whole range from 300 to 3000K, since k varies only from 0.06 to 0.22.

Absorption by NO at 5.3μm

The absorption coefficient of NO for 5.3μm radiation is shown in Fig. 2-7, where k in cm^{-1} $amagat^{-1}$ is plotted against 1000/T. This curve is taken from Ref. 16 up to 3000K, and extrapolated horizontally for higher values of T. The shape of this curve shows excellent absorption, above 1.0, at low temperatures, and near 0.5 at high temperatures. NO is not a thermodynamically stable species under almost any conditions of interest; however, below about 2500K the chemical kinetic rates for its destruction are so slow as to make it a candidate for a low temperature absorber. In the scenario of interest it will form H_2O and N_2 when it dissociates so that there would be a good absorption coefficient from 300K to 3000K if NO is initially present.

Absorption by CO at 5.3μm

The absorption coefficient of CO for 5.3μm radiation is shown in Fig. 2-8, where k in cm^{-1} $amagat^{-1}$ is plotted against 1000/T. This curve is taken from Refs. 16 and 17. It covers the temperature range from 1000 to 6000K, over which k varies from 2.3E-3 to 0.31. The agreement between the values provided by the two different references gives confidence in the prediction of k for CO. Fig. 2-8 shows that only above 2000K may CO be considered a good absorber of 5.3μm radiation, so it acts as a high temperature absorber, while NO and H_2O are low temperature absorbers. CO is stable to very high temperatures (> 6000K).

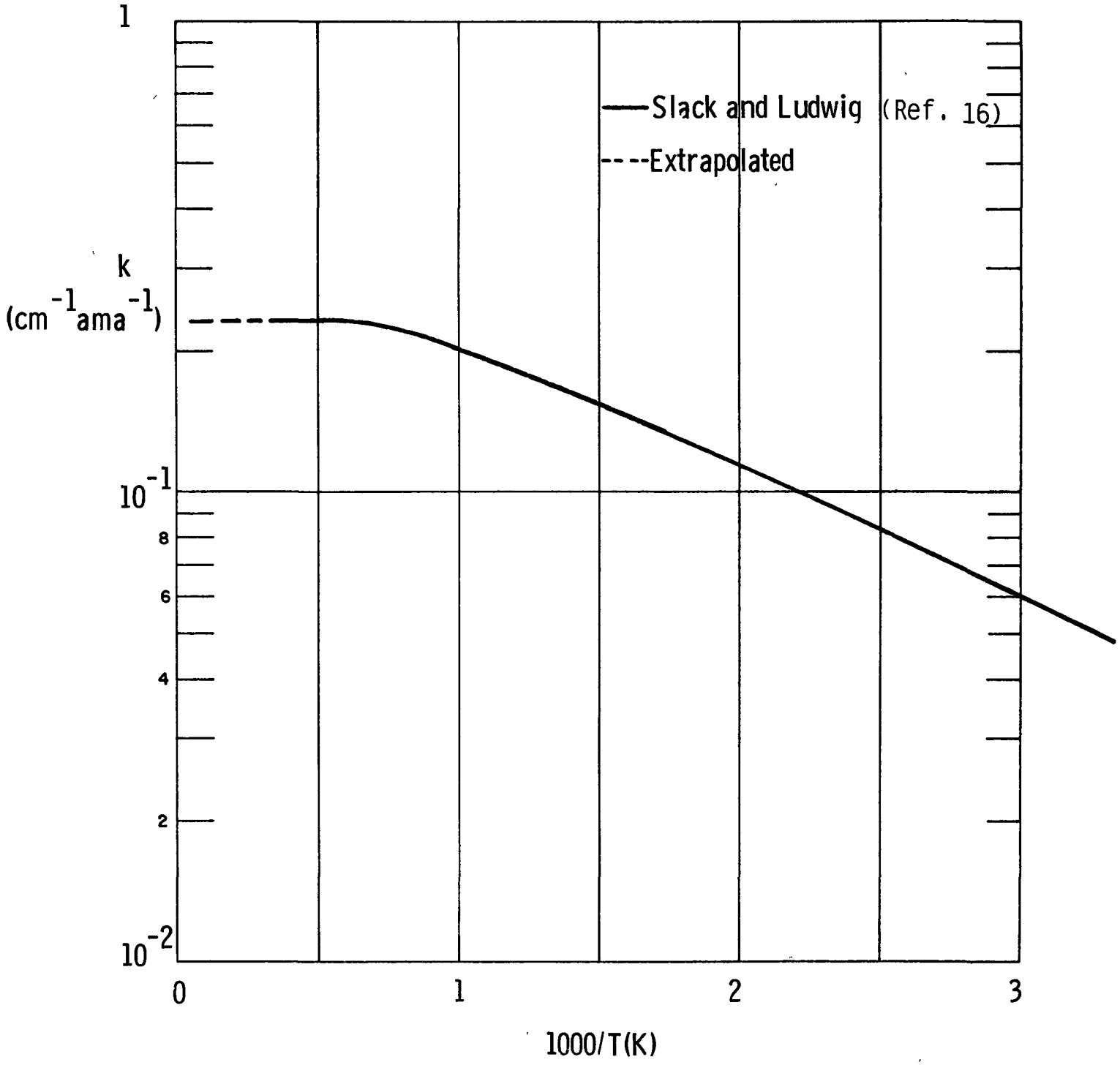

Fig. 2-6 Absorption Coefficient of H_2O at 5.3μm

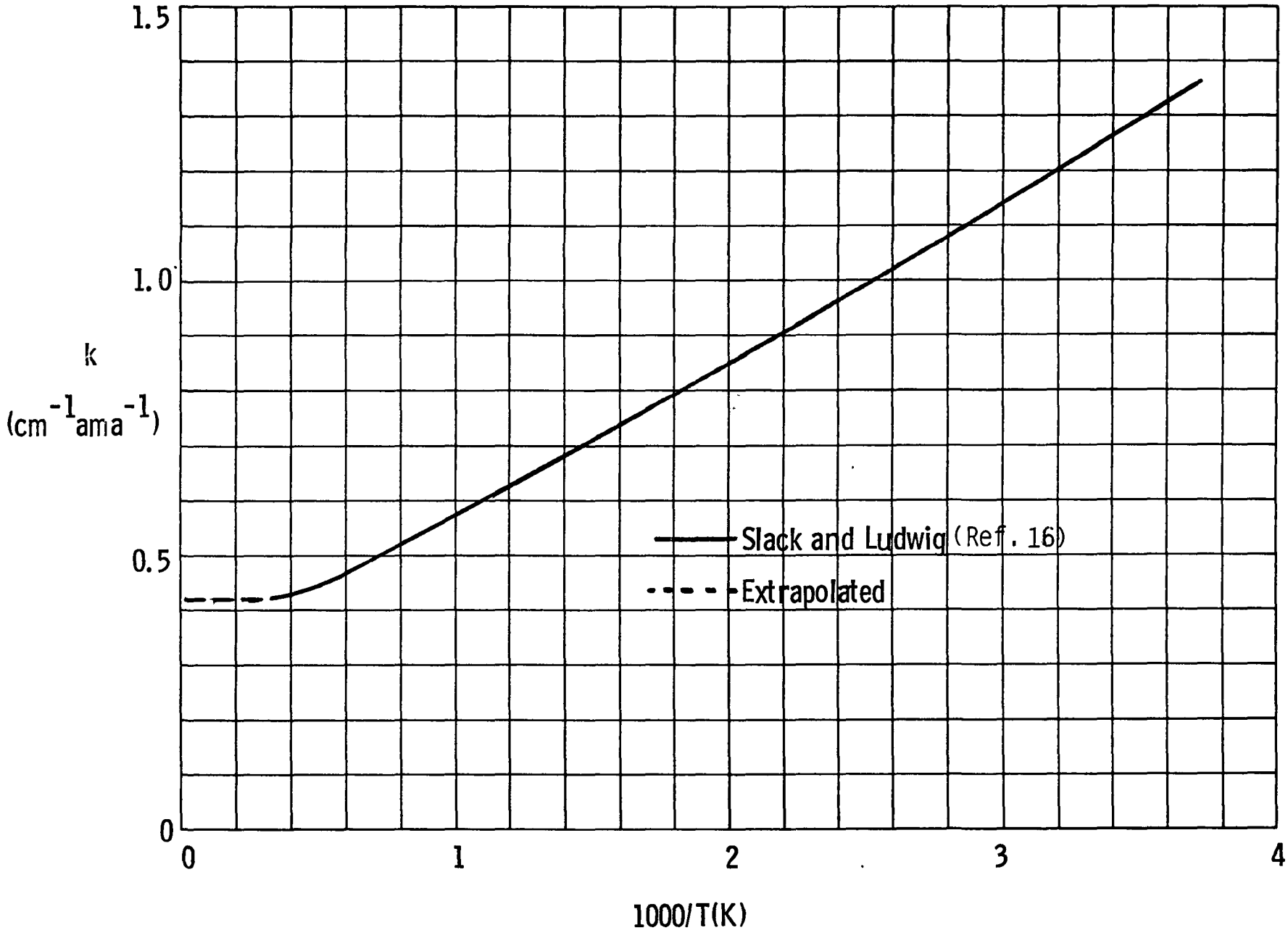

Fig. 2-7 Absorption Coefficient of NO at 5.3μm

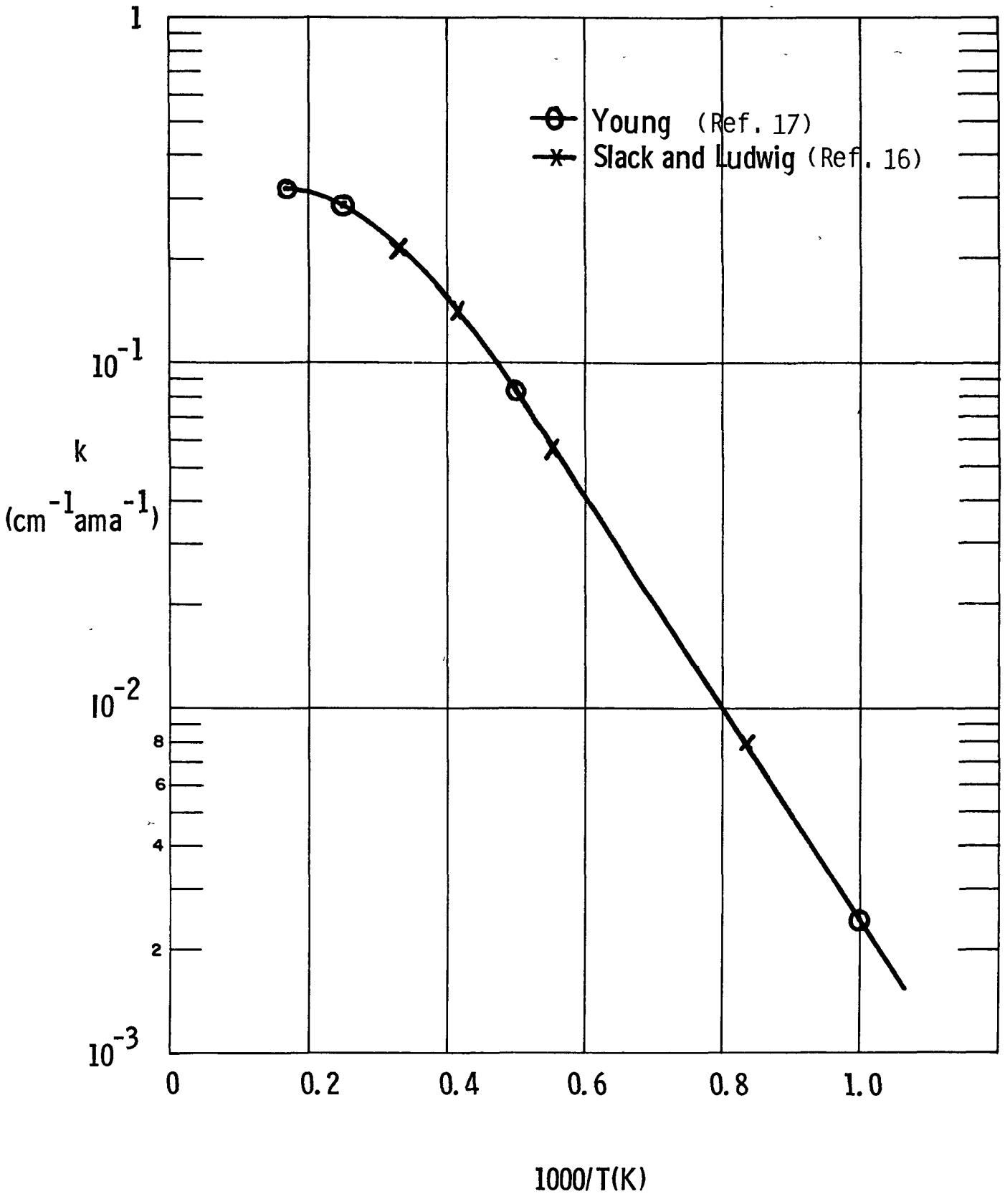

Fig. 2-8 Absorption Coefficient of CO at 5.3μm

Results for Gas Mixtures

The absorption coefficients for individual species can be combined with chemical calculations of the composition of a gas mixture, to provide the total absorption coefficient for the mixture at a given pressure and temperature. We need only multiply each absorption coefficient by the number density of the one or two species which partake in the process leading to that absorption mechanism. Then all the coefficients are added to give the mixture absorption coefficient k_L.

The composition of the gas mixture was calculated by an existing PSI computer program which accepts a list of species, a pressure and a temperature and calculates the equilibrium composition, enthalpy and density. This program can also perform calculations with some species frozen, by omitting from the species list those species which would result from reaction of the species it is desired to freeze.

Calculations have been made for both 10.6μm and 5.3μm radiation at pressures of 1, 3, 10, 30 and 100 atm, for temperatures up to 6000K. For 10.6μm, the mixture considered was $H_2/H_2O/Cs$ in the six composition given by

$$\begin{aligned} H_2/H_2O/Cs &= 0.945/0.05/0.005,\ 0.940/0.05/0.01 \\ &= 0.965/0.03/0.005,\ 0.960/0.03/0.01 \\ &= 0.985/0.01/0.005,\ 0.980/0.01/0.01 \end{aligned}$$

The absorption coefficients are shown for 3, 30 and 100 atm in Figs. 2-9 and 2-10 for all six compositions. At 3 atm, the absorption coefficient never rises above 0.1 cm^{-1} with these compositions and is below 10^{-3} cm^{-1} for temperatures lower than 1000K. The solid curves have 0.005 Cs while the dased curves have 0.01 Cs. The extra cesium makes a noticeable

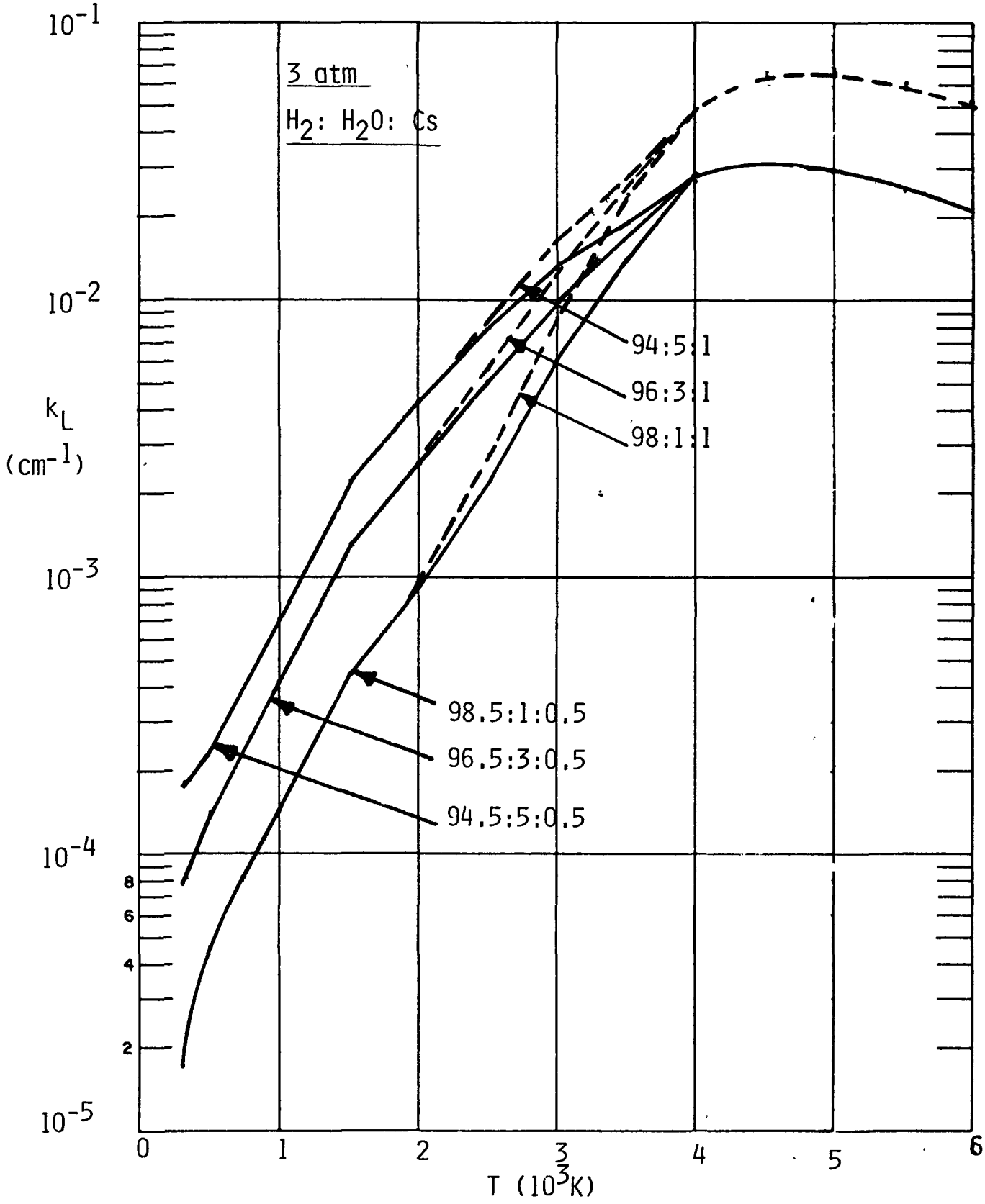

Fig. 2-9 Absorption Coefficient at 10.6μm for 3 atm

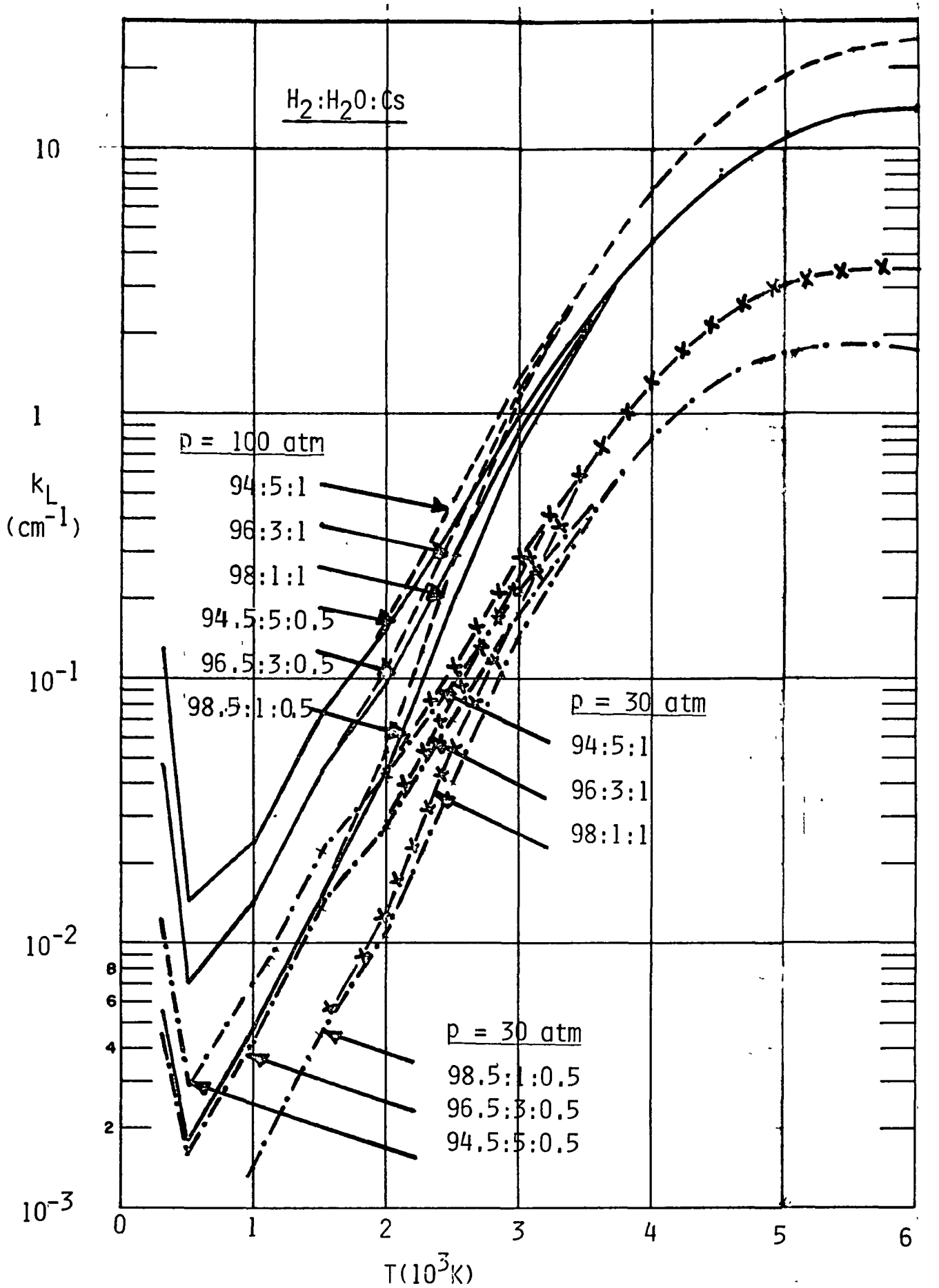

Fig. 2-10 Absorption Coefficient at 10.6μm at 30 and 100 atm

increase in k_L above 2000K, where the cesium begins to produce electrons so Bremsstrahlung can be effective. However, below that temperature, all the absorption comes from water, and both sets of curves are the same because they have the same amount of water.

The effect of pressure in increasing k_L is shown by Fig. 2-10, where the pressure is 30 and 100 atm, rather than 3 atm. Here the highest values of k_L are near 25 cm^{-1} for the 0.01 Cs mixtures and 14 cm^{-1} for the 0.005 Cs mixture. These represent factors of 500 to 700 increase over the corresponding values at 3 atm and show the very favorable increases in k_L that are obtained with the factor of 33 increase in pressure. Again, the pure water absorption is the sole contributor to k_L below 2000K.

In Fig. 2-10, the minimum of water absorption around 500K is clearly seen, with values of 0.002 to 0.02 at 100 atm for these mixtures. This may present some problems for absorption, so it is important to verify that the minimum shown on Fig. 2.5 actually is correct. If it proves correct, then other absorbers for 10.6μm should be studied, since absorption coefficients below 0.01 are probably not desirable.

At the high temperature end, the 100 atm absorption coefficients are more than adequate; it is probably not necessary to operate at such a high pressure. The 30 atm curves show maximum values of k_L of 1 to 3 cm^{-1}.

From these results we can conclude that a 0.005 or 0.01 Cs mixture with a few percent H_2O in H_2 provides good absorption of 10.6μm radiation at 30 atm above 2500K. However, below that temperature, the absorption falls rapidly if our present estimates of water absorption are correct, and

better absorption is needed than that provided by up to 0.05 H_2O. Either other absorbers should be studied, or considerably more water is needed. The addition of water (and consequent subtraction of H_2) increases the molecular weight of the mixture and reduces the specific impulse which can be attained. Therefore, there is a tradeoff between absorption coefficient and amount of molecular absorber.

The calculations for 5.3μm radiation considered two mixtures. Both used CO as the high temperature absorber, but one used water as the low temperature absorber and the other used NO. The mixtures considered were

$$H_2/CO/H_2O = 0.90/0.05/0.05$$
$$= 0.94/0.03/0.03$$
$$= 0.98/0.01/0.01$$

$$H_2/CO/NO = 0.90/0.05/0.05$$
$$= 0.94/0.03/0.03$$
$$= 0.98/0.01/0.01$$

For each mixture, two calculations were made. In the first, all species were assumed to be in equilibrium. In the second, the NO or the H_2O was taken as frozen, unable to react. These provide the two limits between which the actual chemical state will vary. It is important to consider these limits because NO is not a true equilibrium state at low temperatures, and neither is H_2O in the presence of CO. However, both NO and N_2O will actually react very slowly, and in laser heating applications, we do not expect true equilibrium to prevail.

The equilibrium composition calculations show this lack of H_2O at temperature below 1000K. The water is replaced by CO_2 in this region. When we put in NO instead of water, the composition is nearly the same. The NO is replaced by N_2 over the whole temperature range, and the O becomes water above 1000K, and CO_2 below there. As far as the equilibrium species go, the $H_2/CO/NO$ and $N_2O/CO/H_2O$ mixtures are very similar. In both of them, the CO is present at a constant mole fraction above 1000K, and so can serve as the high temperature absorber.

When the composition is combined with the individual species absorption coefficients we get the k_L curves shown in Figs. 2-11 (3 atm) and 2-12 (100 atm).

The results for 3 atm show values of k_L mostly between 0.01 and 10^{-4} cm^{-1}. The pure equilibrium cases are nearly the same whether NO or H_2O is used. They fall off sharply below 1000K because of the disappearance of H_2O. The frozen water curves hold up better below 1000K, though they also fall off below 500K because of the dip in water absorption. They are also slightly higher at the high temperature end. The frozen NO curves are somewhat higher everywhere than the frozen water curves, and they rise sharply at low temperature instead of decaying. This reflects the high absorption of NO at low temperatures.

The results for 100 atm in Fig. 2-12 are qualitatively very similar to the 3 atm case, but all values are about a factor of 30 higher, corresponding to the pressure increase. This improvement is not as great as for the 10.6μm case, because the molecular absorption is proportional only to the first power of number density, while for 10.6μm, the Bremsstrahlung is proportional to the product of the electron and molecular number densities. The values of k_L for 100 atm at the higher seed fractions are mostly between 1 and 0.01 cm^{-1}, which are adequate absorption coefficients, though not as high as for 10.6μm at the same pressure.

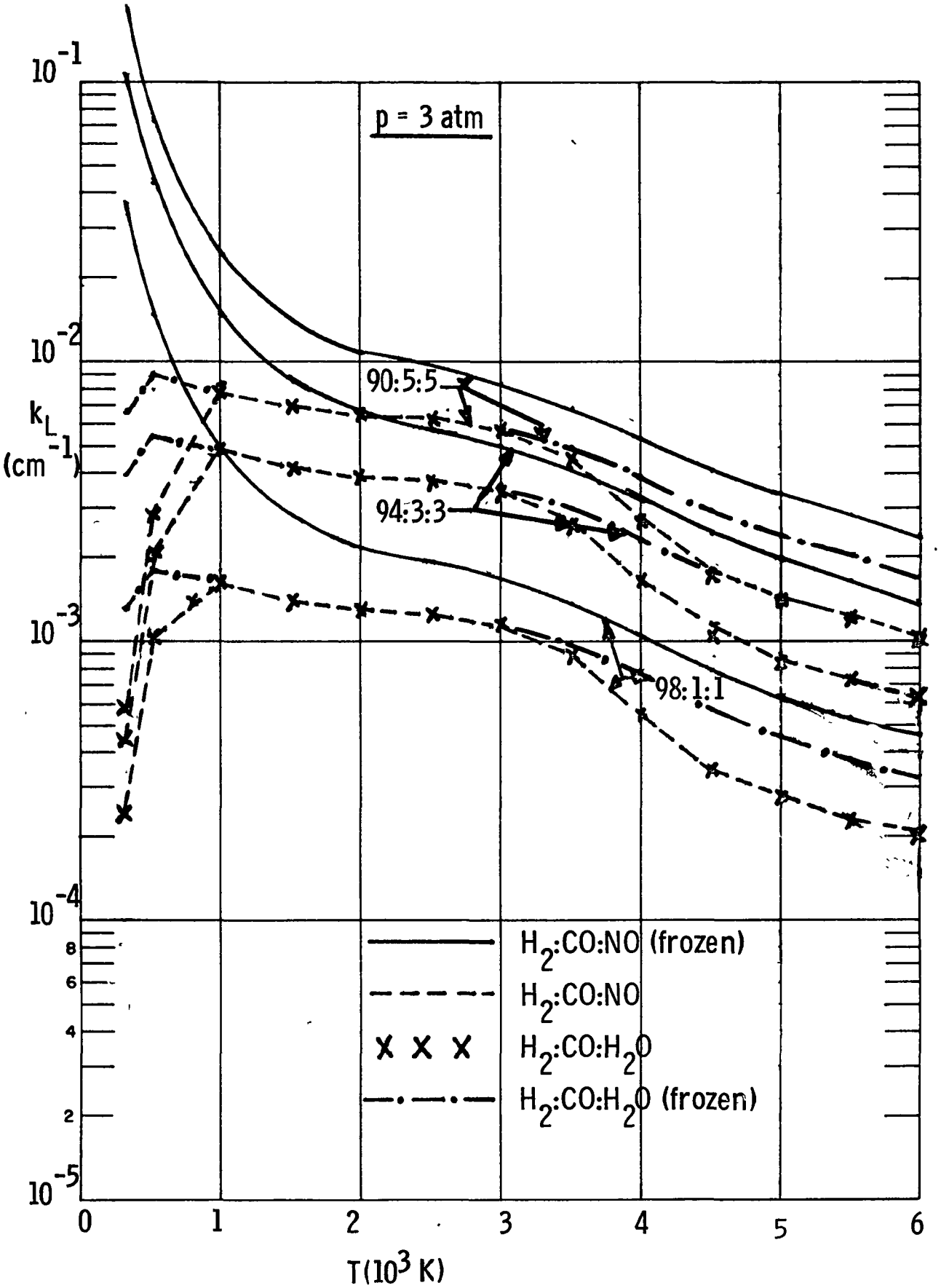

Fig. 2-11 Absorption Coefficient at 5.3μm at 3 atm

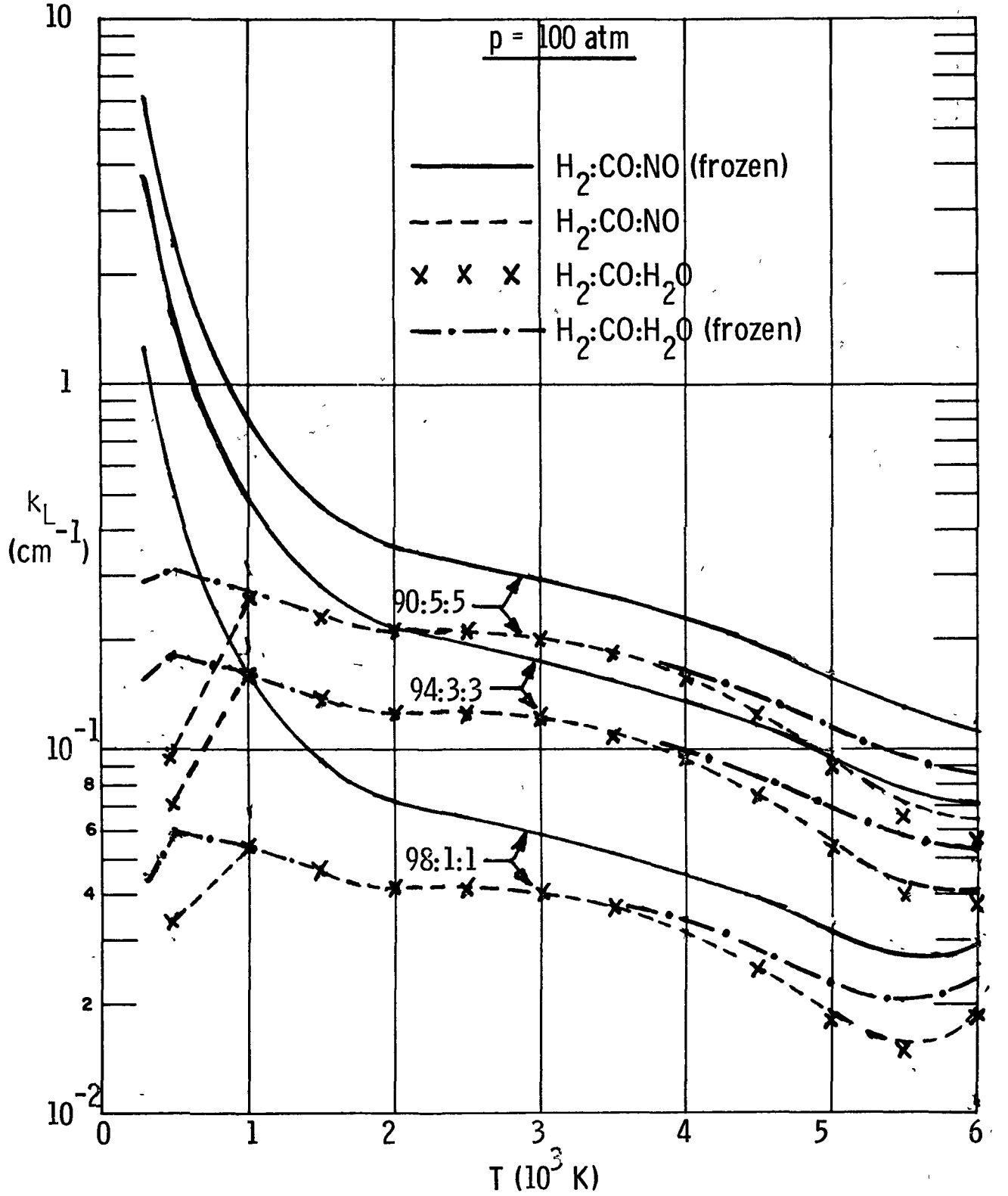

Fig. 2-12 Absorption Coefficient at 5.3μm at 100 atm

The high values of k_L at low temperature provided by frozen NO would be very useful if the chemical kinetics will permit this composition.

For 5.3μm radiation we conclude that frozen NO will permit good absorption at low temperature; frozen water will give lower, though probably adequate absorption. The pressure level must be higher to reach the same values of k_L as for 10.6μm absorption. The trend of absorption with increasing temperature is down for 5.3μm, since no new absorbing species are being created, while the density is decreasing. This is in contrast to 10.6μm, where the trend is up because of the creation of electrons.

III. RADIATIVE AND ABSORPTIVE PROPERTIES MODELING

The use of CW laser radiation to heat gases for propulsion is advantageous because high temperatures can be reached, leading to the possibility of high specific impulse. However, the high temperatures also lead to significant radiation from the gases, which must be handled by the cooling system of the thruster. In the continuous heating mode, where molecular absorbers are used, temperatures up to 6000K can be reached, at pressure levels of up to 100 atm. At temperatures above 2000K, radiation from the vibrational modes of the molecular species in the gas will be the important contributor to the total radiation. For hydrogen, or an alkali metal seed, such as cesium, which ionizes, the free-free (Bremsstrahlung) and free-bound radiation will also be significant at higher temperatures.

In the LSC wave heating mode, where much higher temperatures are reached, line radiation may also be important.

The molecular species considered in this study include NO, CO and H_2O, as well as the primary propellant H_2. At the higher temperatures OH is also formed and must be considered. When NO is used as an absorber, finite rate kinetic calculations show that it will react with H_2 to form H_2O and N_2 at temperatures above 2000K, so radiation from NO is not important and has not been calculated. However, such a calculation could also be made by the procedure described below for the other radiators considered. The species CO_2 is not formed in significant quantities in the mixtures studied so far, but its radiation was also calculated for two reasons. First, it might be a useful absorber for future consideration, and second, there are data and calculations available for CO_2 radiation which can be compared with the results of the calculation method used here.

The radiation from the species H_2, H, H^+, H^-, E, Cs, Cs^+, CO, CO_2, H_2O and OH have been calculated here, including molecular radiation, free-free and free-bound contributions. The method used for the molecular radiation is that described in the books by Penner (Ref. 18) and Penner and Olfe (Ref. 19). It is called the "just-overlapping line" or "continuously-overlapping-line" approximation. This method is particularly applicable at high pressure where lines are broad, for large optical path where the wings of lines become more important, or at high temperature where the number of significant lines in a wavelength interval increases. The purpose of this work is to develop a radiation model which is simple enough to be easily implemented on a computer to calculate the emission from a mixture of the gas species considered, both spectral and total. The results can then be used to construct even simpler and less detailed models of emission for use in the thruster and LSC wave computer programs. We do not require very high accuracy for the models, but desire to obtain the emission to what might be called engineering accuracy.

The radiation from many of these species has been studied before, of course. For the combustion gases CO, CO_2 and H_2O, Hottel long ago produced his famous radiation charts (Ref. 20) based on experiments. However, they were directed to furnace applications, and were limited to temperatures below 2000K and pressure-length products below 10 atm-feet. We are interested in temperatures up to 6000K and higher values of the pressure-length product. For these species, then, our work may be looked on as an extension of the Hottel charts to higher temperatures and pressures. Pure hydrogen is also a very well-studied gas, and up to 10,000K the paper of Olfe (Ref. 21) is particularly useful.

We will see that the results of our model compare very well with the calculations and data of other investigators, and give confidence in the present method of calculating molecular vibrational radiation up to at least 6000K.

3.1 Molecular Vibrational Radiation

Band Strenths for Vibrators

The band strength of a vibrational band (often called the integrated absorption) is an important distinguishing characteristic of the band. We shall use the units amagat^{-1} cm^{-2} where an amagat is the number density at 1 atm and 273.16K, which is 2.687E19 cm^{-3}. Band strengths are normally given at room temperature and their temperature dependence must be determined. It is readily found by use of a simple harmonic oscillator approximation for the vibrator, which will now be described.

When a vibrator makes a transition from a lower state ℓ specified by the quantum number n_1, n_2,... to an upper state u specified by $n_1 + \delta_1$, $n_2 + \delta_2$...., the band strength is

$$\alpha\ (n_i \rightarrow n_i + \delta_i) = \frac{L_o\ c}{8\pi\nu^2}\ A_{u\ell}\ g_u\ \frac{e^{-E_\ell/kT}}{Q_v}\ \left(1-e^{-h_p\nu/kT}\right) \qquad (3\text{-}1)$$

Here c is the speed of light, L_o is Loschmidt's number, E_ℓ is the energy level of the lower state relative to the ground state, $h\nu = E_u - E_\ell$ is the energy change in the transition g_u is the degeneracy of the upper state, Q_v is the vibrational partition function of the molecule and $A_{u\ell}$ is the Einstein coefficient for spontaneous emission for the transition.

In the harmonic oscillator approximation, the populations, degeneracies and Einstein coefficients of the higher level are related to those of the lower level by simple rules so that Eq. (3-1) can be summed over the harmonic oscillator states to give the total band intensity in terms of the properties of the lowest absorbing level. The result for a band is

$$\alpha_T = \sum_{n_i} \alpha(n_i \rightarrow n_i + \delta_i) = \frac{L_o c}{8\pi\nu^2} \quad A_{u\ell}\, g_u\, f(T)$$

$$f(T) = \frac{e^{-E_\ell/kT} \quad (1-e^{-h_p\nu/kT})}{\prod_i \left(1-e^{-h_p c\omega_i/kT}\right)^{\delta_i}} \tag{3-2}$$

Here $\nu = \Sigma c\omega_i \delta_i$, where $c\omega_i$ is the vibrational frequency of mode i, so that ω_i is the corresponding wave number.

In terms of the total band intensity at 300K, that at any temperature can be written as

$$\alpha_T\ (T) = \alpha_T\ (300)\ f(T)/f(300) \tag{3-3}$$

At room temperature $h_p\nu/kT$ is usually large compared to unity, and for transitions from the ground state of the molecule $f(300) \tilde{\sim} 1$.

Emissivity

As radiation traverses a gas, some is re-absorbed, so the radiation emitted from the end of a column of gas is less than that for emission only. The absorption depends on the optical path and the absorption coefficient. We here define the optical path length χ as the physical length times the number density of the radiator in amagats, and define the absorption coefficient P so that $P\chi$ is dimensionless.

The radiation emitted from the end of a homogeneous column of gas is the blackbody function times the absorption factor $1 - e^{-P\chi}$. This is usually expressed as an emissivity ε times the blackbody flux σT^4, where σ is the Stefan-Boltzmann constant. The emissivity is used as the engineering expression for the emitted radiation.

$$\varepsilon = \frac{1}{\sigma T^4} \int d\omega \, B_\omega \, (1-e^{-P\chi}) \tag{3-4}$$

Here the blackbody function is defined in wave number ($\omega = \nu/c$) space as

$$B_\omega = \frac{2\pi h_P c^2 \omega^3}{(e^{h_P c\omega/kT}-1)} \tag{3-5}$$

such that its integral over ω from 0 to ∞ is σT^4. In order to find ε we must evaluate the integral in Eq. (3-4) with the proper variation of P with respect to ω.

We will evaluate the integral using the continuous-overlapping-line approximation. First we apply Eq. (3.4) to a band, centering the integral on the wave number $\bar{\omega}$ of the band center. We take the blackbody function outside the integral, evaluating it at the band center because the band width is small compared to the variation of B_ω. The band is approximated as symmetric about $\bar{\omega}$, and the integral is extended to ∞ since the contributions in the band wings dies off rapidly. The result is

$$\varepsilon = \frac{2B\bar{\omega}}{\sigma T^4} \int_0^\infty (1-e^{-P\chi})\, d(\omega-\bar{\omega}) \qquad (3\text{-}6)$$

The absorption P is taken to be the average of the line strengths for corresponding lines in the R and P branches, divided by the line spacing $2B_e$, and so becomes

$$P = \frac{2j+1}{4B_e}\, \alpha_T \gamma e^{-\gamma j(j+1)} \qquad (3\text{-}7a)$$

Here α_T is the band intensity, γ is defined by

$$\gamma = h_P c B_e / kT \qquad (3\text{-}7b)$$

and j is the rotational quantum number of the upper state.

We treat j as a continuous variable, related to ω by the line spacing $\omega = \bar{\omega} + 2jB_e$ and introduce the variable

$$\xi = \gamma j\,(j+1) + \gamma/4 = \gamma(j+\tfrac{1}{2})^2.$$

so that $d\xi = \sqrt{\gamma}\, dj$, $dj = d\,(\omega - \bar{\omega})/2B_e$.

Then $$P = \frac{\gamma\, \alpha_T \xi}{2B_e}\, e^{\gamma/4}\, e^{-\xi^2}$$

In terms of ξ the expression (3-6) for ε can be written

$$\varepsilon = \frac{B\bar{\omega}}{\sigma T^4}\, \Delta_o\, I(K) \tag{3-8}$$

$$\Delta_o = \frac{B_e}{\sqrt{\gamma}} = \left(\frac{kTB_e}{h_P c}\right)^{\frac{1}{2}}, \quad K = \frac{\chi\sqrt{\gamma}\, \alpha_T e^{\gamma/4}}{B_e} = \frac{\alpha_T \chi_e}{\Delta_o}\, e^{\gamma/4}$$

$$I(K) = 4 \int_0^\infty [1 - \exp\,(-\frac{K\xi}{2}\, e^{-\xi^2})\,]\, d\xi$$

The one parameter integral I(K) can be evaluated numerically. As $K \to 0$, $I \to K$. For K large, an asymptotic analysis shows that I goes like $(\ell n\, K)^{\frac{1}{2}}$. A good fit to the integral is

$$I = 7.2\,[1 - \exp((-K/7.2)]\,,\ K \leq 20$$

$$= 4.13\,[\ell n\ 0.721K]^{\frac{1}{2}}\,,\ K > 20 \qquad (3\text{-}9)$$

With this approximation for I(K), the emissivity is expressed in terms of T, B_e, α_T and χ by Eqs. (3-8), for each band. The band strengths α_T are found from Eqs. (3-2) and (3-3), while the optical path χ is related to the physical path length ℓ by

$$\chi = \ell\ [273.16\ p(atm)/T] \qquad (3\text{-}10)$$

The factor in square brackets is the number of amagats at the desired pressure and temperature. Once the bands and other physical constants of the molecule of interest are described, the emissivity can be easily calculated. It is a function of T and the pressure-length product $p\ell$.

For molecules with multiple bands, the emissivities are added unless the bands overlap. In the case of overlapping bands, a reasonable approximation is to use the sum of the overlapping band strengths.

In flow problems such as the laser heated thruster, radiation models are needed to describe radiant emission, and possibly also radiation transport. To construct such models, one needs to know the spectral emissivity ε_ω, which is the integrand of Eq. (3-4). That can be calculated from the relations already given. The blackbody function is given in Eq. (3-5), the band strength in Eqs. (3-2) and (3-3), and the absorption P in Eqs. (3-7). The rotational quantum number j is related to the wave number and the band center wave number $\bar{\omega}$ by

$$\left|\omega - \bar{\omega}\right| = 2jB_e \qquad (3\text{-}11)$$

It should be recalled that χ is length times the number density of the radiator in amagats, so that P has that number density built in. If one wants the absorption coefficient for a number density n of radiators, it is found from

$$k = nP/2.6868E19 \qquad (3\text{-}12)$$

where k is in cm^{-1} and n is in cm^{-3}.

Emissivity of CO and OH

For diatomic molecules there is only one vibrational mode, and a small number of bands. For OH we consider only the fundamental band, while for CO we consider the fundamental and the first and second overtone bands. For both molecules, the lower state energy $E_\ell = 0$. The parameters for OH and CO are given in Table 3-1.

The calculated emissivities of OH and CO are given in Figs. 3-1 and 3-2 as functions of T for various values of $p\ell$. The dependence on $p\ell$ is nearly linear for OH but shows much less than linear dependence for CO, reflecting the strong effect of reabsorption for this molecule.

TABLE 3-1

Parameters for OH and CO

Molecule	$\omega(cm^{-1})$	$B_e(cm^{-1})$	δ	$\alpha(300)$ $(ama^{-1}\ cm^{-2})$
OH	3570	18	1	100
CO	2143	1.9	1	260
			2	2.2
			3	0.011

TABLE 3-2

Parameters for CO_2

$B_e = 0.39\ cm^{-1}$ $\omega_1 = 1388\ cm^{-1}$ $\omega_2 = 667\ cm^{-1}$ $\omega_3 = 2350\ cm^{-1}$

δ_1	δ_2	δ_3	$\alpha(300)$ $(ama^{-1}\ cm^{-1})$
0	0	1	2770
0	1	0	240
1	0	1	67
1	-1	0	7.5
0	4	1	1.9
0	3	0	0.16

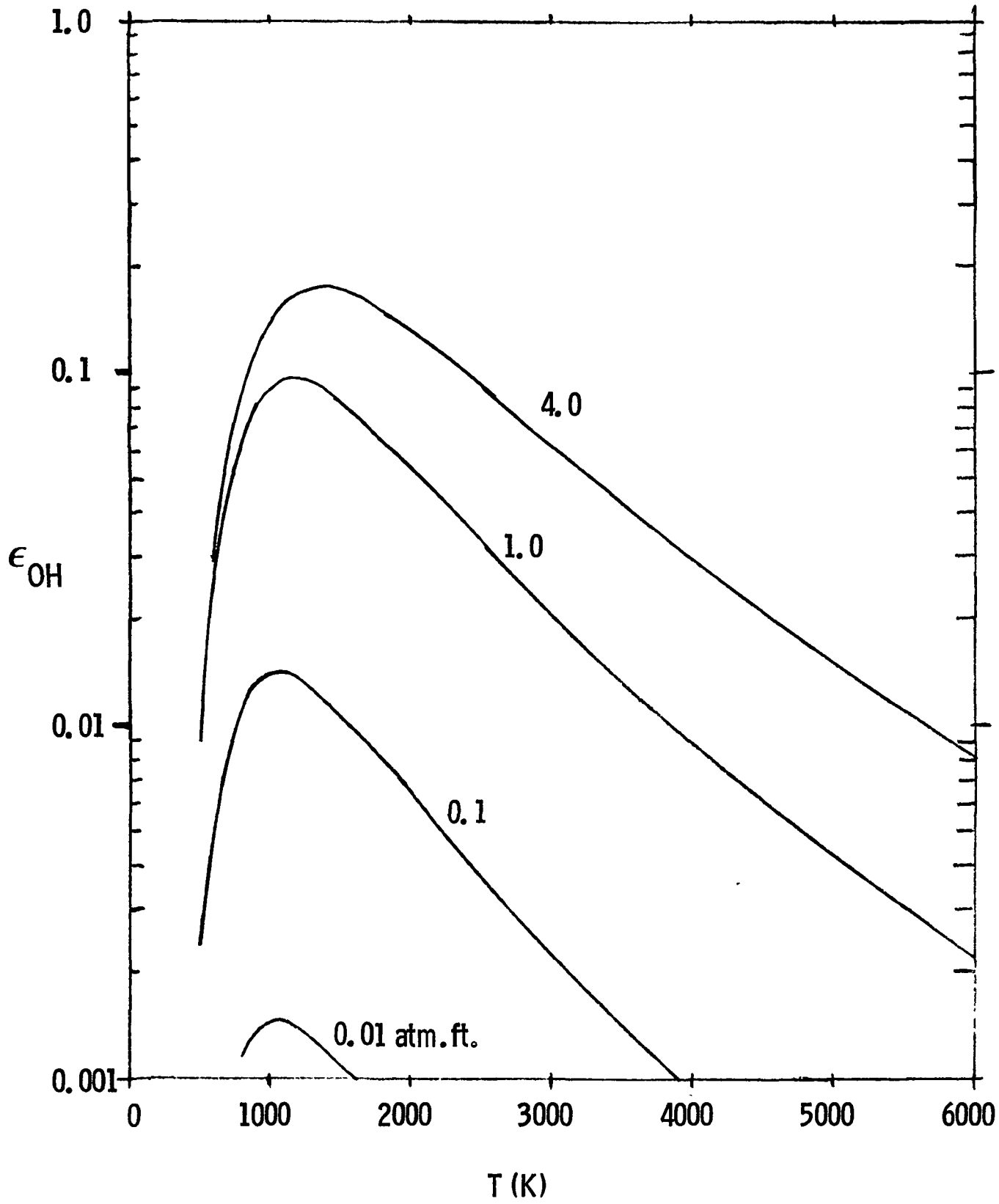

Fig. 3-1. Calculated Emissivity of OH

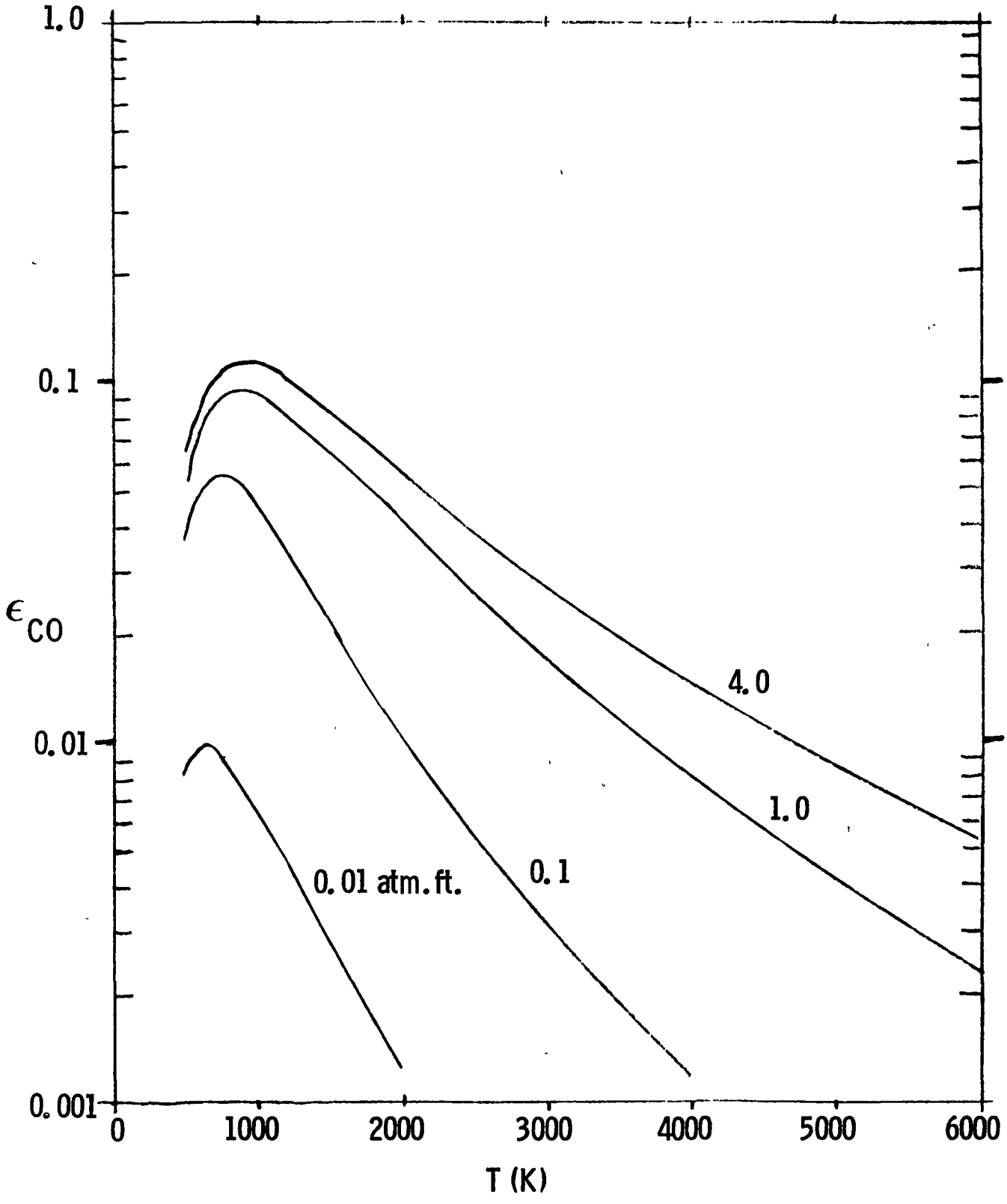

Fig. 3-2. Calculated Emissivity of CO

Emissivity of CO_2

For the triatomic molecule CO_2, the calculation of emissivity is significantly more complicated than for the diatomics. The parameters used are given in Table 3-2. The frequency of each band is given by

$$\nu = c \sum \delta_i \omega_i$$

The band with the negative value of δ_2 corresponds to a series of transitions, the lowest of which is from the 100 state to the 010 state, and has a strong temperature dependence of the band intensity α.

In Eq. (2.4), E_ℓ corresponds to the state given by the negative values of δ:

$$E_\ell = - h_P c \sum_{\delta<0} \delta_i \omega_i$$

If there are no negative values of δ then $E_\ell = 0$.

Another property of CO_2 which must be taken into account is the natural abundance of the carbon 13 isotope, which is about 1%. For CO, the data on emissivity is not certain enough and the bands not strong enough to make this worth considering, but for CO_2 the effect is considerable. The bands of isotopic CO_2 are shifted enough from normal CO_2 that they do not overlap for conditions of interest here, but they are in the same spectral region. The effect of the isotope is therefore approximated by assuming the same band intensities, but at 1% of the partial pressure. We therefore add to the emissivity of normal CO_2 at $p\ell$ the emissivity of CO_2 at $p\ell/100$.

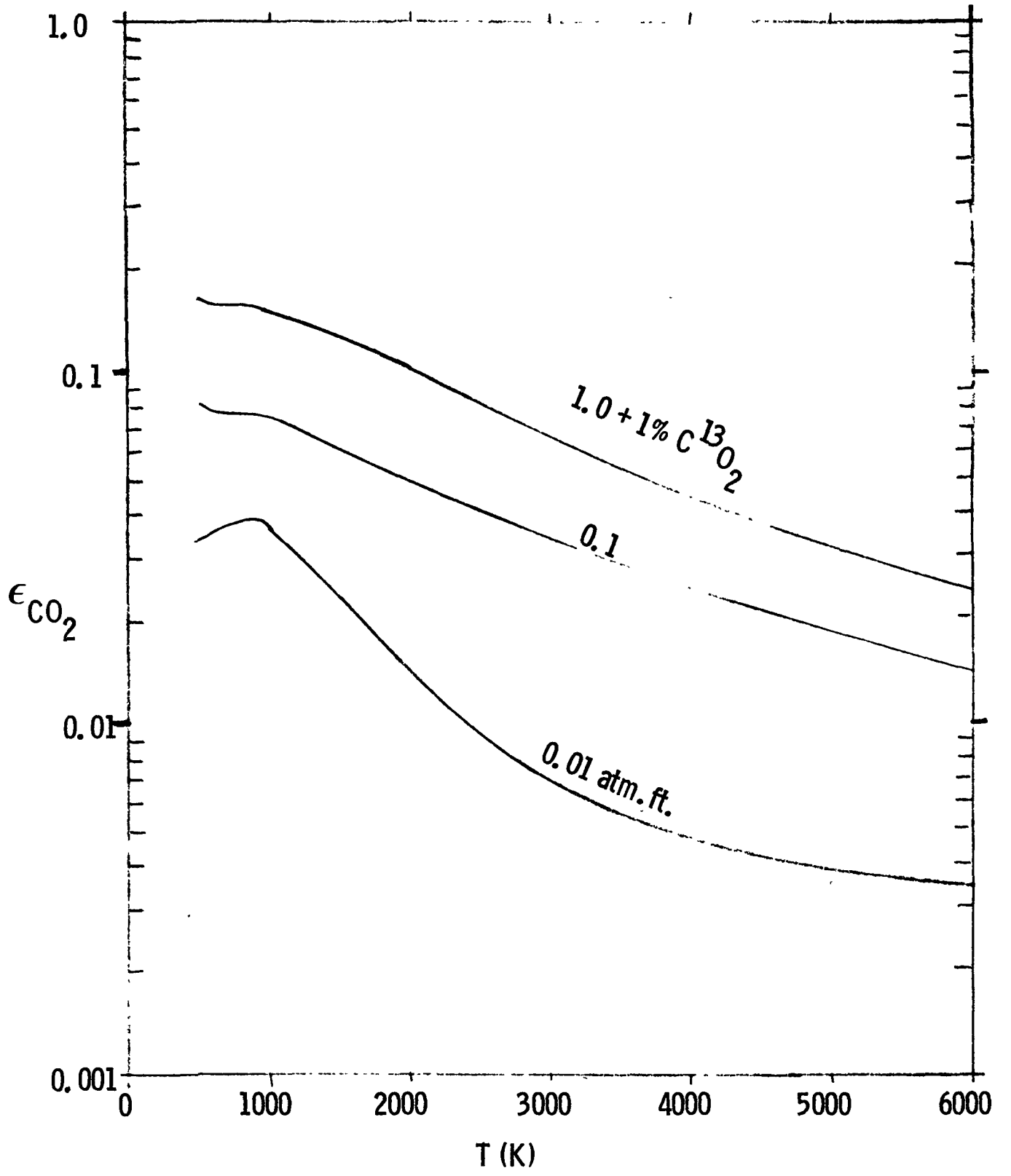

Fig. 3-3. Calculated Emissivity of CO_2

At large $p\ell$ where the CO_2 radiation becomes highly absorbed, this becomes a very important contribution to the emissivity, though always less than a factor of two increase.

The calculated emissivities of CO_2 are shown in Fig. 3-3. They decrease with temperature, except for a slight maximum at the lowest value of $p\ell$.

Emissivity of H_2O

The calculation of the emissivity of H_2O is complicated by the difficulty in describing the rotational structure of the bands. We have taken the width to be given by the variation of intensity with the principal quantum number. The band envelope then approximates that of a linear molecule but with the rotational constant given by the square root of the product of the two layer rotational constants of H_2O. We have also combined the two vibrational stretch modes of H_2O into one to simplify the calculation, leaving only two modes. The pure rotational band was omitted because it contributes significantly to the emissivity only below the temperature range where radiation is important for our application.

The values of the parameters for H_2O used in the calculations are given in Table 3-3. There are five bands, each with two transitions.

The calculated emissivities are given in Fig. 3-4. The drop off below 1000K is partly due to our neglect of the pure rotational contributions.

TABLE 3-3

Parameters for H_2O

B_e = 11.8 cm^{-1} ω_1 = 3655 cm^{-1} ω_2 = 1596 cm^{-1}

δ_1	δ_2	$\alpha(300)$ (ama^{-1} cm^{-2})
0	1	300
1	0	200
1	1	24
2	0	18
2	1	1.0

TABLE 3-4

Vibrational Emissivity of Molecular Hydrogen at a Total Pressure of 100 atm and Path Length of 30 cm

T(K)	n_{H_2} (cm^{-3})	p_{H_2} (atm)	ε (Eq. 3-14)	ε (Ref. 3-14)
1000	7.34 E20	100.	1.14 E-2	1.00 E-2
2000	3.67 E20	100.	5.83 E-3	5.34 E-3
3000	2.41 E20	98.4	1.90 E-3	1.92 E-3
4000	1.56 E20	85.3	5.55 E-4	5.59 E-4
5000	7.78 E19	53.0	9.66 E-5	1.56 E-4

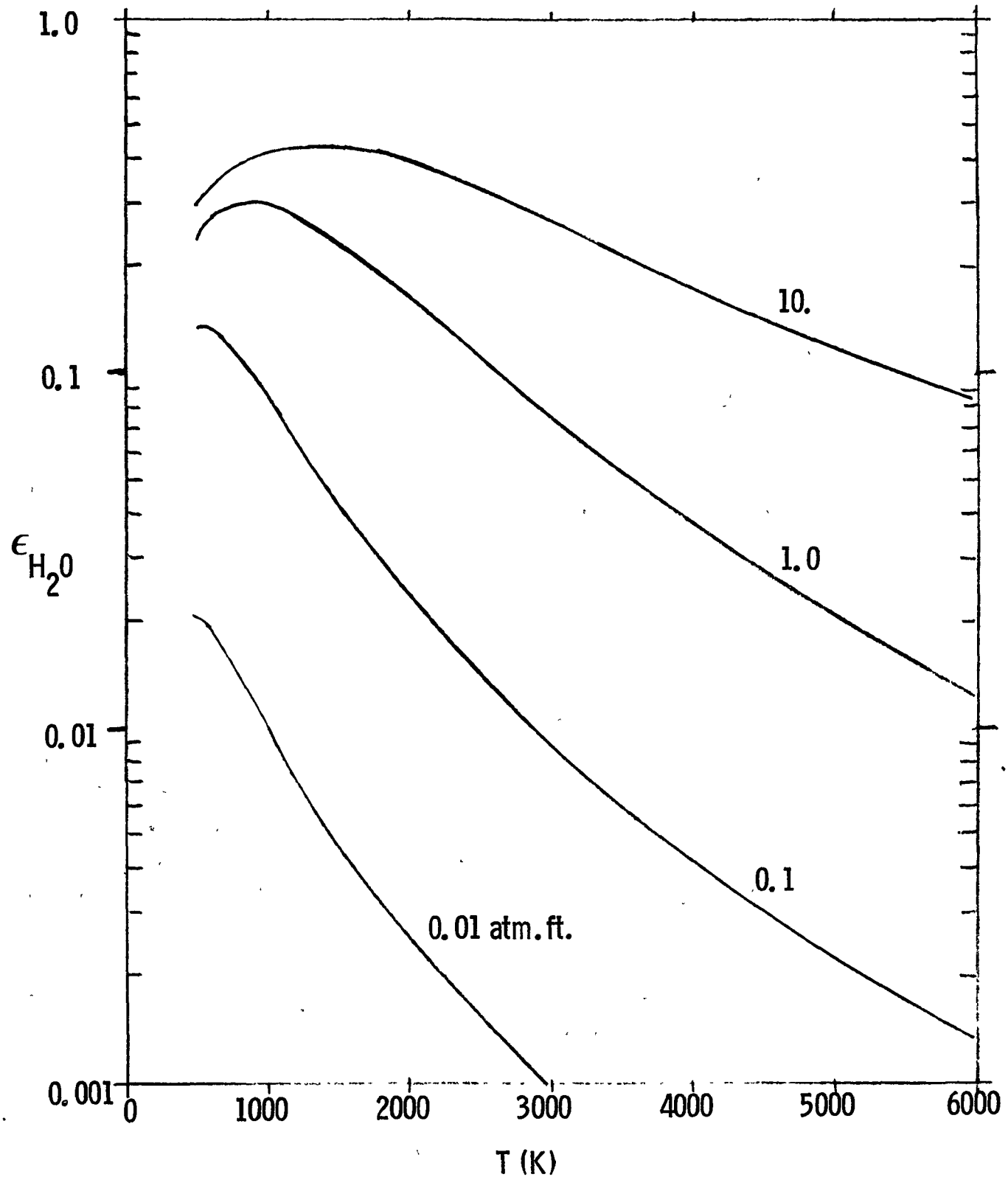

Fig. 3-4. Calculated Emissivity of H_2O

Emissivity of H_2

The vibrational radiation of the H_2 molecule has been considered by Olfe in Ref. 21. He has calculated the band intensity. From his Fig. 5 and Eqs. (10) we can write

$$\alpha_T = 0.019T^{-0.4} \; p_{H_2} \text{ (atm)} \qquad (3\text{-}13)$$

The parameters for H_2 are $\bar{\omega} = 4200$ cm^{-1}, $B_e = 60$ cm^{-1}.

If we use these values in Eqs. (3-8), and (3-10) we can calculate ε for H_2 vibration from the expressions

$$\varepsilon = \frac{3.16E11}{e^{6043/T}-1} \qquad \frac{I(K)}{T^{3.5}} \qquad (3\text{-}14)$$

$$K = 0.8037 \; \ell p_{H_2}^2 / T^{1.9}$$

Olfe presents a calculation for a total hydrogen pressure of 100 atm, $\ell = 30$ cm, and identifies the vibrational contribution in his Fig. 16. By calculating the equilibrium state of hydrogen at this pressure and any T we can find the number density of H_2, and so its partial pressure. Then Eq. (3-14) permits a calculation of ε for $\ell = 30$ cm. The results are given in Table 3-4, together with the values for vibration from Olfe's Fig. 16. The agreement is quite satisfactory up to 4000K, and above that temperature the vibrational contribution is unimportant. So Eq. (3.14) can be used for the total emissivity of hydrogen vibration.

The absorption coefficient is found from Eq. (3-12), using Eqs. (3-7a), (3-11), and (3-13) and the relation between p_{H_2} and n_{H_2}, which is

$$p_{H_2} = 1.3625E\text{-}22\ n_{H_2} T \qquad (3\text{-}15)$$

when p_{H_2} is in atm.

Comparison with Other Calculations and Experiments

There are other calculations and also experimental data with which to compare the results of the present model of molecular emissivities.

For CO, Fig. 3-5 shows the limited data of Hottel (Ref. 20) and the radiation in the thin limit obtained from the calculations of Young (Ref. 22), as well as the present calculations from Fig. 3-2. Young has performed detailed line-by-line calculations. Our results for small optical path are with 10% of Young's over the entire temperature range considered. This in effect justifies, at least for CO, the simple harmonic oscillator approximation for obtaining total emissivity.

Hottel's data is in good agreement with our calculations at $p\ell$ = 1 atm-ft. and fairly good agreement at 0.1 atm-ft. For 0.01 at ft., the data must be regarded with considerable suspicion, since it is in sharp disagreement with both the present results and those of Young.

Based on the comparisions of Fig. 3-5, the present model for CO emissivity is considered satisfactory.

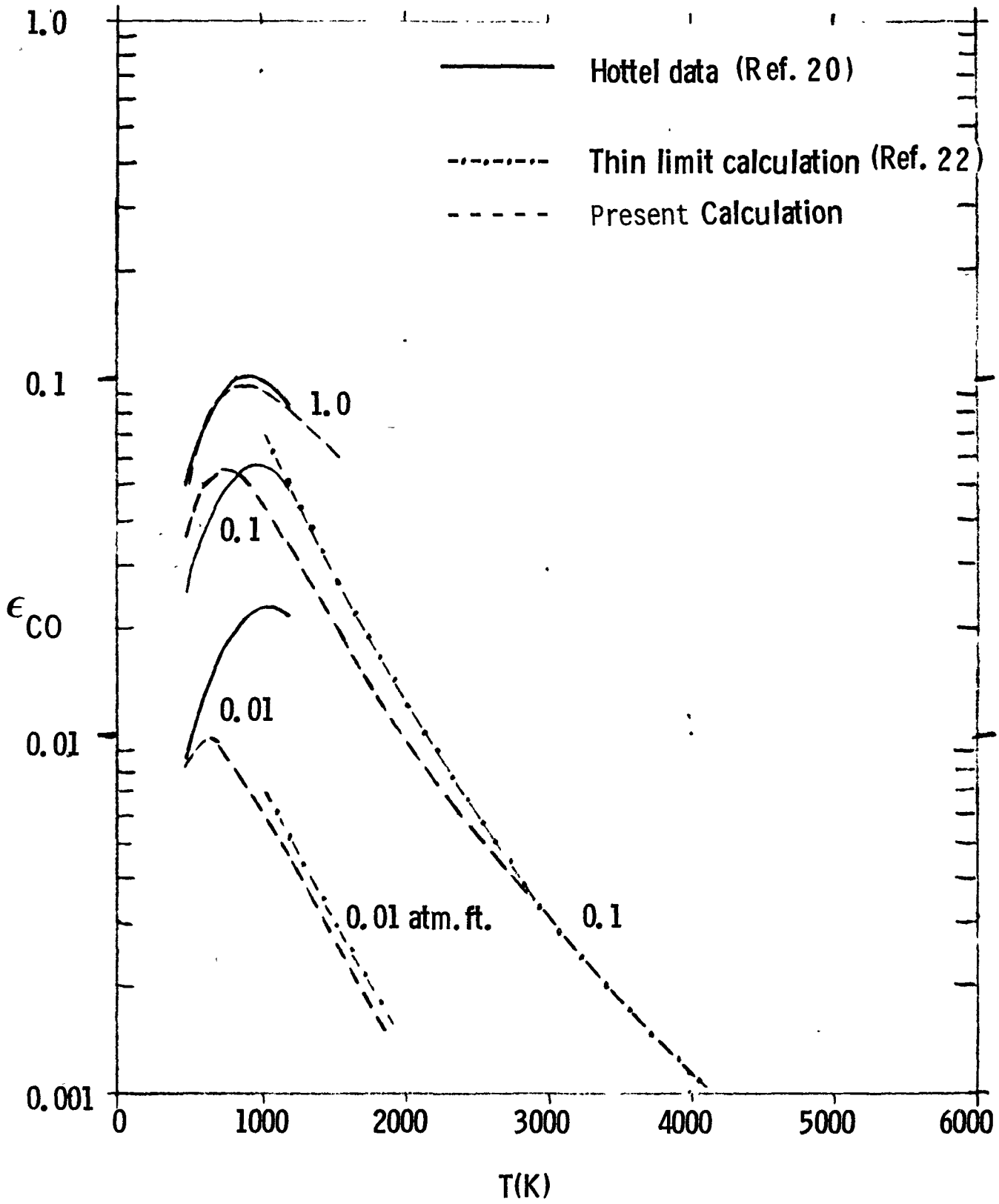

Fig. 3-5. Emissivity of CO

Figure 3-6 presents the data of Hottel (Ref. 20) and the calculations of Penner and Varanasi (Ref. 23) together with the present calculations for CO_2. The agreement is very good, and again, gives confidence in the present model. Hottel gave correction factors for various pressures which account for non-overlapping line effects. Our calculations therefore correspond to the high pressure, continuously-overlapping line results.

Data and calculations for H_2O are presented in Fig. 3-7. The calculations of Penner and Varanasi (Ref. 24) include the effects of finite line width in a calculation very similar to ours. The Ludwig and Ferriso upper limit points are quoted in Ref. 25 as coming from Ref. 26. The Ludwig and Ferriso points are from their calculations of the integral over frequency of results from a band model in Ref. 25. Both these latter results also appear in Ref. 27. Figure 3-7 shows our present calculations to be in good agreement with the other work, particularly at the higher temperatures and/or lower $p\ell$. The main discrepancy can be attributed to the difficulty in characterizing the band width. This problem decreases with increasing temperature because lines associated with higher values of the secondary rotational quantum number fill in between the principal lines at higher temperature, thus making the overlapping line approximation much better.

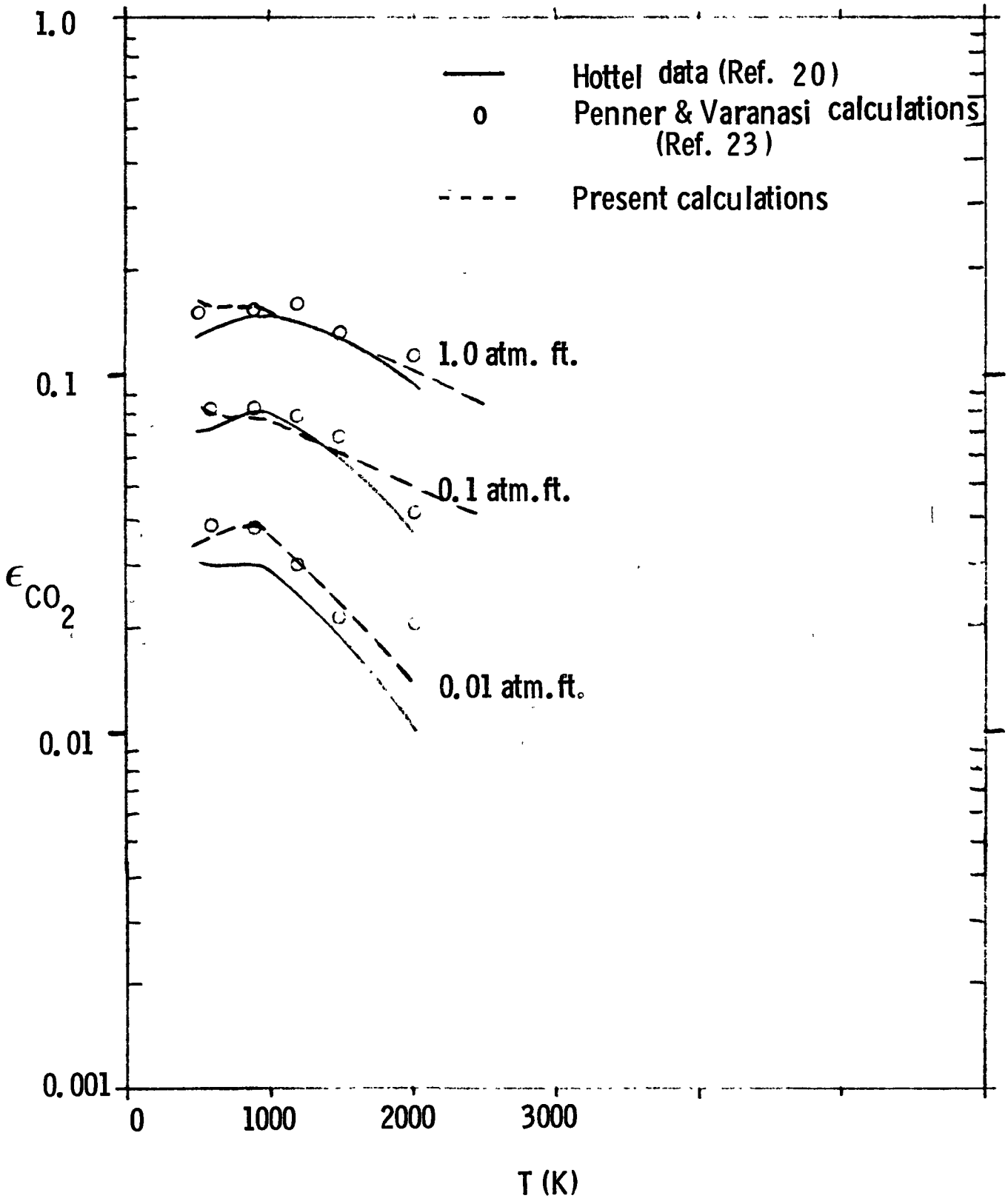

Fig. 3-6. Emissivity of CO_2

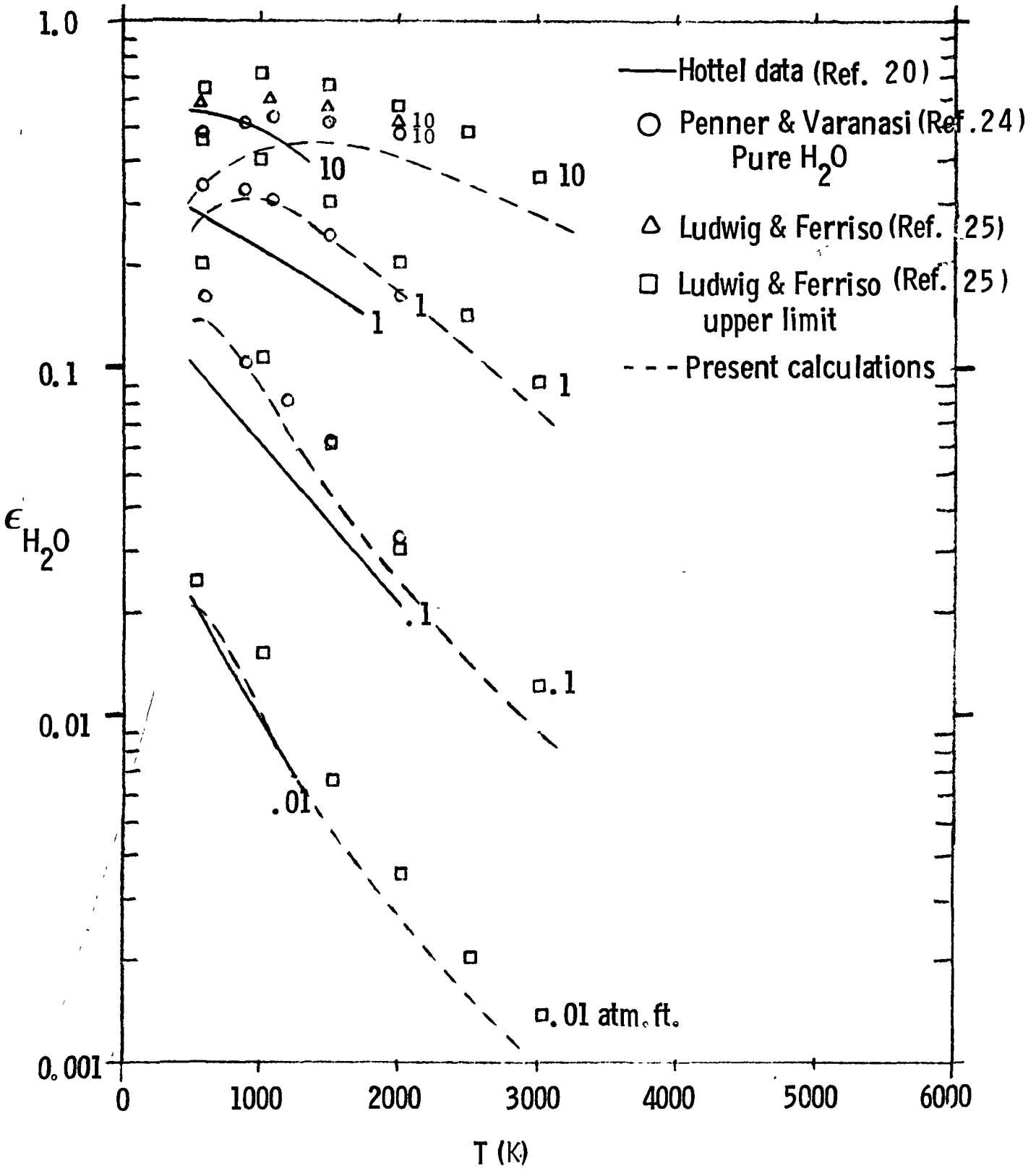

Fig. 3-7. Emissivity of H_2O

3.2 Electronic Radiation Processes

The reverse of the processes which produce absorption in the presence of electrons will produce radiation. These include two free-free processes: one between neutrals and electrons (electron-neutral Bremsstrahlung) and one between ions and electrons (electron-ion Bremsstrahlung). In addition, there are the bound-free processes which include photo-detachment and photo-ionization. We will consider these for both hydrogen, which is the major gas species, and cesium which is the alkali metal seed being used in the present study.

The radiation will be formulated in terms of absorption coefficients k_1 for each process, which is a function of the temperature, composition, wave number, and physical properties of the species. From them, the spectral emissivity ε_ω and total emissivity ε can be obtained for a given path length ℓ, by means of the relations

$$\varepsilon = \int \varepsilon_\omega d\omega, \quad \varepsilon_\omega = \frac{B_\omega \left(1-e^{-\ell \Sigma k_i}\right)}{\sigma T^4} \tag{3-16}$$

where B_ω is the blackbody function already defined in Eq. (3-5). This is the emissivity normal to the center of the base of a hemisphere of radius ℓ.

The absorption coefficients, in turn, are of the form of a cross-section times the number densities of the species participating in the process times the stimulated emission factor $1 - \exp\left(-h_p c\omega/kT\right)$. Below we will present the cross-sections (denoted by σ) for the various processes of importance.

"PAGE MISSING FROM AVAILABLE VERSION"

65-66

For hydrogen molecules, Table 2-1 shows that $T^2A(T)$ may be fitted from 1000 to 25000K by 3.7 E-33$T^{1.45}$ so that the cross-section is

$$\sigma_{EH2} = 3.54E\text{-}33T^{1.45}\ \omega^{-3}$$

and the absorption coefficient is

$$k_{EH2} = 3.54E\text{-}33\ \omega^{-3}T^{1.45}\ n_E\ n_{H2}\left(1-e^{-h_p\ c\omega/kT}\right)\left(cm^{-1}\right) \qquad (3\text{-}19b)$$

Free-Bound Radiation

Free-bound radiation is caused by free electrons being captured by an ion or neutral atom to form a neutral atom or negative ion with the release of energy as radiation. The absorption coefficient is readily found for the bound-free process for neutral hydrogen and cesium, and then used to find the emissivity for the free-bound (reverse) process.

For hydrogen atoms, the bound-free cross-section is given by the sum of the cross-sections for the available bound states

$$\sigma_H = 7.9E\text{-}18 \frac{\sum_{N>\sqrt{Ry/\omega}}^{N_{max}} \left(\frac{Ry}{N\omega}\right)^3 \exp\left(\frac{h_p c}{kT} \frac{Ry}{N^2}\right)}{\sum_{N=1}^{N_{max}} N^2 \exp\left(\frac{h_p c}{kT} \frac{Ry}{N^2}\right)}$$

where Ry is the Rydberg (109737 cm^{-1}) and N_{max} is the principal quantum number of the electronic state of hydrogen which will overlap that of an adjacent atom. For simplicity we took $N_{max} = 40$.

The absorption coefficient for free-bound radiation of hydrogen atoms is found from σ_H by using their number density n_H in the expression

$$k_H = \sigma_H n_H \left(1 - e^{-h_p c\omega/kT}\right) \ (cm^{-1}) \qquad (3\text{-}20)$$

For bound-free absorption of cesium, the cross-section can be approximated adequately by the quantum defect method, which we treat as a perturbation.

The quantum defect method defines the energy level of an electronic state below the ionization level in terms of a modified principal quantum number. This modified quantum number is denoted by n^* and is found to be related to the principal quantum number by a defect δ_ℓ as

$$n^* = n - \delta_\ell$$

Where δ_ℓ is only a function of the angular momentum quantum number, ℓ. For cesium values of δ_ℓ are given in Table 3-5, taken from Ref. 29.

The energy for ionization from an electronic state is then given by

$$\omega_{n\ell} = Ry/(n - \delta_\ell)^2$$

The ionization from the ground electronic state ($n = 6$, $\ell = 0$) is then

$$\omega_{60} = Ry/(1.87)^2 = 0.287\ Ry$$

and the electronic partition function becomes

$$Q_{e\ell} = \sum_{\ell=o}^{5} \sum_{n > n_\ell}^{n_{max},\ell} 2(2\ell + 1)\ \exp\left[-\frac{h_p c}{kT}\ (0.286\ Ry - \omega_{n\ell})\right]$$

where n_ℓ is also given in Table 3.5 as is the upper limit on n, $n_{max,\ell}$.

The bound-free cross-section for each electronic state, (n,ℓ) is then given in the same way as for hydrogen (we performed some reduction of the expression), and is given by

$$\sigma_{n,\ell} = 7.9 \text{ E-18} \quad n^*_{n,\ell} \left(\frac{\omega_{n,\ell}}{\omega}\right)^3$$

$$\equiv 7.9 \text{ E-18} \quad \left(\frac{Ry}{\omega}\right)^3 \quad \frac{1}{(n-\delta_\ell)^5}$$

except that for the ground electronic state ($n=6$, $\ell=0$) we do not allow $\sigma(6,0)$ to be greater than 2 E-18. This then allows acceptable agreement with the limited data of Allen, Ref. 30.

The total cross-section for bound-free absorption by neutral cesium is then

$$\sigma_{Cs} = \sum_{\ell=o}^{5} \sum_{n> n_\ell}^{n_{max,\ell}} \frac{2(2\ell + 1)\ \sigma_{n,\ell}\ \exp\left[-\frac{h_p c}{kT}\ (0.286\ Ry - \omega_{n,\ell})\right]}{Q_{e\ell}}$$

$$\omega > \omega_{n,\ell}$$

and the absorption coefficient is related to the cesium number density n_{Cs} by

$$k_{Cs} = \sigma_{Cs}\ n_{Cs}\ (1 - e^{-h_p c\omega/kT})\ (cm^{-1}) \qquad (3\text{-}21)$$

TABLE 3-5

Quantum Defect Parameters for Cs (Ref. 29)

ℓ	δ_ℓ	n_ℓ	$n_{max,\ell}$
0	4.13	6	12
1	3.6	6	73
2	2.5	5	21
3	0	4	12
4	0	5	6
5	0	6	6

The bound-free absorption by negative hydrogen ions is important when cesium is present, because electrons provided by the cesium attach to the hydrogen atoms. The photo-detachment cross-section for this process is given in Ref. 31. We used this data as a table, given in Table 3-6. The cross-section σ_{HM} was interpolated linearly in this table, using $\log_{10} \omega$ and σ_{HM} as the variables. Then the absorption coefficient is related to the number density n_{HM} of negative hydrogen ions by

$$k_{HM} = \sigma_{HM}\, n_{HM} \left(1 - e^{-h_p c\omega/kT}\right) (cm^{-1}) \qquad (3\text{-}22)$$

TABLE 3-6

Cross-Section for Photo-Detachment of H^- (Ref. 31)

ω (cm^{-1})	$\sigma_{HM} \times 10^{17}$ (cm^2)
1000	0
6050	0
6250	0.3
6670	1.0
7140	1.59
8330	3.4
9090	4.0
10000	4.3
11110	4.4
12500	4.4
14300	4.3
16670	4.0
20000	3.3
25000	2.7
33330	1.9
50000	1.1
10000	0.3

Results

With the absorption coefficients k_i known for the various electronic radiation processes the spectral and total emissivities can be calculated from Eq. (3-16).

For pure hydrogen, we have considered six different processes; electron-ion, electron-H, and electron-H_2 Bremsstrahlung, H and H^- free-bound and molecular vibration. The corresponding absorption coefficients are given by Eqs. (3-17, 3-18, 3-19b, 3-20 and 3-22) for Bremsstrahlung and by Eqs. (3-12, 3-7a, 3-11, 3-13 and 3-15) for vibration. The six absorption coefficients are added to obtain Σk_i for use in Eq. (3-15).

The total emissivity ε for 100 atm, and ℓ = 30 cm is shown in Fig. 3-8 for T up to 10000K as the dashed curve. Also shown as the solid curve are the results of Olfe (Ref. 21, Fig. 16). The agreement is very good down to 2000K. Below there, Olfe's results are higher because he included a rotational contribution which we have neglected. However, the radiation below 2000K is very small because $\sigma T^4 = 5.67$ W/cm^2 at 1000K, so our error there is unimportant. Therefore, the comparison shown in Fig. 3-8 indicates our calculation for hydrogen radiation is quite satisfactory up to at least 10000K.

For pure cesium, we have three contributions to the absorption coefficient: electron-ion and electron-Cs Bremsstrahlung and Cs free-bound. They are given by Eqs. (3-17, 3-19a, 3-21). These three are added to give Σk_i in Eq. (3-15). To assess the importance of cesium as a radiator, we first plot the normalized blackbody function $B_\omega/\sigma T^4$ in Fig. 3-9 as a function of ω, for various values of T. Then, in Fig. 3-10, we show the absorption

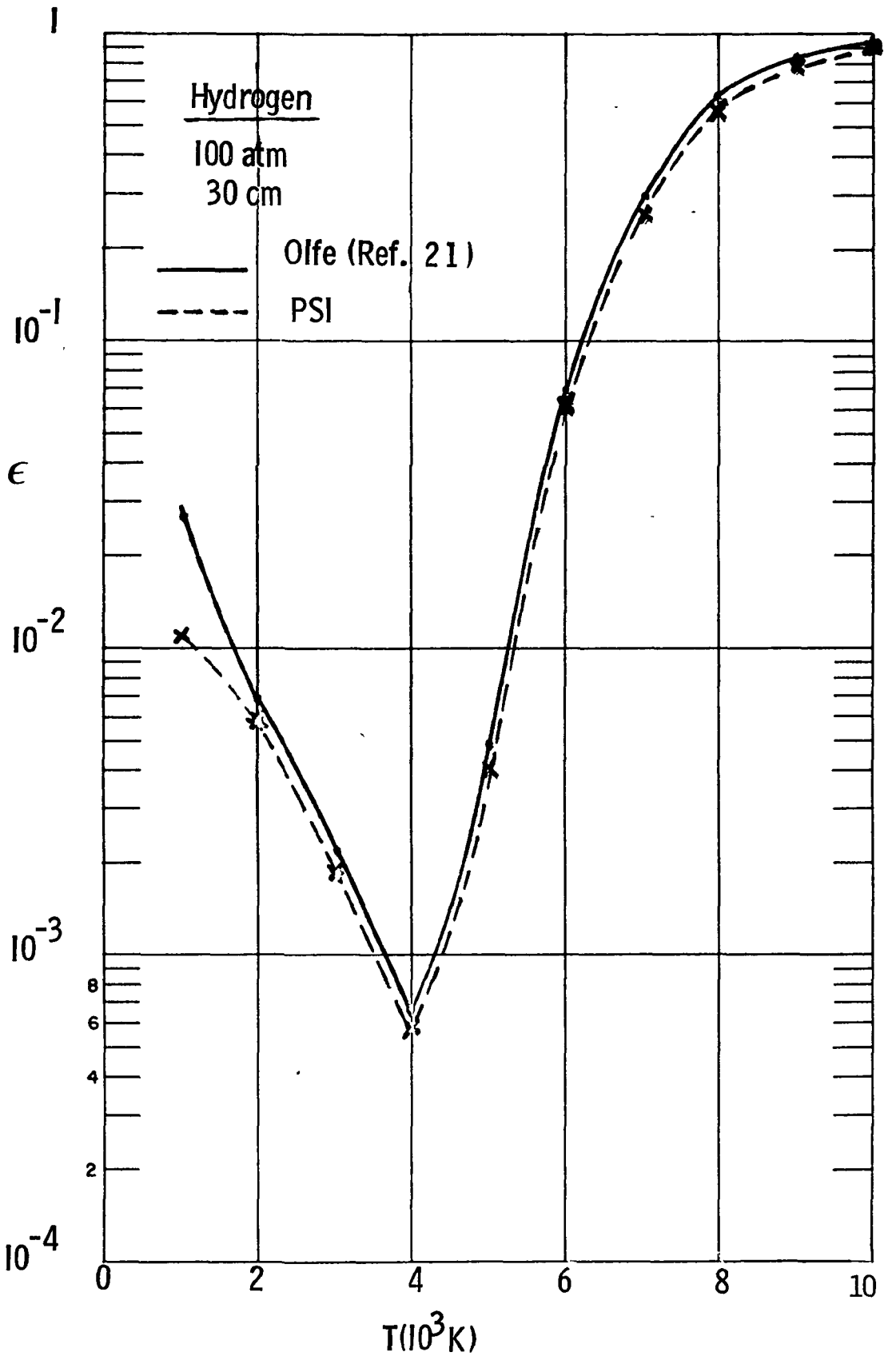

Fig. 3-8. Emissivity of Hydrogen for P=100 atm, ℓ=30 cm.

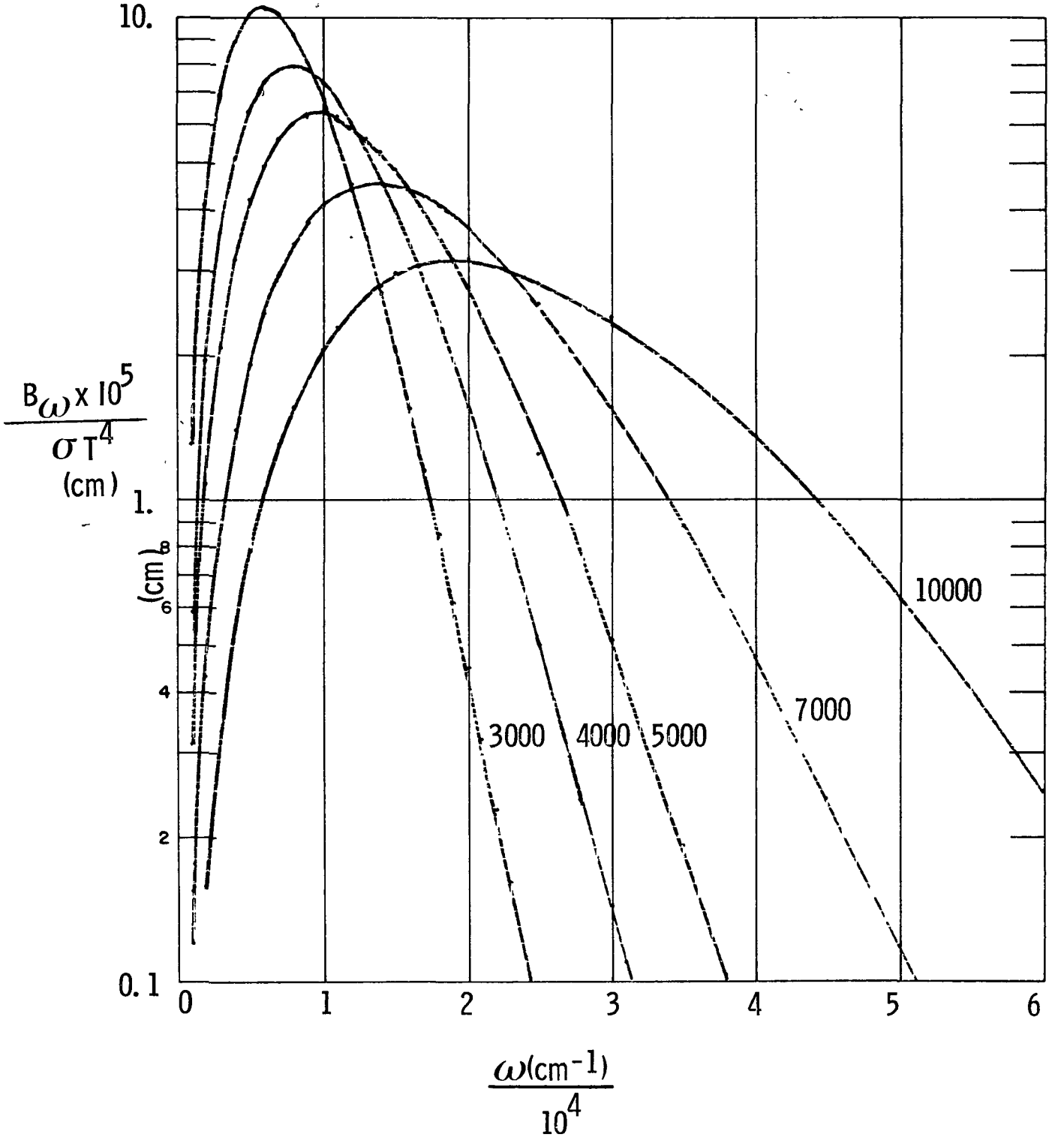

Fig. 3-9. Normalized Blackbody Spectral Function

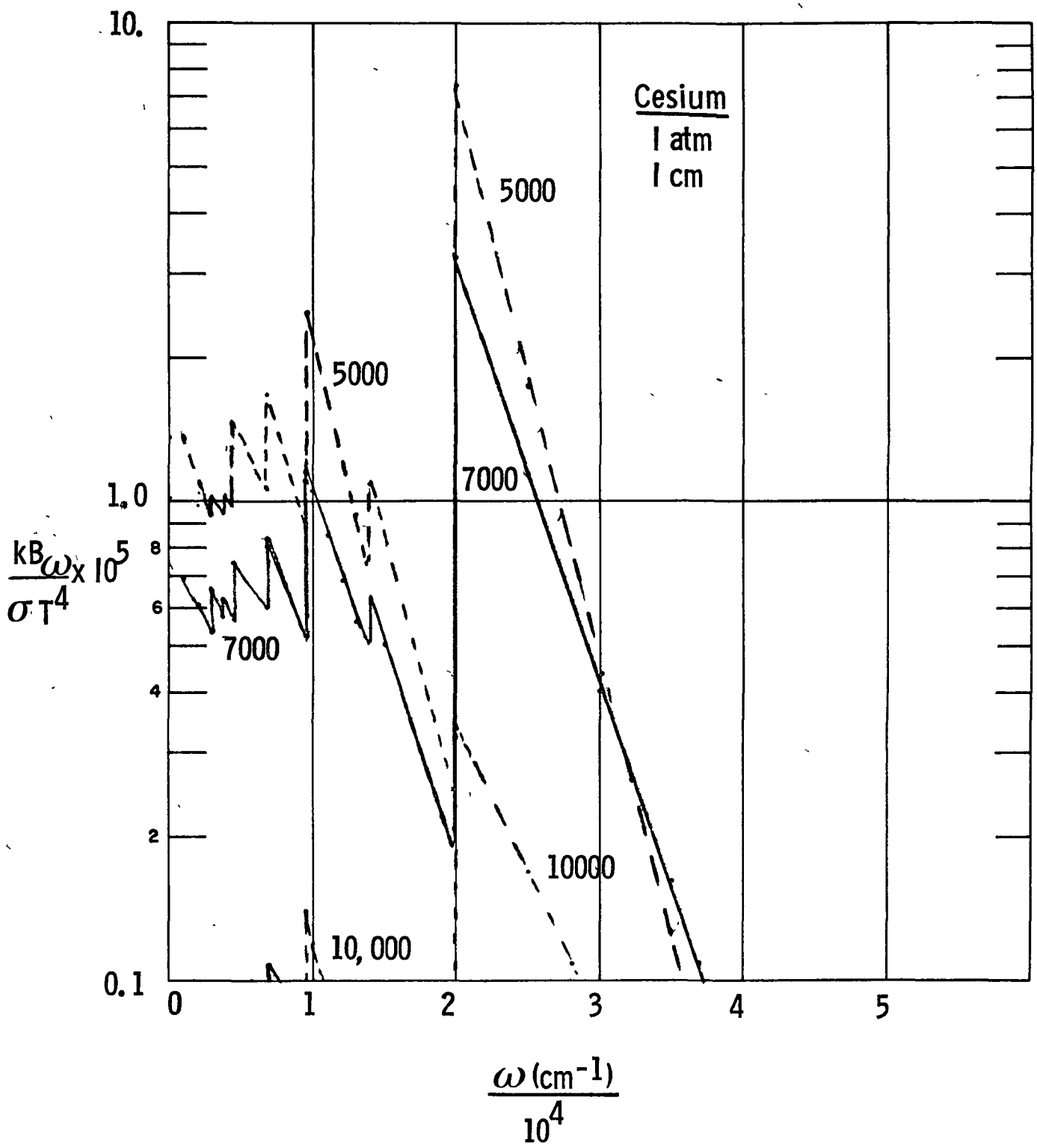

Fig. 3-10. Transparent Spectral Emissivity of Cesium for p = 1 atm, ℓ = 1 cm.

coefficient $k = \Sigma k_i$ times $B_\omega/\sigma T^4$ on the same scale for T = 5000, 7000 and 10000K. This is the spectral emissivity for ℓ small enough so that $k\ell$ is small compared to unity. These calculations are for 1 atm, which is the highest partial pressure of Cs we expect to deal with, since it corresponds to 1% cesium in 100 atm of hydrogen.

Comparison of Figs. 3-9 and 3-10 can give an indication of whether the radiation for any path length ℓ at any given wave number is black or transparent, or between those two limits. If the value on Fig. 3-10 exceeds the corresponding value on Fig. 3-9, then for ℓ = 1 cm, $k\ell > 1$, and the radiation is close to black. For example, this is the case for 5000K at 2E4 cm^{-1}. On the other hand, at 10000K, 1E4 cm^{-1} the value on Fig. 3-10 is much smaller than that on Fig. 3-9, showing that $k\ell<<1$ for ℓ = 1 cm. If ℓ = 10 cm, all the values on Fig. 3-10 must be raised by a factor of 10 to yield $k\ell B_\omega/\sigma T^4$. Then most of the spectrum has $k\ell>1$, and the radiation will be mostly blackbody.

For the approximately cylindrical geometry of the thruster; the path length of importance is the radius (if the cylinder is not short and fat). This is the geometry appropriate to the continuously heated thruster. (If the cylinder is short and fat, as for an LSC wave, then radiation transport must also be included.)

We can conclude that for continuously heated thrusters of operational size (say 10 cm radius), high partial pressures of cesium will give considerable amounts of radiation, which must be taken into account. For laboratory-size thrusters (say 1 cm radius) this radiation will be less of a problem, though still strong in some spectral regions.

To see the effect of pressure and path length, we have used Eq. (3-15) to find the emissivity normal to the center of the base of a hemisphere of radius ℓ at different cesium pressures. The results are shown in Fig. 3-11, which corresponds for cesium to Figs. 3-1 through 3-4 for molecular radiation. For 1 atm pressure, the emissivities are in the 0.1 to 1 range for the longer lengths above 4000K, while for 0.1 atm, they are about a factor of 10 smaller. The highest value of $p\ell$ is only about 0.3 atm ft. on Fig. 3-10, and comparison with Figs. 3-1 through 3-4 shows how much stronger cesium radiates than the molecules considered there. The molecules are band radiators, with a few important bands at most, while the electrons produced by cesium lead to continuum radiation. This accounts for the greater importance of cesium as a radiator compared with the molecules considered here.

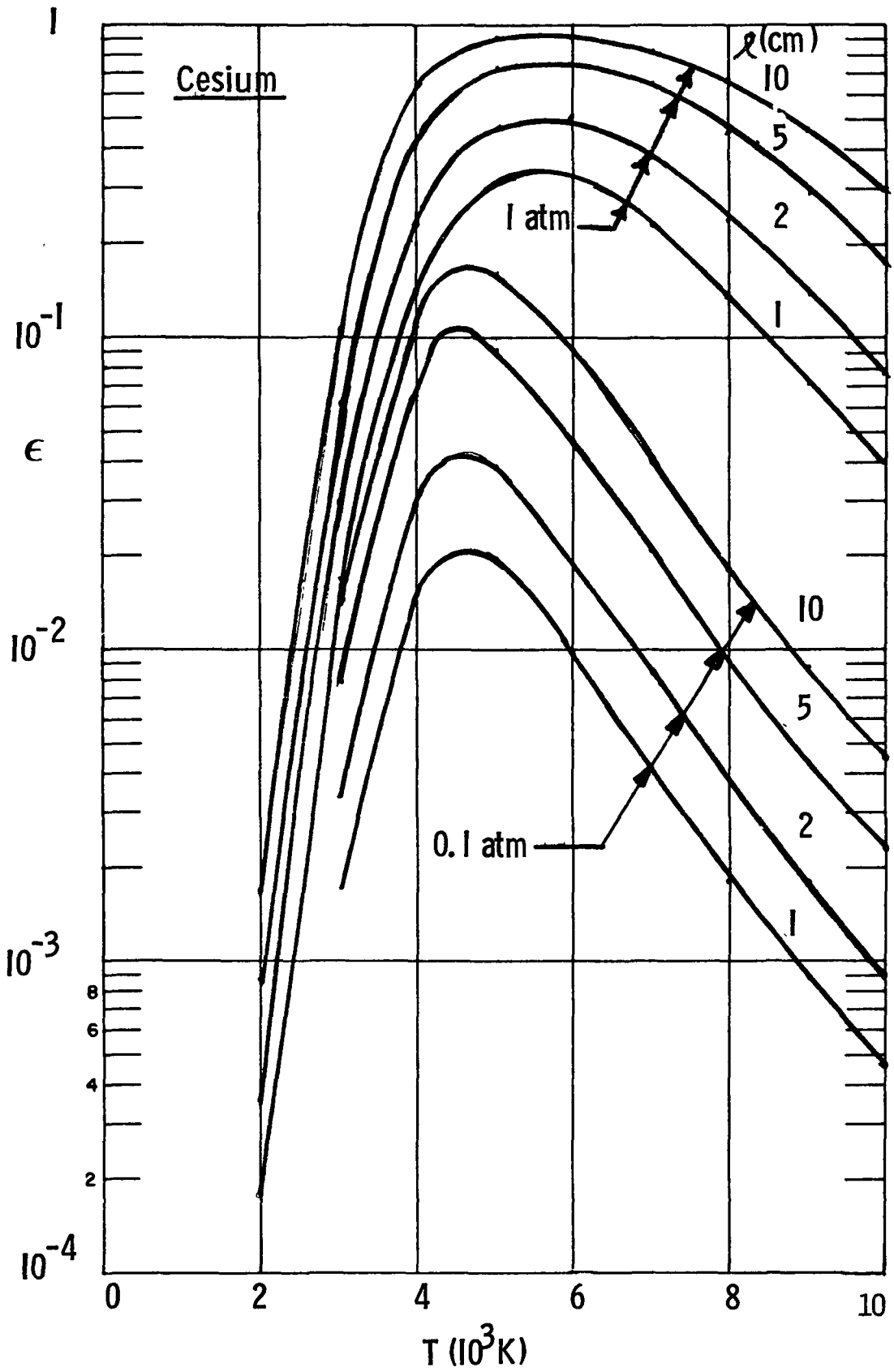

Fig. 3-11. Emissivity of Cesium

IV. THERMODYNAMIC AND TRANSPORT PROPERTIES OF EQUILIBRIUM SEEDED HYDROGEN*

The LSC wave model needs the thermodynamic and transport properties of seeded hydrogen to high temperatures (up to 20000 K or more). The standard equilibrium programs are based on the JANAF Tables and are limited to 6000 K. In the previous work on LSC waves in hydrogen (Ref. 4) a rather simple analytical model of the thermodynamic properties of equilibrium hydrogen was constructed, using molecules, atoms, first ions and electrons. It included vibration-rotation coupling of the molecules, lowering of the ionization potential, and a calculated cut-off for the electronic partition function of the atom. The results were shown in Ref. 4 to be in very good agreement with the elaborate calculations of Ref. 32. For transport properties, the results of Yos in Ref. 33 were utilized.

For seeded hydrogen the model of Ref. 4 has been extended to include a small amount of easily-ionizable alkali metal seed. In addition, the trace species H^- was added because of its importance as a radiator when a low temperature donor of electrons is present. This extended model provides the thermodynamic properties of seeded hydrogen. For the transport properties, the approach of Yos (Ref. 33) was followed with the addition of the seed species, and an update of the cross-section used.

In this section we shall present the models for the thermodynamic and transport properties and some results for a cesium seed, relying for background on Appendix A of Ref. 4. We shall see that the model of

---

* We have included the H^- species in this description even though its inclusion was accomplished after the period covered by this report.

cesium-seeded hydrogen is quite simple to use on a computer and gives quite good results, as far as they can be compared with other calculations. The thermal conductivity of cesium-seeded hydrogen does not differ noticeably from pure hydrogen, so that the difference in the values used here and those from Ref. 4-3 used in Ref. 4-1 are due only to improved values of cross-sections of the hydrogen species.

4.1 Equilibrium Composition

The reactions to be considered are the dissociation of hydrogen molecules, the ionization of the seed atom (denoted by S), the ionization of the hydrogen atom, and the detachment of electrones from H^-. This comprises four reactions among seven species, as follows:

$$H_2 \rightarrow 2H \qquad n_H^2/n_{H2} = K_D \tag{4-1a}$$

$$S \rightarrow S^+ + E \qquad n_E n_{SP}/n_S = K_S \tag{4-1b}$$

$$H \rightarrow H^+ + E \qquad n_E n_{HP}/n_H = K_I \tag{4-1c}$$

$$H^- \rightarrow H + E \qquad n_H n_E/n_{HM} = K_{HM} \tag{4-1d}$$

We have written the corresponding law of mass action to the right of each reaction, with n_i the number densities and K the equilibrium constant for each reaction, which will be defined later. The subscripts H2, H, HP, E, S, SP, HM denote the seven species: hydrogen molecule, atom, first ion, electron, seed atom, seed first ion and hydrogen negative ion. There are seven variables in these four equations, for fixed pressure and temperature.

There are three additional relations which make the solution for the n_i a determinate problem. They are the conservation of charge

$$n_E = n_{HP} + n_{SP} - n_{HM} \tag{4-2a}$$

the specified ratio of seed to hydrogen atoms

$$f = (n_S + n_{SP})/(2n_{H2} + n_H + n_{HP} + n_{HM}) \tag{4-2b}$$

and the pressure

$$p = nkT, \quad n = n_{H2} + n_H + n_{HP} + n_S + n_{SP} + n_{HM} + n_E$$

$$= n_{H2} + n_H + n_S + 2n_{HP} + 2n_{SP} \tag{4-2c}$$

For given p, T, f these 7 relations (4-1a,b,c,d) and (4-2a,b,c) determine the solution for the seven n_i.

The complete solution is quite complex, and we will follow the approach used successfully for pure hydrogen in Ref. 4 by solving simpler problems in each of two regions $T < T^*$ and $T > T^*$ where in degrees K,

$$T^* = 2000 \log_{10} p \text{ (atm)} + 7000 \tag{4-3}$$

In the low temperature region H_2 and H are the main species and the rest are trace species, while in the high temperature region H, H^+ and E are the major species. In both regions the seed is a trace, so we are restricted to seed fractions of a few precent or less, which is adequate for providing laser energy absorption in laser-heated thrusters.

Low Temperature Composition: $T < T^*$

Here the main species are H_2 and H, so that reaction (4-1a) is the principal one. We introduce the number of pairs of H and the associated pressure by

$$n'_o = n_{H2} + n_H/2, \quad p'_H = kT\,(n_{H2} + n_H) = kTn'_o\,(1 + n_H/2n'_o) \quad (4\text{-}4)$$

Then Eq. (4-1a) can be written as

$$\left(\frac{n_H}{2n'_o}\right)^2 = \frac{K_D}{4n'_o}\left(1 - \frac{n_H}{2n'_o}\right) = \frac{K_D\,kT}{4p'_H}\left[1 - \left(\frac{n_H}{2n'_o}\right)^2\right]$$

which provides a solution for n_H as

$$\frac{n_H}{2n'_o} = \left[1 + \frac{4p'_H}{K_D kT}\right]^{-\frac{1}{2}} \quad (4\text{-}5)$$

An equation for n_S is obtained from Eq. (4-2b) by substituting n'_o from (4-4), to get

$$n_S = 2n'_o f + (n_{HP} + n_{HM})\,f - n_{SP} \quad (4\text{-}6)$$

When this is put into Eq. (4-1b), together with Eq. (4-2a) for n_E, a quadratic equation for n_{SP} results, whose solution is

$$n_{SP} = -\frac{1}{2}(K_S + n_{HP} - n_{HM}) + \left[\frac{1}{4}(K_S + n_{HP} - n_{HM})^2 + K_S f\,(2n'_o + n_{HP} + n_{HM})\right]^{\frac{1}{2}} \quad (4\text{-}7)$$

Similar use of Eq. (4-2a) in Eqs. (41c and d) yields from the former a quadratic for n_{HP} whose solution is

$$n_{HP} = -\frac{1}{2}(n_{SP} - n_{HM}) + \left[\frac{1}{4}(n_{SP} - n_{HM})^2 + K_I n_H\right]^{\frac{1}{2}} \quad (4\text{-}8)$$

and from the latter

$$n_{HM} = (n_{SP} + n_{HP})\, n_H / (K_{HM} + n_H) \tag{4-9}$$

Finally, n_{H2} is related to n_H by n_o' from Eq. (4-4) as

$$n_{H2}/n_o' = 1 - n_H/2n_o' \tag{4-10}$$

Since n_{HP} and n_{HM} are small in this low temperature region, an iterative procedure is used to solve for the n_i in the following manner:

1) Guess p_H' from the given pressure p by ignoring all dissociation and ionization in Eqs. (4-2b,c) so that

$$p_H' = p/(1 + 2f)$$

2) Find $n_H/2n_o'$ from Eq. (4-5), n_o' from p_H' in Eq. (4-4), and n_H and n_{H2}, the latter from Eq. (4-10).

3) Assume n_{HP} and n_{HM} negligible in Eq. (4-7) and find n_{SP}.

4) Assume n_{HP} negligible in Eq. (4-9) and find n_{HM}.

5) Find n_{HP} from Eq. (4-8).

6) Recalculate n_{SP} from Eq. (4-7).

7) Find n_S from Eq. (4-2b).

8) Find p_T from Eq. (4-2c) and compare with given p.

9) If p_T is not close enough to p, re-guess p_H' as $p_H' p/p_T$ and repeat steps (1) - (8) until p_T agrees satisfactorily with p.

This process converges in a few iterations to a set of n_i, with n_E given by Eq. (4-2a).

High Temperature Composition: $T > T^*$

Here the main species are H, H^+ and E so that reaction (4-1c) is the principal one. We introduce the number of H nuclei and the associated pressure by

$$2n_o'' = n_H + n_{HP},\quad p_H'' = kT\,(n_H + 2n_{HP}) = 2kTn_o''\,(1 + n_{HP}/2n_o'') \tag{4-11}$$

By using Eq. (4-2a) to eliminate n_E from Eq. (4-1c), replacing n_H by n_o'', and introducing p_H'' from Eq. (4-11), we get

$$\left(\frac{n_{HP}}{2n_o''}\right)^2 \left[1 + \frac{K_I kT}{p_H''}\right] + \frac{n_{SP} - n_{HM}}{2n_o''}\,\frac{n_{HP}}{2n_o''} - \frac{K_I kT}{p_H''} = 0 \tag{4-12}$$

A similar relation for n_{SP} is obtained from Eq. (4-1b). We first use Eq. (4-2a) to eliminate n_E and Eq. (4-2b) to eliminate n_S in favor of f and n_o''. Then we introduce

$$p_S'' = 2kTn_o''\,(f + n_{SP}/2n_o'') \tag{4-13}$$

and Eq. (4-1b) can finally be written

$$\left(\frac{n_{SP}}{2n_o''}\right)^2 \left[1 + \frac{K_s kT}{p_s''}\right] + \frac{n_{SP}}{2n_o''}\,\frac{(n_{HP} - n_{HM})}{2n_o''} - \frac{K_s kTf^2}{p_s''} - K_s f\,\frac{(2n_{H2} + n_{HM})}{(2n_o'')^2} = 0 \tag{4-14}$$

We now have two equations (4-12) and (4-14) for n_{HP} and n_{SP}. The equation for n_{HM} has already been expressed in Eq. (4-9) from reaction (4-1d); from Eq. (4-1a) with the use of Eqs. (4-11) we find

$$\frac{n_{H2}}{2n''_o} = \frac{(1 - n_{HP}/2n''_o)^2}{1 + n_{HP}/2n''_o} \frac{p''_H}{K_D kT}, \quad \frac{n_H}{2n''_o} = 1 - \frac{n_{HP}}{2n''_o} \tag{4-15}$$

The pressure, from Eq. (4-2b, c), can be expressed as

$$p = p''_H + p''_S + kT\,(1 + 2f)\,n_{H2} + kTfn_{HM} \tag{4-16}$$

To obtain the n_i from this set of relations we must first solve the simultaneous equations (4-12) and (4-14) for $n_{HP}/2n''_o$. They are of the form

$$a_1 x_1^2 + x_1 x_2 - b_1 = 0$$

$$a_2 x_2^2 + x_1 x_2 - b_2 = 0$$

These can be put into the form of a quadratic for x_1/x_2:

$$\frac{x_1}{x_2} = -\frac{(b_2 - b_1)}{2b_2 a_1} \sqrt{\left(\frac{b_2 - b_1}{2b_2 a_1}\right)^2 + \frac{a_2 b_1}{a_1 b_2}} \tag{4-17a}$$

which yields the solutions

$$x_1 = \sqrt{\frac{b_1}{a_1 + 1/(x_1/x_2)}}, \quad x_2 = \frac{x_1}{x_1/x_2} \tag{4-17b}$$

With these, we can now set up a procedure for finding the n_i.

1) Guess p''_H from given pressure p by ignoring all dissociation and ionization in Eqs. (4-2b,c) so that

$$p''_H = p/(1 + 2f)$$

2) Guess $p''_S = p - p''_H$

3) Solve for $n_{HP}/2n''_o = x_1$, $n_{SP}/2n''_o = x_2$ from Eqs. (4-17) with $n_{H2} = n_{HM} = 0$, so that

$$a_1 = 1 + K_I kT/p''_H \quad , \quad b_1 = K_I kT/p''_H$$

$$a_2 = 1 + K_S kT/p''_S \quad , \quad b_2 = K_S kTf^2/p''_S$$

4) Find $n_{H2}/2n''_o$ and $n_H/2n''_o$ from Eq. (4-15)

5) Find n''_o from Eq. (4-11)

6) Find n_{H2}, n_H, n_{HP}, n_{SP} using n''_o

7) Find n_{HM} from Eq. (4-9)

8) Repeat steps (3) - (7) with the same a_1 and a_2, but

$$b_1 = \frac{K_I kT}{p''_H} + \frac{n_{HM}}{2n''_o}\,\frac{n_{HP}}{2n''_o} ,$$

$$b_2 = \frac{K_S kTf^2}{p''_S} + \frac{K_S f}{2n''_o}\left(\frac{2n_{H2}}{2n''_o} + \frac{n_{HM}}{2n''_o}\right) + \frac{n_{SP}}{2n''_o}\,\frac{n_{HM}}{2n''_o}$$

9) Find n_S from Eq. (4-2b)

10) Find p_T from Eq. (4-2c) and compare with given p

11) If p_T is not close enough to p, re-guess p''_H as $p''_H p/p_T$ and repeat steps (2) - (10) until p_T agrees satisfactorily with p.

This process converges in a few iterations to a set of n_i, with n_E given by Eq. (4-2a).

4.2 Thermodynamic Properties

The properties of hydrogen were defined in Ref. 4 using the same low temperature - high temperature approximation used here. To find the properties of seeded hydrogen, those properties can be modified rather easily to include the seed.

The density, for example, is defined as

$$\rho = \sum m_i n_i$$

where m_i is the mass of the ith species. The part of the sum over the hydrogenic species was calculated in Ref. 4, and may be called ρ^H. To this we must add the contribution of the seed species n_S and n_{SP} (ignoring the small mass of the electrons), which is

$$\begin{aligned}(n_S + n_{SP})m_S &= (n_S + n_{SP})\ (m_S/m_H)\ \rho^H/(2n_{H2} + n_H + n_{HP} + n_{HM}) \\ &= f(m_S/m_H)\rho^H\end{aligned}$$

Thus we see that

$$\rho = \rho^H + \rho^S = \rho^H\ (1 + m_S/m_H) = \rho^H\ (1 + f\ M_S) \qquad (4\text{-}18)$$

where M_S is the molecular weight of the seed, and f is the seed to H ratio, as defined in Eq. (4-2b).

The enthalpy of the mixture is also a sum over species where h_i is the enthalpy of a given species and $\rho_i = m_i n_i$ is the mass density of that species. Then

$$\rho h = \sum \rho_i h_i = \sum_{\text{hydrogen}} \rho_i h_i + \sum_{\text{seed}} \rho_i h_i \qquad (4\text{-}19)$$

We may write this, using Eq. (4-18), as

$$h = \frac{\rho^H}{\rho}(h^H + h^S) = \frac{h^H + h^S}{1 + M_S f} \tag{4-20a}$$

where the first term is the hydrogen contribution and the second is the seed contribution

$$h^H = \sum_{\text{hydrogen}} \rho_i h_i / \rho^H, \qquad h^S = \sum_{\text{seed}} \rho_i h_i / \rho^H \tag{4-20b}$$

The pure hydrogen contribution has been given in Ref. 4, Appendix A. With the present notation it is

$$h^H = \frac{5kT}{2m_H}\left[(0.7 + 0.2\,\psi_v)\frac{n_{H2}}{n_o} + \left(1 + 0.2\frac{\theta_D}{T} + 0.4\frac{\theta_{IL}}{T}\left(1 - \frac{S_2}{S_1}\right)\right)\frac{n_H}{2n_o}\right.$$
$$\left. + \left(2 + 0.2\frac{\theta_D}{T} + 0.4\frac{\theta_{IL}}{T}\right)\frac{n_{HP}}{2n_o}\right] \tag{4-21}$$

Here, the dissociation temperature, θ_D, lowered ionization temperature θ_{IL}, vibrational enthalpy function ψ_v, original number of hydrogen molecules n_o, and hydrogen atom electronic partition function sums S_1 and S_2 are

$$\theta_D = \frac{h^o_D m_{H2}}{k}, \quad \theta_{IL} = \frac{h^o_{IL} m_H}{k}, \quad \psi_v = \frac{\theta_v/T}{e^{\theta_v/T} - 1}$$

$$\theta_v = 5978\text{K}, \quad n_o = n_{H2} + (n_H + n_{HP})/2 \tag{4-22}$$

$$S_i = \sum_{j=1}^{L} j^2 \exp\,(\theta_{IL}/T^2 j^2), \quad S_2 = \sum_{j=1}^{L} \exp\,(\theta_{IL}/T^2 j^2)$$

The species H^- was not included in Ref. 4. Although it is included in the composition here because of its importance in radiation, it is a minor species and its contribution to the enthalpy and specific heat will be ignored. Such an approximation was found excellent for pure hydrogen in Ref. 4.

We can construct the seed contribution to the enthalpy in a similar manner. For each species there is a translational contribution $5kT/2m_i$. For atoms and ions there can be an additional electronic contribution $h_{e\ell}$ and for ions, their ionization energy per unit mass h^o_{IS}. The electronic contribution is expressed in terms of an electronic partition function $Q_{e\ell}$ as

$$h_{e\ell} = \frac{kT^2}{m} \frac{\partial \ell n Q_{e\ell}}{\partial T} \tag{4-23a}$$

where $Q_{e\ell}$ is a sum over states with energy ε_j and weight g_j:

$$Q_{e\ell} = \sum_{j=0} g_j e^{-\varepsilon_j/kT}, \quad \frac{\partial \ell n Q_{e\ell}}{\partial T} = \frac{\sum_{j=0} \varepsilon_j g_j e^{-\varepsilon_j/kT}}{Q_{e\ell} kT^2}$$

so that

$$h_{e\ell} = \frac{\sum_{j=0} \varepsilon_j g_j e^{-\varepsilon_j/kT}}{m Q_{e\ell}} \tag{4-23b}$$

The enthalpies then are

$$h_E = 5kT/2m_E \tag{4-24a}$$

$$h_S = 5kT/2m_S + h_{e\ell S} \tag{4-24b}$$

$$h_{SP} = 5kT/2m_S + h_{e\ell SP} + h^o_{IS} \tag{4-24c}$$

When put into the second sum in Eq. (4-20b) the masses cancel, and we have

$$\sum_{\text{seed}} \rho_i h_i = \frac{5kT}{2}(n_S + 2n_{SP}) + n_S m_S h_{e\ell S} + n_{SP} m_S (h_{e\ell SP} + h^o_{IS})$$

The factor 2 multiplying n_{SP} includes the contribution of the electrons from the seed. Note that for many seeds the electronic contribution to the ion enthalpy is negligible because the excited state energies ε_i are very large. The density of the hydrogen is $\rho^H = 2n_o m_H$, with n_o defined in Eq. (4-22), so Eq. (4-20b) yields

$$h^S = \frac{5kT}{2m_H}\left[\frac{n_S}{2n_o} + \frac{2n_{SP}}{2n_o} + 0.4\,\frac{n_S}{2n_o}\,\frac{m_S h_{e\ell S}}{kT} + 0.4\,\frac{n_{SP}}{2n_o}\,\frac{m_S(h_{e\ell SP}+h^o_{IS})}{kT}\right] \tag{4-25}$$

The specific heat of the mixture is obtained from

$$c_p = \left(\frac{\partial h}{\partial T}\right)_p = \frac{1}{1 + M_S f}\left[\left(\frac{\partial h^H}{\partial T}\right)_p + \left(\frac{\partial h^S}{\partial T}\right)_p\right] \tag{4-26}$$

obtained by differentiating Eq. (4-20a), where h^H and h^S are given in Eqs. (4-21) and (4-25).

Actually, the low-temperature, high-temperature approximation permits some simplification because for the hydrogen only the species H_2 and H, or H and H^+ appear, so that only two of the three terms in Eq. (4-21) are needed at any one time. The same is true of the derivatives of the n_i, which are needed for c_p.

Low Temperature Properties: $T < T^*$

Here the species H^+ is ignored ($n_{HP} = 0$) so the hydrogen enthalpy from Eq. (4-21) becomes

$$h^H = \frac{5kT}{2m_H}\left[(0.7 + 0.2\psi_v)\ \frac{n_{H2}}{n_o} + \left(1 + 0.2\ \frac{\theta_D}{T}\right)\frac{n_H}{2n_o}\right] \qquad (4\text{-}27)$$

The term $1 - S_2/S_1$ is ignored because the first terms in the sums are equal, and they dominate at low temperatures. There is no corresponding simplification for h^S, except that for most seeds the term $h_{e\ell SP}$ is negligible in Eq. (4-25).

The species ratios n_i/n_o have already been given in the previous subsection, where n_o was called n_o' for the low temperature approximation. For c_p, the derivatives of n_i/n_o are needed; without H^- they can be given by a simplified version of the procedure outlined above for n_i/n_o, as follows.

The two reactions occurring here are (4-1a) and (4-1b). With only electrons from the seed, not from the hydrogen, these are

$$n_H^2 = K_D n_{H2} \quad , \quad n_{SP}^2 = K_S n_S \qquad (4\text{-}28)$$

The original number of H_2 molecules, and the seed fraction from Eq. (4-2b) are

$$n_o = n_{H2} + n_H/2 \ , \quad f = (n_S + n_{SP})/2n_o \qquad (4\text{-}29)$$

while Eq. (4-2c) shows the pressure to be

$$p = kT\ (n_{H2} + n_H + n_S + 2n_{SP}) = n_o kT\left(1 + n_H/2n_o + f + n_{SP}/n_o\right) \qquad (4\text{-}30)$$

We can solve Eq. (4-29) for n_{H2} and n_S as

$$\frac{n_{H2}}{n_o} = 1 - \frac{n_H}{2n_o}, \quad \frac{n_S}{2n_o} = f - \frac{n_{SP}}{2n_o} \tag{4-31}$$

and put them into Eq. (4-28) to get

$$\left(\frac{n_H}{2n_o}\right)^2 = \frac{K_D}{4n_o}\left(1 - \frac{n_H}{2n_o}\right), \quad \left(\frac{n_{SP}}{2n_o}\right)^2 = \frac{K_S}{2n_o}\left(f - \frac{n_{SP}}{2n_o}\right)$$

By using Eq. (4-30) to eliminate the first n_o on the right we find

$$\left(\frac{n_H}{2n_o}\right)^2\left[\frac{4p}{K_D kT} + 1\right] = 1 + 2\left(1 - \frac{n_H}{2n_o}\right)\left(f + \frac{n_{SP}}{2n_o}\right)$$

$$\left(\frac{n_{SP}}{2n_o}\right)^2\left[\frac{p}{K_S kT} + 1\right] = f^2 + \frac{1}{2}\left(1 + \frac{n_H}{2n_o}\right)\left(f - \frac{n_{SP}}{2n_o}\right)$$

We can now differentiate with respect to T at constant p, remembering that K_D and K_S are functions of T (to be given later). The result is two linear simultaneous equations for the derivatives of $n_H/2n_o$ and $n_{SP}/2n_o$, which are needed for c_p. These equations are

$$\left[2\frac{n_H}{2n_o}\left(\frac{4p}{K_D kT} + 1\right) + 2\left(f + \frac{n_{SP}}{2n_o}\right)\right]\left(\frac{\partial}{\partial T}\frac{n_H}{2n_o}\right)_p$$

$$-2\left(1 - \frac{n_H}{2n_o}\right)\left(\frac{\partial}{\partial T}\frac{n_{SP}}{2n_o}\right)_p = \left(\frac{n_H}{2n_o}\right)^2 \frac{4p}{K_D kT}\,\frac{d\ln K_D T}{dT} \tag{4-32a}$$

$$-\frac{1}{2}\left(f-\frac{n_{SP}}{2n_o}\right)\left(\frac{\partial}{\partial T}\ \frac{n_H}{2n_o}\right)_p+\left[2\,\frac{n_{SP}}{2n_o}\left(\frac{p}{K_S kT}+1\right)+\frac{1}{2}\left(1+\frac{n_H}{2n_o}\right)\right]\ \left(\frac{\partial}{\partial T}\ \frac{n_{SP}}{2n_o}\right)_p$$

$$=\left(\frac{n_{SP}}{2n_o}\right)^2\frac{p}{K_S kT}\ \ \frac{d\ln K_S T}{dT} \qquad (4\text{-}32b)$$

The solution of these two equations gives the necessary derivatives. The other derivatives of n_H/n_o and $n_S/2n_o$ are found from Eq. (4-31) as

$$\left(\frac{\partial}{\partial T}\ \frac{n_{H2}}{n_o}\right)_p=-\left(\frac{\partial}{\partial T}\ \frac{n_H}{2n_o}\right)_p\qquad\left(\frac{\partial}{\partial T}\ \frac{n_S}{2n_o}\right)_p=-\left(\frac{\partial}{\partial T}\ \frac{n_{SP}}{2n_o}\right)_p \qquad (4\text{-}33)$$

Using Eqs. (4-31) and (4-33), the derivatives of h^H and h^S may be written from Eqs. (4-27) and (4-25) as

$$\left(\frac{\partial h^H}{\partial T}\right)_p=\frac{5k}{2m_H}\left[(0.7+0.2\,\Phi_v)\left(1-\frac{n_H}{2n_o}\right)+\frac{n_H}{2n_o}+\left(0.3+0.2\,\frac{\theta_D}{T}-0.2\,\psi_v\right)T\left(\frac{\partial}{\partial T}\ \frac{n_H}{2n_o}\right)\right]_p \qquad (4\text{-}34a)$$

$$\left(\frac{\partial h^S}{\partial T}\right)_p=\frac{5k}{2m_H}\left[f+\frac{n_{SP}}{2n_o}+\left(f-\frac{n_{SP}}{2n_o}\right)\left(\frac{d}{dT}\,\frac{m_s h_{el\,S}}{k}\right)+\frac{n_{SP}}{2n_o}\left(\frac{d}{dT}\,\frac{m_s h_{el\,SP}}{k}\right)+\left(1+\frac{m_\varepsilon}{kT}\left(h_{el\,SP}-h_{el\,S}\right)+\frac{\theta_{IS}}{T}\right)T\left(\frac{\partial}{\partial T}\,\frac{n_{SP}}{2n_o}\right)\right]_p \qquad (4\text{-}34b)$$

Here we have defined

$$\theta_{IS} = m_S h_I^o/k \text{ and } \phi_v = d\psi_v T/dT = \psi_v^2 \, e^{\theta v/T} \tag{4-35a}$$

and the derivative of $h_{e\ell}$ is found from Eq. (4-23b) to be

$$\frac{d}{dT}\frac{mh_{e\ell}}{k} = \frac{-1}{Q_{e\ell}^2 T^2}\left[\left(\sum_{j=0}\frac{\varepsilon_j g_j}{k} e^{-\varepsilon_j/kT}\right)^2 - Q_{e\ell}\sum_{j=0}\frac{\varepsilon_j^2 g_j}{k^2} e^{-\varepsilon_j/kT}\right] \tag{4-35b}$$

When the solutions of Eq. (4-3a) are inserted into Eq. (4-34), the expression for c_p follows immediately from Eq. (4-26), and h is found by putting Eqs. (4-27) and (4-25) into Eq. (4-20a).

High-Temperature Properties: $T > T^*$

A similar procedure is used here, where there are no H_2 species. The hydrogen enthalpy, Eq. (4-21), is

$$h^H = \frac{5kT}{2m_H}\left[\left[1 + 0.2\frac{\theta_D}{T} + 0.4\frac{\theta_{I_2}}{T}\left(1 - \frac{S_2}{S_1}\right)\right]\frac{n_H}{2n_o} + \left(2 + 0.2\frac{\theta_D}{T} + 0.4\frac{\theta_{IL}}{T}\right)\frac{n_{HP}}{2n_o}\right] \tag{4-36}$$

The reactions occurring are now (4-1b) and (4-1c). The conservation requires $n_E = n_{HP} + n_{SP}$, ignoring the H^- species, so the reaction equations may be written

$$(n_{HP} + n_{SP})\, n_{HP} = K_I\, n_H, \quad (n_{HP} + n_{SP})\, n_{SP} = K_S\, n_S \tag{4-37}$$

In this regime

$$n_o = (n_H + n_{HP})/2, \qquad f = (n_S + n_{SP})/2n_o$$

$$p = kT\,(n_H + 2\,n_{HP} + n_S + 2n_{SP}) = 2\,n_o kT\,(1 + n_{HP}/2n_o + f + n_{SP}/2n_o) \quad (4\text{-}38)$$

so that

$$\frac{n_H}{2n_o} = 1 - \frac{n_{HP}}{2n_o}, \qquad \frac{n_S}{2n_o} = f - \frac{n_{SP}}{2n_o} \quad (4\text{-}39)$$

The reactions, Eqs. (4-37), become

$$\left(\frac{n_{HP}}{2n_o}\right)^2 + \frac{n_{HP}n_{SP}}{4n_o^2} = \frac{K_I}{2n_o}\left(1 - \frac{n_{HP}}{2n_o}\right)$$

$$\left(\frac{n_{SP}}{2n_o}\right)^2 + \frac{n_{HP}n_{SP}}{4n_o^2} = \frac{K_S}{2n_o}\left(f - \frac{n_{SP}}{2n_o}\right)$$

and elimination of the first n_o on the right in favor of the pressure from Eq. (4-38) yields

$$\left(\frac{n_{HP}}{2n_o}\right)^2\left[\frac{p}{K_I kT} + 1\right] + \frac{n_{HP}n_{SP}}{4n_o^2}\,\frac{p}{K_I kT} = 1 + \left(1 - \frac{n_{HP}}{2n_o}\right)\left(f + \frac{n_{SP}}{2n_o}\right)$$

$$\left(\frac{n_{SP}}{2n_o}\right)^2\left[\frac{p}{K_S kT} + 1\right] + \frac{n_{HP}n_{SP}}{4n_o^2}\,\frac{p}{K_S kT} = f^2 + \left(f - \frac{n_{SP}}{2n_o}\right)\left(1 + \frac{n_{HP}}{2n_o}\right)$$

The derivatives of these yield the two linear equations as

$$\left[\left(2\frac{n_{HP}}{2n_o}+\frac{n_{SP}}{2n_o}\right)\left(\frac{p}{K_I kT}+1\right)+f\right]\left(\frac{\partial}{\partial T}\frac{n_{HP}}{2n_o}\right)_p-\left[1-\left(\frac{p}{K_I kT}+1\right)\frac{n_{HP}}{2n_o}\right]\left(\frac{\partial}{\partial T}\frac{n_{SP}}{2n_o}\right)_p$$

(4-40a)

$$=\frac{n_{HP}}{2n_o}\left(\frac{n_{HP}}{2n_o}+\frac{n_{SP}}{2n_o}\right)\frac{p}{K_I kT}\frac{d\ell n\ K_I T}{dT}$$

$$-\left[f-\left(\frac{p}{K_S kT}+1\right)\frac{n_{SP}}{2n_o}\right]\left(\frac{\partial}{\partial T}\frac{n_{HP}}{2n_o}\right)_p+\left[\left(2\frac{n_{SP}}{2n_o}+\frac{n_{HP}}{2n_o}\right)\left(\frac{p}{K_S kT}+1\right)+1\right]\left(\frac{\partial}{\partial T}\frac{n_{SP}}{2n_o}\right)_p$$

(4-40b)

$$=\frac{n_{SP}}{2n_o}\left(\frac{n_{SP}}{2n_o}+\frac{n_{HP}}{2n_o}\right)\frac{p}{K_S kT}\frac{d\ell n\ K_S T}{dT}$$

The solution of these gives the derivatives needed for c_p, along with the derivative of Eq. (4-39), which is

$$\left(\frac{\partial}{\partial T}\frac{n_H}{2n_o}\right)_p=-\left(\frac{\partial}{\partial T}\frac{n_{HP}}{2n_o}\right)_p,\quad\left(\frac{\partial}{\partial T}\frac{n_S}{2n_o}\right)_p=-\left(\frac{\partial}{\partial T}\frac{n_{SP}}{2n_o}\right)_p \tag{4-41}$$

The derivative of h^H is found from Eq. (4-36), using Eqs. (4-39) and (4-41). The result is

$$\left(\frac{\partial h^H}{\partial T}\right)_p = \frac{5k}{2m_H}\left[1 + \frac{n_{HP}}{2n_o} + 0.4\,\frac{\theta_{IL}^2}{T^2}\left(1 - \frac{n_{HP}}{2n_o}\right)\left(\frac{S_4}{S_1} - \frac{S_2^2}{S_1^2}\right) + \left(1 + 0.4\,\frac{\theta_{IL}}{T}\,\frac{S_2}{S_1}\right) T\left(\frac{\partial}{\partial T}\,\frac{n_{HP}}{2n_o}\right)_p\right] \qquad (4\text{-}42)$$

where we define

$$S_4 = \sum_{j=1}^{L} j^{-2} \exp\left(\theta_{IL}/T^2 j^2\right) \qquad (4\text{-}43)$$

The expression for $(\partial\, h^S/\partial T)_p$ is the same as Eq. (4-34b) and need not be repeated.

Again the expression for c_p is given in Eq. (4-26), when the solution for the derivatives from Eqs. (4-40) are inserted in Eqs. (4-34b) and (4-42). The enthalpy is found by using Eqs. (4-25) and (4-36) in Eq. (4-20a).

Comparison of the results presented above with those given for pure hydrogen in Appendix A of Ref. 4 shows them to agree for no seed, f = 0 after correction of some misprints in Ref. 4. (In Eq. (A-27b) of that reference θ_I should be θ_{IL}, and in Eq. (A-29b), the first θ_{IL}/T should be $(\theta_{IL}/T)^2$). In the case of no seed, of course, the simultaneous equation pairs Eqs. (4-32) and Eqs. (4-40) reduce to single equations for the derivatives of $n_H/2n_o$ and $n_{HP}/2n_o$. These latter ratios are called β and α in Ref. 4.

4.3 Equilibrium Constants

The K_i quantities on the right side of Eq. (4-1) are the equilibrium constants for the reactions, which come from the law of mass action. For a reaction of the form

$$A \rightarrow B + C$$

this relates the partial pressure p_A, p_B, p_C to the temperature, the internal partition functions Q_i and the molecular masses.

$$\frac{p_B p_C}{p_A} = \left(\frac{2\pi}{k_P^2}\ \frac{m_B m_C}{m_A}\right)^{3/2} (kT)^{5/2}\ \frac{Q_{iB}\ Q_{iC}}{Q_{iA}}\ e^{-h_A^o\ m_A/kT} \equiv KkT \qquad (4\text{-}44)$$

Here h_p is Planck's constant, and h_A^o is the heat per unit mass of A to be supplied to produce B + C. The ratio on the left can be converted to $n_B n_C/n_A$ by merely changing the power of kT from 5/2 to 3/2, since $p_i = n_i kT$. This law of mass action can now be applied to each of the reactions (4-1) to find the appropriate K, which is the right side of the above expression divided by kT.

Hydrogen Dissociation: Reaction (4-1a)

Here $A = H_2$, $B = C = H$, and $h_A^o = h_D^o$. The internal partition function for H_2 is the product of the contributions of states due to electrons, $Q_{el\,H2}$, rotation, Q_r vibration Q_v, and vibration-rotation coupling, Q_c. Standard statistical mechanics gives these as

$$Q_{el\,H2} = 1\ ,\quad Q_r = T/2\theta_r,\quad \theta_r = 85.34,\quad Q_v = (1-e^{-\theta_v/T})^{-1}$$

$$Q_c = 1 + \frac{28.45}{T} + 1.785\ E\text{-}5T + \frac{5.04\ E\text{-}2}{e^{\theta_v/T}-1} + \frac{5.68\ E\text{-}2\ \theta_v/T}{(e^{\theta_v/T}-1)^2}$$

The first recognizes that the electronic states of H_2 are too high to be included (greater than 132,000K), so the ground-state statistical weight is used. The second is the fully-excited rotation form of Q_r, which is satisfactory for high temperature, since θ_r = 85.34F. The factor 2 accounts for the symmetry of the hydrogen molecule. The third expression is the vibration of a harmonic oscillator, θ_v = 5978K. The coupling expression Q_c comes from Ref. 34 p.163, Eq. (7.39), where it is given as $Q_{vjm} = Q_c\, Q_r\, Q_v$, and the constants are found from the spectroscopic constants for H_2, as explained in Ref. 4, Appendix A.

The only internal partition function for H is due to electronic states, and can be expressed as

$$Q_{e\ell H} = 2S_1\, e^{-\theta_{IL}/T}, \quad \theta_{IL} = h^o_{IL}\, m_H \Big/ k$$

where S_1 is the sum given in Eq. (4-22). The upper limit L of the sum S_1, (and of sums S_2 and S_4 defined in Eqs. (4-22) and (4-43) must be finite since the terms grow like j^2 for large j. Related to this is the fact that that energy h^o_{IL} in θ_{IL} is not the usual ionization energy h^o_I for hydrogen, but a lowered value. They are both associated with the pressure of free electrons in an ionized mixture. A description of how to calculate L and θ_{IL} from the number of electrons and θ_I= 157,900K is given in Appendix A of Ref. 4.

Finally, $h^o_D\, m_{H2}/k$ = 52,000K = θ_D. So the equilibrium constant K_D for the dissociation reaction is

$$K_D = \left(\frac{\pi m_H k}{h_P^2}\right)^{3/2} \frac{T^{3/2}\, Q^2_{e\ell H}}{Q_c\, Q_v\, Q_r}\, e^{-\theta_D/T} \qquad (4\text{-}45a)$$

$$\theta_D = h^o_D\, m_{H2}/k = 52{,}000\text{K}$$

The logarithmic derivative of $K_D T$ is needed for Eq. (4-32a), in the low temperature regime. We ignore the derivatives of Q_c and $Q_{e\ell H}$, and use Q_r and Q_v from Eq. (4-44).

The result is

$$\frac{d\ell n\ K_D T}{dT} = \frac{1}{T}\left(\frac{3}{2} - \psi_v + \frac{\theta_D}{T}\right) \qquad (4\text{-}45b)$$

Hydrogen Ionization: Reaction (4-1c)

Here A = H, B = H+, C = E. The internal partition functions are $Q_{iE} =$, $Q_{iHP} = 1$ and $Q_{e\ell H}$ already given. The equilibrium constant is then

$$K_I = \left(\frac{2\pi m_E k}{h_P^2}\right)^{3/2} \frac{T}{S_1}^{3/2} \qquad (4\text{-}46a)$$

$$\theta_I = h_I^o\ m_H/k = 157{,}900\ K$$

The logarithmic derivative of this is used in Eq. (4-40a), and is

$$\frac{d\ell n\ K_I T}{dT} = \frac{1}{T}\left(\frac{5}{2} + \frac{\theta_{IL}}{T}\ \frac{S_2}{S_1}\right) \qquad (4\text{-}46b)$$

Hydrogen Detachment: Reaction (4-1d)

Here A = H^-, B = H, C = E. The only new internal partition function is that for H^-, $Q_{el\,HM} = 1$, so the equilibrium constant is

$$K_{HM} = \left(\frac{2\pi m_E k}{h_P^2}\right)^{3/2} T^{3/2} \; 2 \; Q_{elH} \; e^{-\theta_A/T} \tag{4-47}$$

$$\theta_A = h_A^o \, m_H/k = 8759K$$

Seed Ionization: Reaction (4-1b)

Here A = S, B = S+, C = E. The internal partition functions for S and S+ depend on the particular seed of interest. In any case

$$K_S = \left(\frac{2\pi m_E k}{h_P^2}\right)^{3/2} T^{3/2} \; \frac{2Q_{elSP}}{Q_{elS}} \; e^{-\theta_{IS}/T} \tag{4-48a}$$

$$\theta_{IS} = h_{IS}^o m_S/k$$

The logarithmic derivative of K_S appears in Eqs. (4-32b) and (4-40b). The derivatives of Q_{el} can be related to h_{el} by Eq. (4-23a), so we may write

$$\frac{d\ell n \; K_S T}{dT} = \frac{1}{T}\left(\frac{5}{2} + \frac{\theta_{IS}}{T} + \frac{m_S h_{elSP}}{kT} - \frac{m_S h_{elS}}{kT}\right) \tag{4-48b}$$

The seed we have used so far is cesium. For this seed the properties are

$$\theta_{IS} = 45200K, \qquad Q_{e\ell SP} = 1 \tag{4-49}$$

$$Q_{e\ell S} = \sum_{j=0} g_j \, e^{-\varepsilon_j/kT}$$

where the weights g_j are energies ε_j can be found in the standard tabulations, such as the JANAF tables. We have used 23 terms in the sum, and the values of g_j, ε_j and ε_j/k are tabulated in Table 4-1.

We have now specified all the properties necessary to find the equilibrium composition and thermodynamic properties of the hydrogen-seed mixture. For pure hydrogen, they reduce to those of Ref. 4, which were shown there in Table A1 to agree very well with the elaborate calculations of Patch, Ref. 32, up to 100 atm and 20000K.

TABLE 4-1

Statistical Weights and Energies for Cesium

j	g_j	ε_j (cm^{-1})	ε_j/k (K)
0	2	0	0
1	2	11178	16083
2	4	11732	16880
3	4	14499	20861
4	6	14597	21002
5	2	18536	26670
6	2	21766	31317
7	4	21947	31577
8	4	22589	32501
9	6	22632	32563
10	2	24317	34987
11	8	24472	35210
12	6	24472	35210
13	6	25764	37069
14	26	26616	38295
15	34	27364	39371
16	72	28446	40928
17	38	29429	42342
18	28	30172	43411
19	66	29148	41938
20	96	29679	42702
21	130	30042	43224
22	168	30302	43598

4.4 Transport Properties

The calculation of the transport properties of gas mixtures has been studied extensively. An exact theory is extremely complicated, and has been worked for only a few cases, such as ionizing argon. Most engineering calculations are based on various kinds of mixture rules. Perhaps the most successful such calculations were done by Yos (Ref. 33), who presented results of calculations for air, oxygen, nitrogen and hydrogen; each gas was considered a mixture of its equilibrium constituents. Yos' work has been widely used and revised. A recent revision (Ref. 35) did not include hydrogen, but it did up-date some of the cross-sections which are needed for a hydrogen mixture.

There is little information available on alkali metal vapor, especially at high temperature, and none that could be found on seeded hydrogen. Since the seed is a small fraction of the mixture, one might feel that the transport properties of pure hydrogen would be satisfactory. However, the seed produces electrons at low temperatures, and they are a good conductor of heat because of the ease with which they transport energy. So it was considered necessary to check the possible effect of seeing on hydrogen thermal conductivity. This was accomplished by using the Yos method to calculate the transport properties of cesium-seeded hydrogen, and comparing the results with pure hydrogen. This new calculation also afforded the opportunity to use the more recent cross-sections of Ref. 35 to up-date the properties for pure hydrogen. This results in significant differences from Yos' thermal conductivity at high temperatures.

We will see that the thermal conductivity of hydrogen is not affected noticeably by seeding with a percent of cesium, especially when the degree of uncertainty in the cross-sections used is taken into account. It is therefore sufficiently accurate for the LSC wave model in seeded hydrogen to use pure hydrogen transport properties.

Thermal Conductivity

Yos expresses the thermal conductivity λ_c as the sum of three terms giving the contributions of the translational motion λ_{tr}, the internal degrees of freedom, λ_{int}, and the change in composition due to reactions λ_r. Each contribution is expressed in terms of the number density of the ith species n_i, the stochiometric coefficients of the ith species in the nth reaction a_{ni} and a number of other parameters, as follows:

$$\alpha_{ij} = \frac{1 + (1 - m_i/m_j)(0.45 - 2.54\, m_i/m_j)}{(1 + m_i/m_j)^2} \tag{4-50}$$

$$v_{ij} = \left[\frac{2m_i m_j}{\pi(m_i + m_j)\, kT}\right]^{\frac{1}{2}} \tag{4-51}$$

$$\Delta_{ij}^{(1)} = \frac{8}{3}\, v_{ij}\, \pi\, \bar{\Omega}_{ij}^{(1,1)}, \quad \Delta_{ij}^{(2)} = \frac{16}{5}\, v_{ij}\, \pi\, \bar{\Omega}_{ij}^{(2,2)} \tag{4-52}$$

The $\pi\, \bar{\Omega}$ are collision integrals, defined as weighted averages of the collision cross-sections:

$$\pi\, \bar{\Omega}_{ij}^{(t,s)} = \frac{\int_0^\infty d\gamma \int_0^\pi d\chi\; e^{-\gamma^2}\, \gamma^{2s+3}\, (1 - \cos^t \chi)\, 4\pi\, \sigma_{ij} \sin\chi}{(s+1)\,! \left[1 - \frac{1 + (-1)^t}{2\,(t+1)}\right]} \tag{4-53}$$

Here σ_{ij} (χ, g) is the differential scattering cross-section for the pair of species i - j, χ is the scattering angle in the center of mass system and γ is the relative velocity of the colliding particles normalized by v_{ij}.

The denominator is the rigid sphere value of the double integral in the numerator, which is obtained by putting $4\pi\,\sigma_{ij} = 1$.

In addition, the internal contribution involves the dimensionless internal specific heat. $\bar{c}_{int,\,i}$ and the reaction contribution involves the dimensionless heat of reaction $\Delta\,\bar{h}_n/T$. In these terms the thermal conductivity is

$$\lambda_C = \lambda_{tr} + \lambda_{int} + \lambda_r \tag{4-54}$$

where

$$\lambda_{tr} = \frac{15k}{4} \sum_i \frac{n_i}{\sum_j \alpha_{ij}\, n_j \Delta^{(2)}_{ij}} \tag{4-55a}$$

$$\lambda_{int} = k \sum_i \frac{n_i\, \bar{c}_{int,i}}{\sum_j n_j\, \Delta^{(1)}_{ij}} \tag{4-55b}$$

$$\lambda_r = k \sum_n \frac{(\Delta\bar{h}_n/T)^2}{\sum_i (a_{ni}/n_i) \sum_j (a_{ni}n_j - a_{nj}n_i)\, \Delta^{(1)}_{ij}} \tag{4.55c}$$

The sums on i and j go over all species, while the sum on n goes over all reactions.

In order to evaluate this expression we need the number densities, whose calculation has been described above, the internal specific heats, which can be obtained from the internal partition functions already given, the stochiometric coefficients, which follow from the reactions, and the collision integrals $\pi \bar{\Omega}_{ij}^{(s,t)}$ for s = t = 1 and s = t = 2. In these calculations we will ignore the minor species H-.

The reactions (4-1a) and (4-1b) proceed in the low temperature region. The Yos formulation requires them to be written as a sum on the left equals zero on right. When they are so expressed we see that

$$T < T^*: \quad a_{1H2} = 1, \quad a_{1H} = -2, \; a_{2S} = 1, \; a_{2SP} = -1, \; a_{2E} = -1 \qquad (4\text{-}56a)$$

In the high temperature region reactions (4-1b) and (4-1c) proceed so that

$$T > T^*: \quad a_{2S} = 1, \; a_{2SP} = -1, \; a_{2E} = -1, \; a_{3H} = 1, \; a_{3HP} = -1, \; a_{3E} = -1 \qquad (4\text{-}56b)$$

The other values of a_{ni} are zero in the two regions.

The dimensionless heats of reaction are defined as

$$\Delta\bar{h}_n/T = \sum_i a_{ni} \, h_i \, m_i/k$$

For reaction (4-1a) this is

$$\frac{\Delta\bar{h}_1}{T} = \frac{2m_H}{kT} \quad (h_{H2} - h_H)$$

The two enthalpies can be inferred from Eq. (4-21), or found in Eqs. (A-24) and (A-23) of Ref. 4. The molecular enthalpy is the sum of translational, rotational and vibrational contributions

$$h_{H2} = \frac{7kT}{2m_{H2}} + \frac{kT}{m_{H2}} \psi_v \tag{4-57}$$

where ψ_v is defined in Eq. (4-22). The atom enthalpy is the sum of translational, dissociation and electronic contributions

$$h_H = \frac{5kT}{2m_H} + h_D^o + h_{IL}^o \left(1 - \frac{S_2}{S_1}\right) \tag{4-58}$$

where S_1 and S_2 are given in Eq. (4-22). When these are put into the heat of reaction for reaction (4-1a) we ignore the electronic contribution, since this reaction is only considered in the low temperature regime. We then find

$$\frac{\Delta\bar{h}_1}{T} = \psi_v - \frac{3}{2} - \frac{\theta_D}{T} \tag{4-59}$$

For reaction (4-1b) we have

$$\frac{\Delta\bar{h}_2}{T} = \frac{m_S}{k}(h_S - h_{SP}) - \frac{m_E}{k} h_E$$

The enthalpies have already been given in Eqs. (4-24)and the heat of reaction becomes

$$\frac{\Delta\bar{h}_2}{T} = \frac{1}{Q_{el_S}} \sum_{j=0} \frac{\varepsilon_j g_j}{kT} e^{-\varepsilon_j/kT} - \frac{\theta_{IS}}{T} - \frac{5}{2} \tag{4-60}$$

For the third reaction, (4-1c),

$$\frac{\Delta\bar{h}_3}{T} = \frac{m_H}{k}(h_H - h_{HP}) - \frac{m_E h_E}{k}$$

The ion enthalpy has translational, dissociation and ionization contributions

$$h_{HP} = \frac{5kT}{2m_H} + h_D^o + h_{IL}^o \tag{4-61}$$

so that use of this and Eqs. (4-58) and (4-24a) yield

$$\frac{\Delta\bar{h}_3}{T} = -\frac{5}{2} - \frac{\theta_{IL}}{T}\frac{S_2}{S_1} \tag{4-62}$$

These three expressions, Eqs. (4-59), (4-60) and (4-62), provide the heat of reaction terms for λ_r.

The internal specific heats $\bar{c}_{int}$ can be found from the enthalpies by differentiation. The electrons and the H+ have no internal degrees of freedom and so $\bar{c}_{int} = 0$ for them. For the other species, we ignore the 5k/2m term in the enthalpy and form $\bar{c}_{int} = m(\partial h/\partial T)_p/k$ from the other terms.

For H_2, use of Eq. (4.53) yields

$$\bar{c}_{int,\,H2} = 1 + \Phi_v \tag{4-63}$$

where Φ_v has been defined in Eq. (4-35a).

For H only the last term m Eq. (4-58) contributes, and differentiation yields

$$\bar{c}_{int,\,H} = \left(\frac{\theta_{IL}}{T}\right)^2 \left(\frac{S_4}{S_1} - \frac{S_2^2}{S_1^2}\right) \tag{4-64}$$

where S_4 is defined in Eq. (4-43).

For both S and S+, the only term which contributes can be seen from Eqs. (4-24b, c) to be $h_{e\ell}$ so

$$\bar{c}_{int,\,S} = \frac{m_S}{k} \frac{dh_{e\ell S}}{dT}, \quad \bar{c}_{int,\,SP} = \frac{m_S}{k} \frac{dh_{e\ell SP}}{dT} \tag{4-65}$$

where the expression for the derivative is given in Eq. (4-35b). For most seeds, including the cesium case calculated later, the excited states of S+ are so high that they may be ignored, and $\bar{c}_{int,\,SP} = 0$.

Equations (4-63) - (4-65) provide all the non-zero expressions for $\bar{c}_{int}$ that are needed in λ_{int}.

Finally, there are the collision integrals $\pi\,\bar{\Omega}_{i,j}^{(1,1)}$ and $\pi\,\bar{\Omega}_{i,j}^{(2,2)}$. We are considering 6 species: H_2, H, H+, E, S, SP. Thus the matrix of the integral is 6 x 6, but because of symmetry there are only 21 different values in each of the two matrices.

The interactions between charged particles are associated with Coulomb forces. In Ref. 35 the Yos collision integrals for these interactions are updated to (cgs units)

$$\pi \bar{\Omega}^{(1,1)}_{i,j} = \pi \bar{\Omega}^{(2,2)}_{i,j} = Q_c$$

$$Q_c = \frac{\pi}{2} \left(\frac{e^2}{kT}\right)^2 \left\{ \ln \left[\frac{1}{(\pi n_E)^{1/2}} \left(\frac{kT}{e^2}\right)^{3/2} \right] - 0.577 \right\} \qquad (4\text{-}66a)$$

In MKS units this becomes

$$Q_c = \frac{4.38E\text{-}10}{T^2} \left\{ \frac{1}{2} \ln \left(\frac{6.82E\text{-}13\ T^3}{n_E} \right) - 0.577 \right\} \qquad (4\text{-}66b)$$

Reference 35 further suggests that for collisions involving electrons we use $0.6\ Q_c$, while using Q_c for all other Coulomb collisions. This then provides both collision integrals for the collision pairs: H+ - E, S+ - E, H+ - H+, S+ - S+, E-E, H+ - S+.

The values for the H - E system, as given by Yos, but in MKS units, are

$$\pi \bar{\Omega}^{(1,1)}_{H\text{-}E} = 5.28E\text{-}19 \left\{ -\frac{1}{2}\left(\frac{T_o}{T}\right)^2 + \frac{3}{4}\left(\frac{T_o}{T}\right) + \left[\left(\frac{T_o}{T}\right)^2 - \left(\frac{T_o}{T}\right) + \frac{3}{4}\right]\left(\frac{T_o}{T}\right)^{1/2} \exp\left(\frac{T_o}{T}\right) \frac{\sqrt{\pi}}{2}\ \mathrm{erfc}\left(\frac{T_o}{T}\right)^{1/2} \right\} \qquad (4\text{-}67a)$$

$$\pi \bar{\Omega}^{(2,2)}_{H-E} = 1.76E\text{-}19 \left\{ \frac{1}{2} \left(\frac{T_o}{T}\right)^3 - \left(\frac{T_o}{T}\right)^2 + \frac{15}{8} \left(\frac{T_o}{T}\right) \right.$$

$$\left. + \left[-\left(\frac{T_o}{T}\right)^3 + \frac{3}{2} \left(\frac{T_o}{T}\right)^2 - \frac{9}{4} \left(\frac{T_o}{T}\right) + \frac{15}{8} \right] \left(\frac{T_o}{T}\right)^{\frac{1}{2}} \exp\left(\frac{T_o}{T}\right) \frac{\sqrt{\pi}}{2} \operatorname{erfc}\left(\frac{T_o}{T}\right)^{\frac{1}{2}} \right\} \quad (4\text{-}67b)$$

where T_o = 3300K, the factor $\sqrt{\pi}/2$ is a correction to Yos' erroneous $\sqrt{\pi/2}$, and erfc is the complementary error function.

For charge exchange, H+ - H Yos gives, in MKS units,

$$\pi \bar{\Omega}^{(1,1)}_{HP-H} = 2.52E\text{-}18 - 4.92E\text{-}19 \log \frac{T}{1.008}$$

$$+ 2.42E\text{-}20 \left(\log \frac{T}{1.008}\right)^2 \quad (4\text{-}68)$$

while $\pi \bar{\Omega}^{(2,2)}_{HP-H}$ is taken from Yos' Fig. 1.

The other collision integrals for hydrogen species with other hydrogen species or electrons are also taken from Fig. 1 of Yos. These are H-H_2, H-H, H_2-H_2 and H_2 - E. In the latter case, the two collision integrals are taken to be equal. The collision integrals for H_2 - H+ are ignored since in our model of the thermodymanics H_2 appears only in the low temperature regime and H+ only in the high temperature regime.

We have so far covered 13 interactions, leaving only the 8 interactions between the seed species and themselves, or the seed species and the hydrogen species where only one of the two interacting species is ionized. These are: H_2 - S, H - S, H+ - S, H_2 - S+, H - S+, S - S+, E - S, S - S.There is little if any information on these interactions. The last three are pertinent to the pure seed, but even information on them is lacking for alkali metals at high temperatures. Fortunately, the seed will be at most, a few percent of the mixture, so rough approximations will be satisfactory. We took the seed atom and ion to be equivalent to the hydrogen atom and ion, so that we took the collision integrals for the following interactions to be the same.

$$H_2 - S = H_2 - H; \quad H - S = H - H; \quad E - S = E - H;$$

$$S - S = H - H; \quad S - S+ = H - H+$$

The remaining three, H_2 - S+, H - S+, H+ - S, are harder to estimate. The latter two cannot be approximated by H - H+ because that is a charge exchange process with a large cross-section, while replacing one partner by a seed does not yield a charge exchange process. We did calculations with several values, of the order of 10^{-18} to 10^{-20} m^2.

Table 4-2 summarizes the source of the collision integrals. The curves of Fig. 1 of Ref. 33 used were read at T = 1000 (500) 10,000 (1000) 16,000 (2000) 30,000 and interpolated linearly in log $\pi \bar{\Omega}$.

All the information is now available to calculate the thermal conductivity λ. First calculations were made for hydrogen to compare with Yos to check the program. Calculations were made using both Yos' Coulomb

TABLE 4-2

Source of Collision Integrals

	H_2	H	H+	E	S	S+
H_2	Fig.1	Fig.1	—	Fig.1	H_2-H	Est.
H		Fig.1	Eq.(4-68) Fig. 1	Eqs.(4-67)	H-H	Est.
H+			Eqs.(4 66)	0.6* Eqs.(4-66)	Est.	0.6* Eqs.(4-66)
E				0.6* Eqs.(4-66)	E-H	0.6* Eqs.(4-66)
S					H-H	H-H+
S+						Eqs.(4-66)

Note: Fig. 1 refers to Fig. 1 of Ref. 33.

cross-section, which is

$$Q_c = \left(\frac{e^2}{kT}\right)^2 \quad \frac{1}{2} \quad \log\left[\frac{9}{4\pi}\left(\frac{kT^3}{e^2}\right) \quad \frac{1}{n_E} + \frac{16}{n_E^{3/2}}\left(\frac{kT}{e^2}\right)^2\right]$$

$$= \frac{3.21E\text{-}10}{T^2} \log \left[\frac{1.536E14T^3}{n_E} + \frac{5.732E10T^2}{(n_E)^{3/2}}\right] \qquad (4\text{-}69)$$

and the one suggested by Aerotherm in Ref. 35, which is given in Eqs. (4-66). The results are shown in Fig. 4-1 as plots of λ vs T for p = 1, 10, 100 atm up to 30,000K. The solid lines use the Yos expression for Q_c, while the dashed lines use the more recent Aerotherm expression.

The solid lines are in excellent agreement with the tables in Yos' report (Ref 33). The dashed lines show the effect of the more recent Coulomb cross-section at the higher temperatures and pressures, where ionized species are very significant. The curves have two bumps, the lower temperature bump reflecting dissociation of H_2 and the higher temperature bump the ionization of H.

Calculations were then made for cesium-seeded hydrogen with a ratio Cs/H = 0.01. The results show only small changes from pure hydrogen at the same total pressure, of the order of a few percent, over a factor of 10 change in the value of the collision integrals which had to be estimated. We conclude that small amounts of cesium seed do not have a significant effect on hydrogen thermal conductivity, expecially in view of the uncertainty in the various collision integrals.

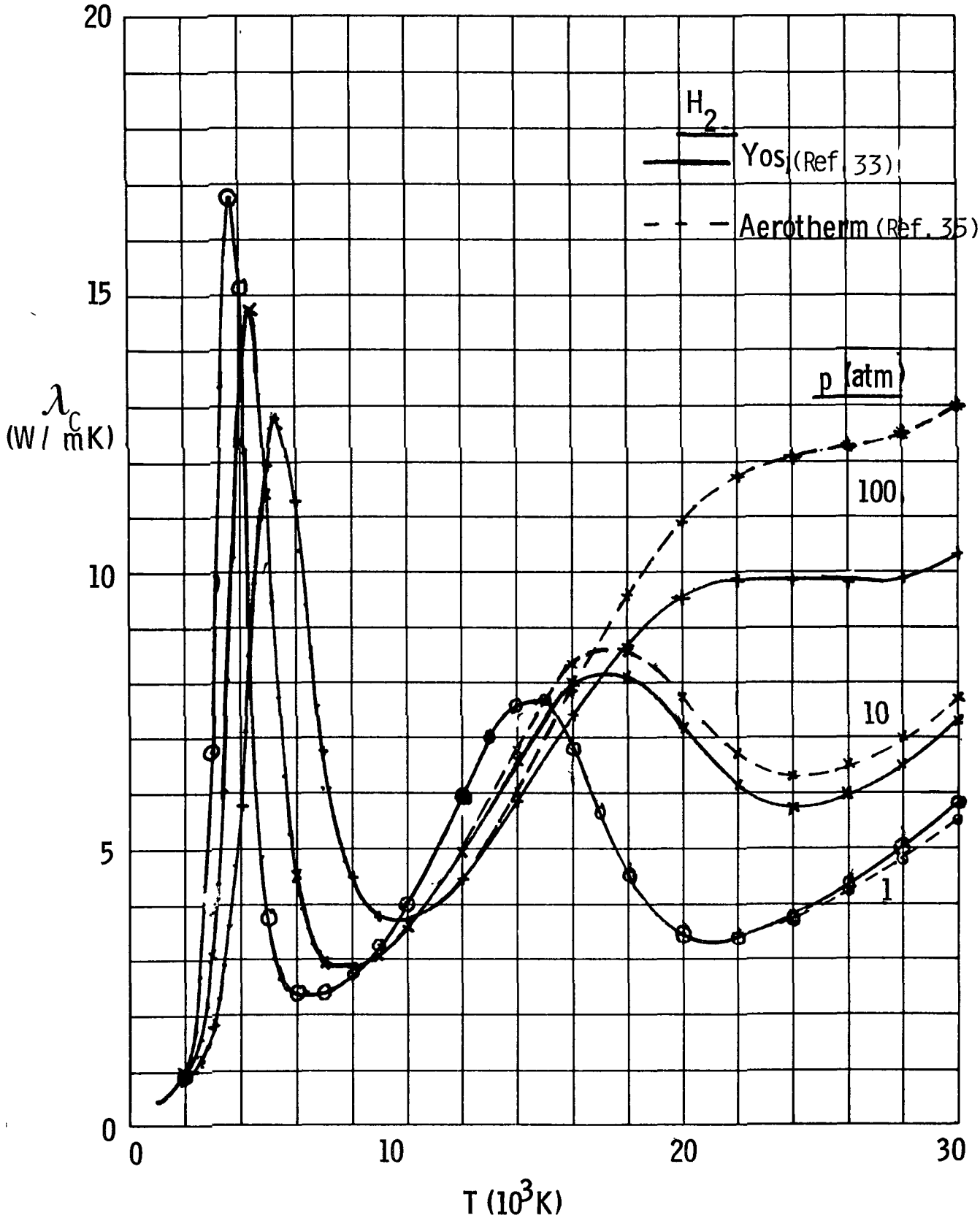

Fig. 4-1 Thermal Conductivity of Equilibrium Hydrogen

Study of Eqs. (4-55) make this conclusion plausible. Addition of new species adds terms to the denominators of each component of λ, decreasing each term in the sums; but it also adds more terms to the sums over i. These are compensating effects, and the net effect is small for small amounts of seed.

The conclusion that pure hydrogen conductivity is a good approximation is important for simplifying the computer models of laser-heated thrusters. It means that λ_C can be treated as independent of composition, but only dependent on T and P. Thus we can input λ_C as a table independent of seeds, and interpolate, rather than having to change λ_C for each seed fraction.

The calculations by Yos' method described above are limited to T > 1000K by the collision integrals given in Fig. 1 of Ref. 33. Below 1000K there are only two species, H_2 and S, so the calculations are quite simple, having only λ_{tr} and λ_{int} components. It can be verified that at 1000K also there is only a few percent difference between pure H_2 and Cs/H = 0.01. In fact, a good fit to the calculations at 1000K and 2000K is

$$\lambda_C = \lambda_C \text{ (hydrogen)} \; / \; (1 + 0.02f) \qquad (4\text{-}70)$$

which shows the small effect of small seed fractions f.

The pure hydrogen expression for T < 1000K can be obtained by using the value λ_C = 0.434 W/mK calculated at 1000K, and the value 0.177 W/mK given on page 574 of Ref. 36 as experimentally measured. A linear fit gives

$$\lambda_C = 3.67E\text{-}4\ T + 6.69E\text{-}2 \qquad (4\text{-}71)$$

for pure hydrogen, T < 1000K.

Viscosity

Yos also gives an expression for viscosity in Ref. 33. in the same terms as his conductivity expression. It is

$$\mu = \sum_i m_i n_i / \sum_j n_j \Delta^{(2)}_{i,j} \qquad (4\text{-}72)$$

where $\Delta^{(2)}_{i,j}$ has already been defined in terms of a collision integral in Eq. (4-52).

We can expect a smaller alkali seed fraction to have a larger effect on μ than on λ_C, because of the large mass of the seed atom compared to hydrogen. (The molecular weight of cesium for example is 133.) Calculations bear this out. At low temperature, up to 4000K, the viscosity of Cs/H = 0.01 is as much as a factor of 2 larger than that of pure H_2. This difference is reduced to only a few percent in the middle range of temperature but begins to become significant again at temperatures near 20,000K. These effects will have to be considered if viscosity becomes an important parameter.

V. DEVELOPMENT OF THRUST CHAMBER DESIGN COMPUTER PROGRAM

The two modes of heating the propellant being considered necessitate two different computer programs. In the continuous heating mode, both the low and moderate temperature absorbers are present. Laser energy absorption occurs continuously from the input temperature to the high temperature at which all the laser energy has been absorbed. The axial gradients are not large, so viscous and heat conduction effects in the axial direction can be neglected. For this case we need a flow model which includes radial gradients, laser absorption, equilibrium chemistry, and radiation losses.

In the discontinuous heating mode, there is no low temperature absorber. Absorption occurs in an LSC wave standing in the flow channel, and the low temperature heating is accomplished by the LSC wave mechanism of forward energy transport by radiation and conduction. Here we need a flow model which includes axial conduction and radiation transport, laser absorption, and radiation losses. The radial gradients are not important here, except possibly near the edges of the heated zone.

In previous work performed at PSI, (Ref. 4), a one-dimensional LSC wave model for pure hydrogen was constructed. That model is the basis for the seeded hydrogen LSC wave thruster being considered here. The additions needed to include seeding are in the thermodynamics, the thermal conductivity, the laser absorption, and the radiation transport and losses. The models needed for the first three additions have been discussed in the previous sections of this report. The radiation transport and loss model for seeded hydrogen has not yet been developed. Since the LSC wave model for pure hydrogen is thoroughly described in Ref. 4, and the version for seeded hydrogen is not complete yet, we will not discuss the seeded LSC wave model in this report.

The continuous heating flow model has formulated almost completely, and will be described here. The resulting computer program is based upon an axisymmetric wake flow program which was available at PSI. To adapt this

program to the continuously-heated thruster we had to add laser energy absorption, radiation losses, and provide for the presence of outer walls.

5.1 Equations of Motion

We consider flow in an axisymmetric channel, where the axial gradients are small compared to the radial gradients. This enables us to make the boundary layer approximation that the viscous terms need only include the radial gradients, not the axial ones. Let us denote the axial and radial coordinates by x,r, and the axial and radial velocity components by u,v. The mass conservation equation is then

$$\frac{\partial r\rho u}{\partial x} + \frac{\partial r\rho v}{\partial r} = 0 \qquad (5\text{-}1a)$$

In the usual fashion, the boundary layer approximation applied to the radial momentum equation tells us that the pressure is constant over a cross-section, so p = p(x). Then the axial momentum conservation equation is

$$\rho u \frac{\partial u}{\partial x} + \rho v \frac{\partial u}{\partial r} = - \frac{dp}{dx} + \frac{1}{r} \frac{\partial}{\partial r} \left(r \mu \frac{\partial u}{\partial r} \right) \qquad (5\text{-}1b)$$

The energy conservation equation must include the radiation flux terms, which will account for both the laser radiation and the radiation from the gas. Written with enthalpy h as the dependent variable, and with a radiation flux vector whose axial and radial components are denoted by S_x and S_r, the equation is

$$\rho u \frac{\partial h}{\partial x} + \rho v \frac{\partial h}{\partial r} + \frac{1}{r} \frac{\partial r S_r}{\partial r} + \frac{\partial S_x}{\partial x} = u \frac{dp}{dx}$$

$$+ \mu \left(\frac{\partial u}{\partial r} \right)^2 + \frac{1}{r} \frac{\partial}{\partial r} \left\{ r \left[\lambda_{Cf} \frac{\partial T}{\partial r} + \sum \rho D_i h_i \frac{\partial C_i}{\partial r} \right] \right\}$$

Note that λ_{Cf} is the frozen thermal conductivity, not including the reaction contribution, which is the summation term in the bracket. Thus λ_{Cf} is the sum of the translational and internal contributions, as given in Eqs. (4-55a) and (4-55b).

The term in square brackets on the right is the heat flux in the radial direction. It is composed of the conduction part proportional to the temperature gradient, and the diffusive part, which involves the enthalpy per unit mass h_i of the i-th species, a diffusion coefficient D_i for that species, and the gradient of its mass fraction C_i. The form of the diffusion term is the simplified one usually used, where the diffusion velocity has been expressed by Fick's law as $D_i \, \partial C_i/\partial r$, to avoid the considerable complication of considering multicomponent diffusion.

The heat flux term can be simplified by introducing the relation between the mixture enthalpy h and the species enthalpy and mass fraction.

$$h = \sum h_i C_i$$

If we differentiate, and recognize that h_i depends only on T, we find

$$dh = \sum h_i dC_i + c_{pf} dT, \quad c_{pf} = \sum c_{p_i} C_i, \quad c_{p_i} = dh_i/dT$$

The quantity c_{pf} is the frozen specific heat of the mixture, which is just the weighted sum of the specific heats of the individual components.

By replacing the temperature derivative by the enthalpy derivative in the last term of the energy equation, it becomes

$$\rho u \frac{\partial h}{\partial x} + \rho v \frac{\partial h}{\partial r} + \frac{1}{r} \frac{\partial r S_r}{\partial x} + \frac{\partial S_x}{\partial x} = u \frac{dp}{dx} + \mu \left(\frac{\partial u}{\partial r} \right)^2$$

$$+ \frac{1}{r} \frac{\partial}{\partial r} \left\{ r \frac{\lambda_{Cf}}{c_{pf}} \left[\frac{\partial h}{\partial r} + \sum (Le_i - 1) h_i \frac{\partial C_i}{\partial r} \right] \right\} \qquad (5\text{-}1c)$$

where the Lewis number is defined as

$$Le_i = \rho D_i \, c_{pf} / \lambda_{Cf}$$

which is the ratio of diffusion of species to diffusion of heat. This equation shows the considerable simplification which occurs if $Le_i = 1$, when the species concentration gradients do not need to be included.

The three conservation equations determine the three independent variables u, v and h in the two-dimensional x, r coordinate system. This formulation is appropriate for a gas mixture in chemical equilibrium, when the chemical state is determined by the specification of two thermodynamic variables, such as T and p, plus the mixture composition in terms of the fraction of each kind of chemical nucleus contained in the mixture. It is also possible to formulate the problem in terms of non-equilibrium reacting chemistry; such a formulation was contained in the original wake program from which the present program was adopted. However, it was found that the laser energy addition caused problems with the nonequilibrium chemistry calculation. Since nonequilibrium was not considered to be required for the laser-heated thruster application, at least during the heating phase of the flow which is being addressed here, the program was converted to the chemical equilibrium formulation given above.

Part of the radiant energy flux vector $\underline{S}$ is the laser beam. We will take a parallel beam travelling parallel to the x axis, for which $S_x = I$ and $S_r = 0$. Then the laser contributes a term $\partial I/\partial x$ on the left of Eq. (5-1c), but the laser energy is absorbed according to

$$\partial I/\partial x = -k_L I \tag{5-2}$$

where k_L is the laser absorption coefficient discussed in Section II. Thus the laser provides a term $k_L I$ on the right side of Eq. (5-1c). (Note that we may permit I to depend on both x and r, even though it is only propagating in the x direction.) The remaining part of the radiant energy flux vector is due to radiation transport in the gas and will be denoted by $\underline{S}^R$, and the terms on the left of Eq. (5-1c) containing this vector will be carried as $\nabla \cdot \underline{S}^R$, the divergence of the vector.

The final form of the energy equation is then

$$\rho u \frac{\partial h}{\partial x} + \rho v \frac{\partial h}{\partial r} + \nabla \cdot \underline{S}^R = u \frac{dp}{dx} + \mu \left(\frac{\partial u}{\partial r}\right)^2 + k_L I$$

$$+ \frac{1}{r} \frac{\partial}{\partial r} \left\{ r \frac{\lambda_{Cf}}{c_{pf}} \left[\frac{\partial h}{\partial r} + \sum (Le_i - 1) h_i \frac{\partial C_i}{\partial r} \right] \right\} \qquad (5\text{-}1d)$$

These cylindrical conservation equations are singular on the axis $r = 0$, and must be expressed in limiting form there. On the axis, symmetry requires that $v = 0$ and $\partial u/\partial r = 0$. Near the axis a Taylor expansion then gives

$$v = r\left(\frac{\partial v}{\partial r}\right)_a, \quad u = u_a + \frac{r^2}{2}\left(\frac{\partial^2 u}{\partial r^2}\right)_a, \quad \frac{\partial u}{\partial r} = r\left(\frac{\partial^2 u}{\partial r^2}\right)_a \qquad (5\text{-}3)$$

where the subscript a means on the axis. For the variables h and C_i, relations like those for u apply. These relations enable us to express Eqs. (5-1a, 5-1b and 5-1d) on the axis. All the terms with the operator $v\partial/\partial r$ vanish. The viscous terms are the ones with the factor $1/r$. For the momentum equation, the viscous term is

$$\frac{1}{r} \frac{\partial}{\partial r} r\mu \frac{\partial u}{\partial r} = \mu \frac{\partial^2 u}{\partial r^2} + \frac{\mu}{r} \frac{\partial u}{\partial r} + \frac{\partial \mu}{\partial r} \frac{\partial u}{\partial r}$$

The first two terms have the same limit on the axis because of Eq. (5-3), while the last term is of order r^2 there and may be ignored. So we find that

$$\left(\frac{1}{r} \frac{\partial}{\partial r} r\mu \frac{\partial u}{\partial r}\right)_a = 2\left(\mu \frac{\partial^2 u}{\partial r^2}\right)_a$$

Exactly similar treatment can be accorded the last term in Eq. (5-1d). The second term in the mass conservation is treated similarly (after division by r) using the expression for v in Eq. (5-3). The resulting equations <u>on the axis</u> become

$$\frac{\partial \rho u}{\partial x} + 2\rho \frac{\partial v}{\partial r} = 0 \qquad (5\text{-}4a)$$

$$\rho u \frac{\partial u}{\partial x} = - \frac{dp}{dx} + 2\mu \frac{\partial^2 u}{\partial r^2} \qquad (5\text{-}4b)$$

$$\rho u \frac{\partial h}{\partial x} + \nabla \cdot \underline{S}^R = k_L I + u \frac{dp}{dx} + 2 \frac{\lambda_{Cf}}{c_{pf}} \left[\frac{\partial^2 h}{\partial r^2} + \sum (Le_i - 1)\, h_i \frac{\partial^2 C_i}{\partial r^2} \right] \qquad (5\text{-}4c)$$

5.2 Transformation of Equations of Motion

The numerical solution of the conservation equations is accomplished by using the stream function Ψ as one of the independent variables, instead of r. This satisfies the mass conservation equation exactly by setting

$$\rho u r = \frac{\partial \Psi}{\partial r}, \quad \rho v r = - \frac{\partial \Psi}{\partial x}, \quad \Psi = \int_0^r \rho u r dr, \quad r^2 = 2 \int_0^{\psi} d\Psi / \rho u \qquad (5\text{-}5)$$

The stream function has the significance of being the mass flow through a cross-section of radius r, except for a factor of 2π. We now transform from x, r to ξ, Ψ, where $\xi = x$, but is given a different name to avoid confusion. The transformation laws are

$$\frac{\partial}{\partial r} = \rho u r \frac{\partial}{\partial \Psi}, \quad \frac{\partial}{\partial x} = \frac{\partial}{\partial \xi} - \rho v r \frac{\partial}{\partial \Psi} \qquad (5\text{-}6a)$$

$$v = u(\partial r / \partial x)_{\Psi = \text{const}}$$

Thus the convective derivative operator becomes

$$\rho u \frac{\partial}{\partial x} + \rho v \frac{\partial}{\partial r} = \rho u \frac{\partial}{\partial \xi}$$

and the viscous operator becomes

$$\frac{1}{r} \frac{\partial}{\partial r}\left(rf \frac{\partial}{\partial r}\right) = \rho u \frac{\partial}{\partial \Psi}\left(r^2 f \rho u \frac{\partial}{\partial \Psi}\right) \tag{5-6b}$$

where f is any function.

Using these transformation equations, we find the momentum and energy conservation expressions Eqs. (5-1b and 5-1d) to become

$$\frac{\partial u}{\partial \xi} = -\frac{1}{\rho u}\frac{dp}{d\xi} + \frac{\partial}{\partial \Psi}\left(\rho u r^2 \mu \frac{\partial u}{\partial \Psi}\right) \tag{5-7a}$$

$$\frac{\partial h}{\partial \xi} + \frac{\nabla \cdot \underline{S}^R}{\rho u} = \frac{k_L I}{\rho u} + \frac{1}{\rho}\frac{dp}{d\xi} + \rho u r^2 \mu \left(\frac{\partial u}{\partial \Psi}\right)^2$$

$$+ \frac{\partial}{\partial \Psi}\left\{\frac{\rho u r^2 \lambda_{Cf}}{c_{pf}}\left[\frac{\partial h}{\partial \Psi} + \sum (Le_i - 1) h_i \frac{\partial C_i}{\partial \Psi}\right]\right\} \tag{5-7b}$$

The corresponding equations on the axis are to be found from Eqs. (5-4b and 5-4c). We need to evaluate the second radial derivatives in terms of Ψ. From Eq. (5-5) we see that near the axis

$$\Psi = \rho_a u_a r^2/2, \quad r = (2\Psi/\rho_a u_a)^{\frac{1}{2}}$$

Then from Eq. (5-6a and 5-6b) we find

$$\frac{\partial}{\partial r} = \rho_a u_a r \frac{\partial}{\partial \Psi} \rightarrow (2\rho_a u_a \Psi)^{\frac{1}{2}} \frac{\partial}{\partial \Psi}$$

$$\frac{\partial^2}{\partial r^2} = \rho_a u_a r \frac{\partial}{\partial \Psi}\left(\rho_a u_a r \frac{\partial}{\partial \Psi}\right) \rightarrow 2\rho_a u_a \sqrt{\Psi} \frac{\partial}{\partial \Psi}\left(\sqrt{\Psi} \frac{\partial}{\partial \Psi}\right)$$

$$= 2\rho_a u_a \left(\Psi \frac{\partial^2}{\partial \Psi^2} + \frac{1}{2} \frac{\partial}{\partial \Psi}\right) = \rho_a u_a \frac{\partial}{\partial \Psi}$$

The last step follows because $\Psi = 0$ on the axis. Thus the second r derivatives in the axis equations become first Ψ derivatives. Then Eqs. (5-4b and 5-4c) <u>on the axis</u> transform to

$$\frac{\partial u}{\partial \xi} = -\frac{1}{\rho u} \frac{dp}{d\xi} + 2\mu \frac{\partial u}{\partial \Psi} \tag{5-8a}$$

$$\frac{\partial h}{\partial \xi} + \frac{\nabla \cdot \underline{S}^R}{\rho u} = \frac{k_L I}{\rho u} + \frac{1}{\rho} \frac{dp}{d\xi}$$

$$+ \frac{2\lambda_{Cf}}{c_{pf}} \left[\frac{\partial h}{\partial \Psi} + \sum (Le_i - 1) h_i \frac{\partial C_i}{\partial \Psi}\right] \tag{5-8b}$$

We now have two equations in the unknowns h, u to be solved, when expressions for I, $\nabla \cdot \underline{S}^R$, λ_{Cf}/c_{pf} and $dp/d\xi$ are given.

5.3 Wall Shape

The use of the Ψ coordinate instead of r means that r has to be calculated by Eq. (5-5), once the solution has been obtained at a given cross section x. Since u = 0 at the wall, $r = r_w$, the integration must be done carefully near the wall. The behavior of ρu near the wall can be obtained from the transformation Eq. (5-6a), which shows that

$$\frac{\partial \rho u}{\partial r} = \rho u r \frac{\partial \rho u}{\partial \Psi} = \frac{r}{2} \frac{\partial (\rho u)^2}{\partial \Psi}$$

Since we expect the r-derivative of ρu to be finite at the wall, while u is zero there, it is clear that the Ψ-derivative of ρu must be infinite, but the Ψ-derivative of $(\rho u)^2$ is finite. Thus we may write a Taylor series

$$(\rho u)^2 = (\Psi - \Psi_w) \left[\partial (\rho u)^2 / \partial \Psi\right]_w$$

near the wall. The relation between r and Ψ from Eq. (5-5) can be written

$$\int_{\Psi}^{\Psi_w} \frac{d\Psi}{\rho u} = \int_{r}^{r_w} r dr = \frac{1}{2} (r_w^2 - r^2)$$

Using the expansion for $(\rho u)^2$ on the left, we find

$$r_w^2 = r^2 + 4 \left(\frac{\Psi_w - \Psi}{\left[-\partial (\rho u)^2 / \partial \Psi\right]_w} \right)^{1/2} \qquad (5\text{-}9a)$$

where we have recognized that $\Psi_w > \Psi$ and the gradient is negative since ρu decreases to zero at the wall.

A finite difference expression for this equation for r_w is obtained by putting the derivative equal to the difference quotient from r to r_w, remembering that $\rho u = 0$ at the latter location. Then Eq. (5-9a) becomes

$$r_w^2 = r^2 + 4(\Psi_w - \Psi)/\rho u \qquad (5\text{-}9b)$$

This can be applied to find r_w at Ψ_w, when r is known at Ψ, by using ρu at Ψ. It carries the integral of Eq. (5-5) from Ψ to Ψ_w.

The fact that the wall shape is determined as a result of the calculation, instead of as an input, means that the calculation is an indirect one. However, there is a parameter available to control the wall shape $r_w(x)$, since we have not yet specified the pressure gradient $dp/d\xi$. In the stream function formulation, we are free to specify $dp/d\xi$ to adjust the wall shape to a desirable one. Since the flow is heating, the density will tend to decrease, and the streamlines will tend to diverge, increasing the channel size. To counteract this trend, if we want to maintain an approximately uniform channel area, we may increase the flow velocity u. Reference to the momentum equation (5-7a) shows that we then need to maintain a negative pressure gradient $dp/d\xi$. How to specify $dp/d\xi$ so as to obtain a desired wall shape is an art that will have to be learned as experience with the flow computer program progresses.

5.4 Laser Beam Shape

Absorption of energy from the laser beam is a heating term $k_L I$ in the energy equation (5-8b). The intensity I is determined by the absorption equation (5-2). Notice that I is a function of x, r and not ξ, Ψ since

it does not follow the streamlines. Thus the solution of Eq. (5-2) is computed in x, r coordinates, and then the relation between Ψ and r at a fixed $x = \xi$ is used to convert $I(x,r)$ to $I(\xi, \Psi)$ for use in the energy equation. Conversely, k_L is a function of the thermodynamic variables, which are defined in the ξ, Ψ system, and it is transferred to the x, r system for use in Eq. (5-2).

An initial profile, at $x = 0$, is needed for $I = I_i(r)$ to start the integration of Eq. (5-2). There are many profiles that could be chosen, such as a uniform (top hat) profile or a truncated Gaussian. We have chosen to use the far-field pattern of a beam made by uniformly illuminating a circular aperture. This profile is

$$I_i(r) = I_o \left[2J_1(ar)/ar\right]^2 \tag{5-10}$$

where J_1 is the first order Bessel function, I_o is the intensity at $r = 0$ and a is a parameter giving the width of the beam.

The power P in this beam up to any radius r is found by integration to be

$$P_r = \int_o^r 2\pi r\, I_i(r)\, dr = \frac{4\pi I_o}{a^2} \left[1 - J_o^2(ar) - J_1^2(ar)\right] \tag{5-11}$$

The total power to $r = \infty$ is $4\pi I_o/a^2$, which shows that 2/a may be interpreted as the radius over which a uniform beam of intensity I_o would have the same total power as I_i.

The parameter a may also be related to the first zero of I_i, which occurs at

$$ar_1 = 3.83171$$

Thus we can write I_i as

$$I_i = I_o \left[2J_1(y)/y\right]^2, \quad y = 3.83171\, r/r_1 \tag{5-12}$$

where the parameter is now the radius r_1 at the first zero of I_i.

In order to allow for the presence of a buffer gas near the wall, where no laser heating takes place, we also introduce a cut-off radius r_c, beyond which the laser intensity is zero. Then the initial laser profile is

$$I_i = I_o \left[2J_1(y)/y\right]^2, \quad r < r_c$$
$$= 0 \qquad\qquad r > r_c \tag{5-13}$$

This provides three parameters with which to specify the incoming laser profile. I_o is the center-line intensity; r_1 is the location of the first zero, which specifies the width of the profile; r_c gives the radius beyond which there is no laser beam.

The laser power entering the thruster is found by putting $r = r_c$ in Eq. (5-11). By defining y_c as in Eq. (5-12) with $r = r_c$, we can write

$$P_c = 4\pi I_o r_c^2 \left[1-J_o^2(y_c) - J_1^2(y_c)\right] \Big/ y_c^2, \; y_c = 3.83171\, r_c \Big/ r_1 \tag{5-14}$$

If desired, P_c can replace one of the three parameters I_o, r_1, r_c in specifying the initial laser profile.

The distribution of intensity, power and area is shown in Fig. 5-1 as a function of r/r_1, up to the first zero $r = r_1$. I_i/I_o is obtained from Eq. (5-12). The power is obtained from Eq. (5-11), normalized by $P_1 = P(r=r_1)$, which is found by recognizing that $J_1(ar_1) = 0$, and $J_o(ar_1) = 0.40276$ so

$$\frac{P_r}{P_1} = \frac{1-J_o^2(y) - J_1^2(y)}{0.83778}$$

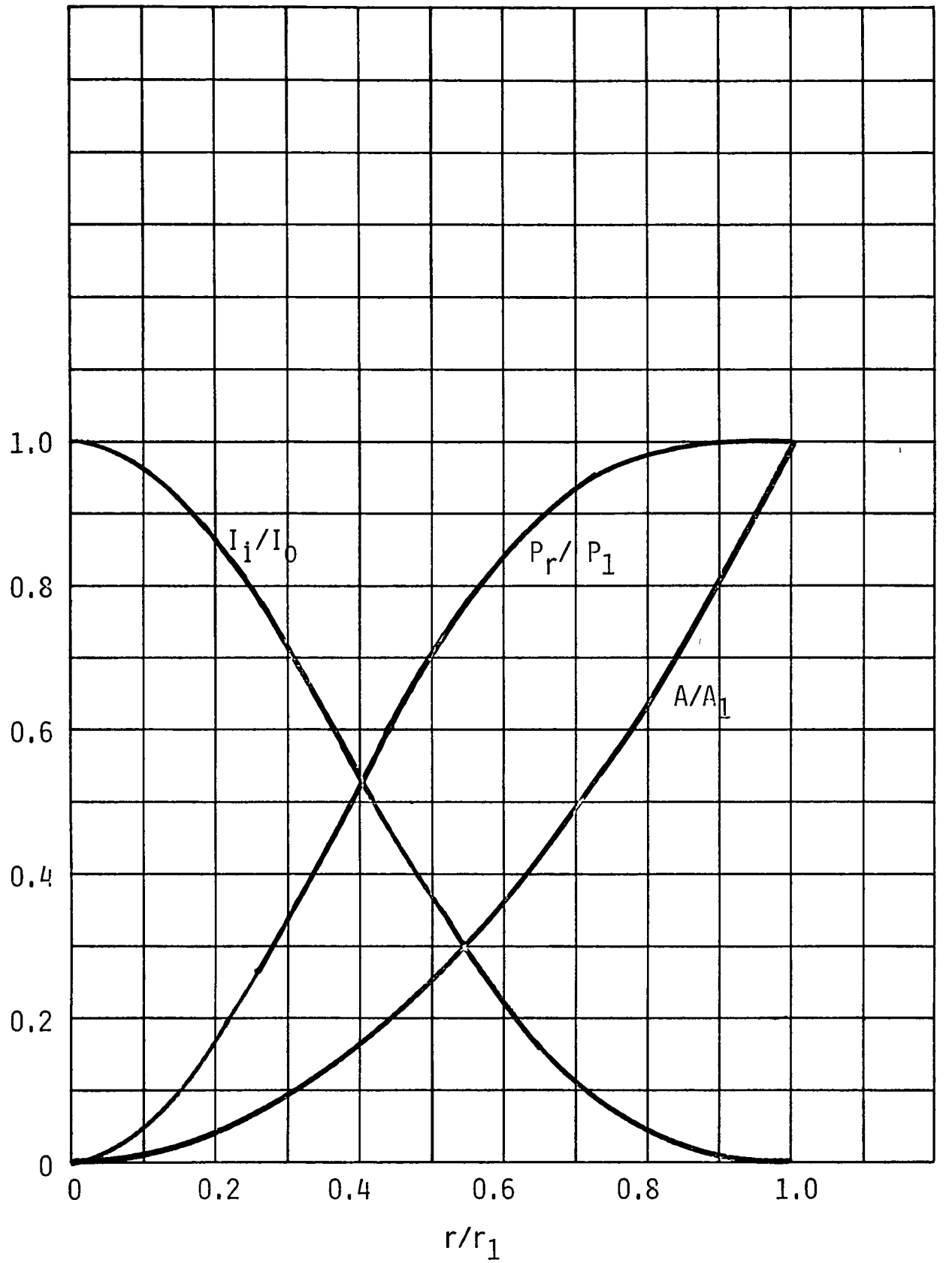

Fig. 5-1 Profiles of Intensity and Power for the Incoming Laser Beam.

The area is just $A = \pi r^2$ and at r_1 it is $A_1 = \pi r_1^2$ so that

$$A/A_1 = (r/r_1)^2$$

It can be seen from Fig. 5-1 that the intensity drops off rapidly with r, and 90% of the power is inside $r/r_1 = 0.65$. The region outside this radius is nearly unheated. In a sense, this laser profile automatically provides a practically unheated buffer zone if the cut-off radius is taken as r_1.

5.5 Radiation Model

The term $\nabla \cdot \underline{S}^R$ in the energy equation (5-8b) is the flux of radiation. What is needed for this term is an engineering model of the radiative flux. Such a model can be based on the rather detailed information about absorption coefficients presented in Section III. However, it is not feasible to use complete spectral information because integration over the wavenumber range for all calculated points in the flow field would be very time-consuming.

Although computation of radiative transfer within a gas is an extremely difficult numerical problem, there are several features of the laser-heated thruster which suggest a simplified model may be applicable. First, the shape of the laser beam (Fig. 5-1) suggests that the temperature at the center of the channel will be much hotter than that in the outer region near the cooled walls. Therefore, the radiative losses will be most important in the high temperature central region; it is reasonable to sacrifice accuracy in the outer region in favor of a more realistic description near the center.

Second, the absorption coefficients increase rapidly as the temperature increases, so they are several orders of magnitude larger in the hot region than in the cold region. Therefore, if re-absorption is unlikely to occur in the hot region (optical depth less than 0.5) it is

also unlikely to occur in the cold region, because the decrease in absorption coefficient with decreasing temperature is much greater than the increase in size of the cold region over the hot region. On the other hand, if the hot region is optically thick so that re-absorption must be considered, the radiation trapping there reduces the radiation loss and causes the temperature to remain rather constant. Outside the hot region, where the gas is optically thin and losses occur, the temperature is expected to drop rapidly.

This physical picture suggests the use of a thick-thin model of the radiation flux, in which each region is characterized by absorption coefficients and a thickness, and depending on the resulting optical depth, is described by either an optically thick (re-absorbing) or an optically thin (emitting) flux model. The physical picture just described also suggests that the transition from one description to the other is expected to occur abruptly, and the results will be insensitive to the details of the transition.

In order to avoid dealing with the spectral variation over the whole range, a band model is used. The spectral information available from the detailed description in Section III is examined, and used to identify a few important bands, for which approximate absorption coefficients are constructed. Integration over these bands can then be performed analytically.

The result of combining the thick-thin description and the band model is a rather simple engineering model of the radiation loss which is easily implemented in the flow field code, and yet still should give a description of the radiation flux within engineering accuracy.

In the region where a radiation band is optically thin, emission dominates over absorption. This approximation leads to an expression for the radiation source $\nabla \cdot \underline{S}^R$ involving the Planck mean absorption coefficient, and can be expressed as (Ref. 37)

$$(\nabla \cdot \underline{S}^R)_{thin} = 4\pi \int_{thin} d\omega \; k_\omega \; B_\omega / \pi \qquad (5\text{-}15)$$

where B_ω is the blackbody function defined in Eq. (3-5), and the integration is taken over the thin bands.

In the region where a radiation band is optically thick, the logarithmic rate of change of B_ω with respect to optical depth is small. The only readiation which reaches a given point comes from points where B_ω does not differ much from its value at the given point. This approximation leads to the Rosseland mean absorption coefficient, and to an expression for the radiation flux vector as

$$\underline{S}^R = -\frac{4}{3}\nabla T \int_{thk} \frac{1}{k_\omega}\frac{dB_\omega}{dT}\, d\omega$$

where the integration is taken over the thick bands. To form the divergence of $\underline{S}^R$ we recognize that only the gradient in the r direction need be kept, since we have taken the axial gradients to be small. Thus

$$(\nabla \cdot \underline{S}^R)_{thk} = \frac{1}{r}\frac{\partial}{\partial r}\left(rS_r^R\right) = -\frac{4\pi}{3r}\frac{\partial}{\partial r}\left(\lambda_R\, r\, \frac{\partial T}{\partial r}\right) \qquad (5\text{-}16a)$$

$$\lambda_R = \frac{1}{\pi}\int_{thk} \frac{1}{k_\omega}\frac{dB_\omega}{dT}\, d\omega \quad . \qquad (5\text{-}16b)$$

This is often called the radiation conduction approximation because the form of Eq. (5-16a) is exactly the same as the conductive and diffusive terms in the energy equation. In fact, λ_R plays the role of a radiative thermal conductivity.

The sum of Eqs. (5-15) and (5-16) provides the $\nabla \cdot \underline{S}^R$ term in the energy equation. We need now to specify the bands, the absorption coefficient for each band, and some criteria for deciding when and how a band changes from thick to thin at different points in the flow field.

For each band we will specify the absorption coefficient k_i in the form

$$k_i = k_i^* \left(1 - e^{-h_p c\omega/kT}\right) \qquad (5\text{-}17)$$

where we have separated out the stimulated emission factor. The k_i^* will be independent of the wavenumber, since it is appropriate to an average over the band. Thus the integrations indicated in Eqs. (5-15) and (5-16) can be performed in general over the band limits ω_ℓ to ω_u. Using the expression for B_ω from Eq. (3-5), we can write Eq. (5-15) for a band as

$$(\nabla \cdot \underline{S}^R)_{thin} = 8\pi h_P c^2 k_i^* \int_{\omega_\ell}^{\omega_u} d\omega\ \omega^3\ e^{-h_P c\omega/kT}$$

$$= k_i^*\ \frac{60}{\pi^4}\ \sigma\ T^4 \left[-e^{-x}\ (x^3 + 3x^2 + 6x + 6)\right]_{x_\ell}^{x_u} \tag{5-18}$$

where $x = h_P c\omega/kT$. A similar use of Eqs. (3-5) and (5-17) in Eq. (5-16b) shows that for a band

$$\lambda_R = \frac{15}{\pi^5}\ \frac{\sigma T^3}{k_i^*} \int_{x_\ell}^{x_u} \frac{x^4\ e^{-x}\ dx}{(1 - e^{-x})^3}\ .$$

This integral is not expressible in finite form, but can be integrated by parts to yield a form easily calculated. The result is

$$\lambda_R = \frac{15}{\pi^5}\ \frac{\sigma T^3}{k_i^*} \left\{ \frac{-x^4}{2} \left[\frac{1}{(1 - e^{-x})^2} - 1 \right] - \frac{2\ x^3\ e^{-x}}{1 - e^{-x}} \right.$$

$$\left. + 2x^2\ (x + 3)\ \ell n\ (1 - e^{-x}) - 6 \sum_{n=1} \frac{e^{-nx}}{n^2} \left[2\ (1 + \frac{1}{n})\ (x + \frac{1}{n}) + x^2 \right] \right\}_{x_\ell}^{x_u} \tag{5-19}$$

Band Model Example

In order to try out the band model, a model was constructed for a particular case and implemented in the computer program. The case chosen was a mixture $H_2/H_2O/Cs = 0.945/0.05/0.005$ at p = 30 atm, for a radius of about 12 cm. The detailed spectral absorption coefficients were calculated for this case by the methods described in Section III. The absorption coefficient for the equilibrium mixture is shown in Fig. 5-2, as a function of ω, for T = 2000, 4000 and 6000 K. The components of this absorption coefficient are presented similarly for the same three temperatures in Fig. 5-3. The components are that of hydrogen molecule vibration, KV, hydroxyl KOH, water KH_2O, the three cesium contributions KCS and the four hydrogen atom contributions KH. Another important ingredient of the model is the normalized blackbody function

$$RE = B_\omega/\sigma T^4$$

which is presented in Fig. 5-4 for the three temperatures. It provides the limits of the radiation at each wave number, and shows where radiation cannot be important regardless of the size of the absorption coefficient.

The band model was constructed after study of these plots to extract the important part of the radiation. It was concluded that the radiation for this case could be expressed to sufficient accuracy by the use of three bands (with ω in cm^{-1}):

$$\begin{aligned} &\text{Band 1:} \quad 0 < \omega < \quad 0.8E4 \\ &\text{Band 2:} \quad 0.8\ E4 < \omega < \quad 2E4 \qquad (5\text{-}20) \\ &\text{Band 3:} \quad 2E4 < \omega < \infty \quad . \end{aligned}$$

In the first band radiation from cesium and from electron-atom hydrogen Bremsstrahlung are important. In the second and third bands radiation from cesium and free-bound H^- are important. The absorption coefficients for the three bands are expressed as

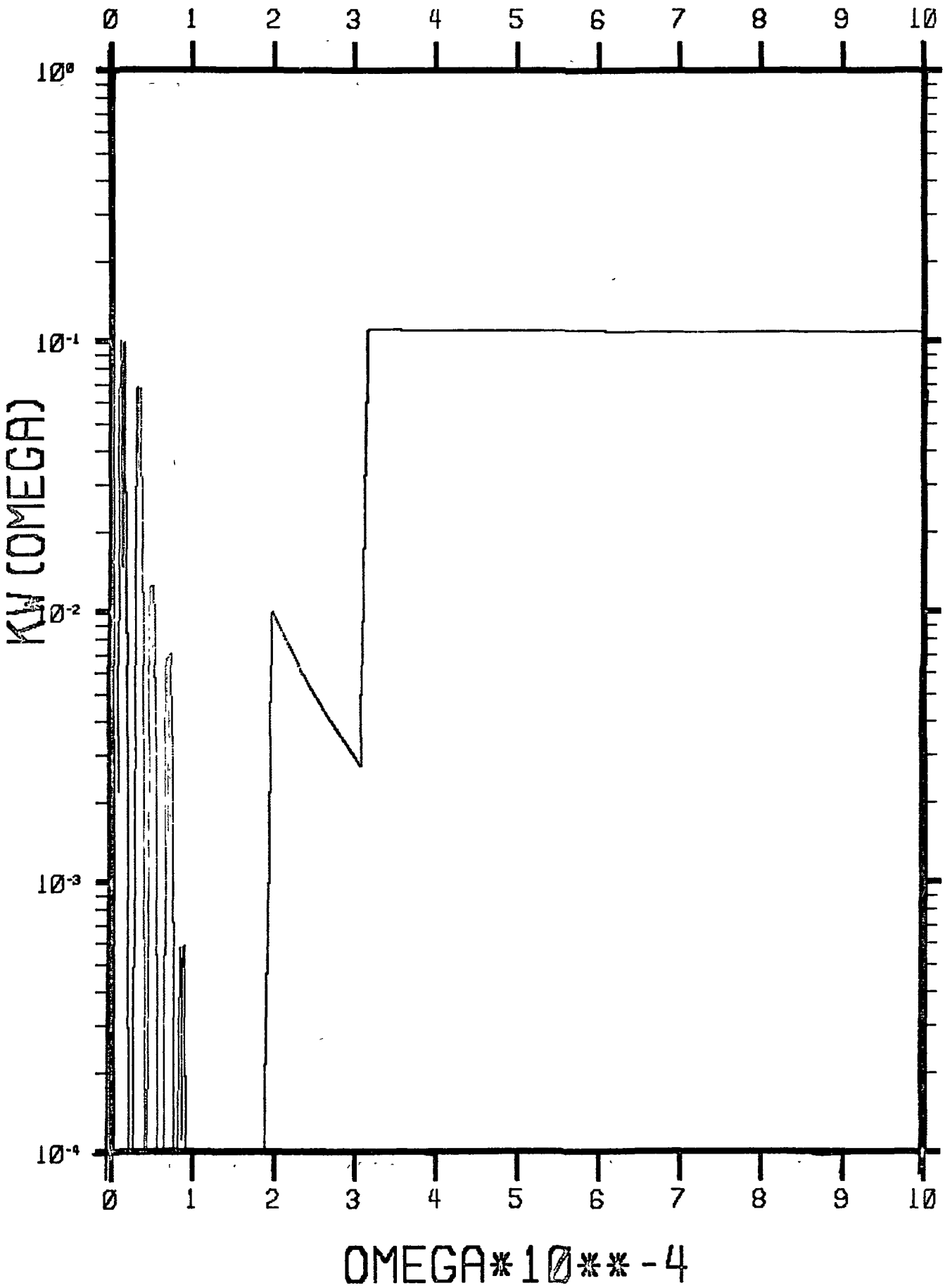

Fig. 5-2a Absorption Coefficient as a Function of Wavenumber for $H_2/H_2O/Cs$ = 0.945/0.05/0.005. T = 2000 K, p = 30 atm.

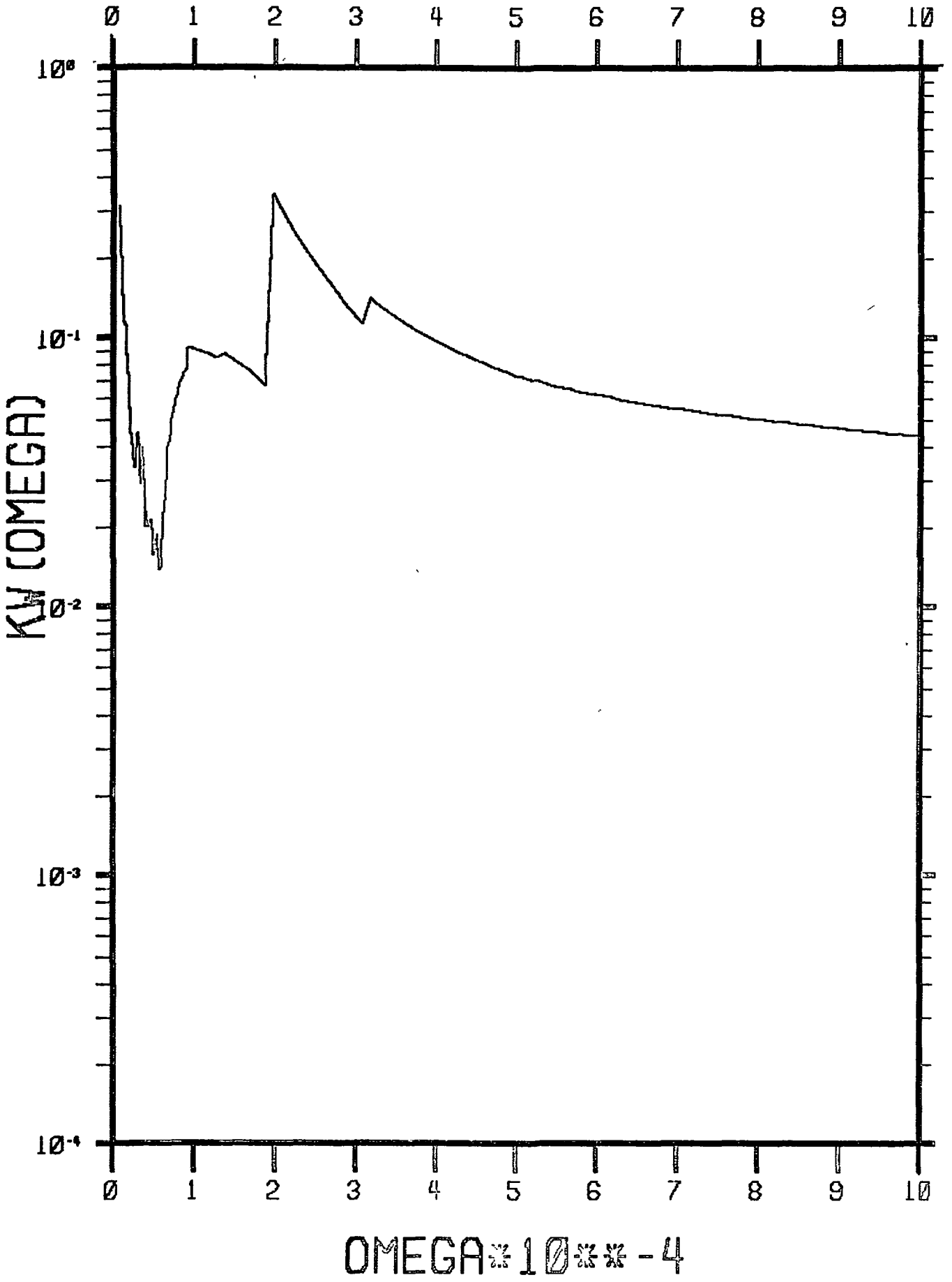

Fig. 5-2b Absorption Coefficient as a Function of Wavenumber for $H_2/H_2O/Cs$ = 0.945/0.05/0.005. T = 4000 K, p = 30 atm.

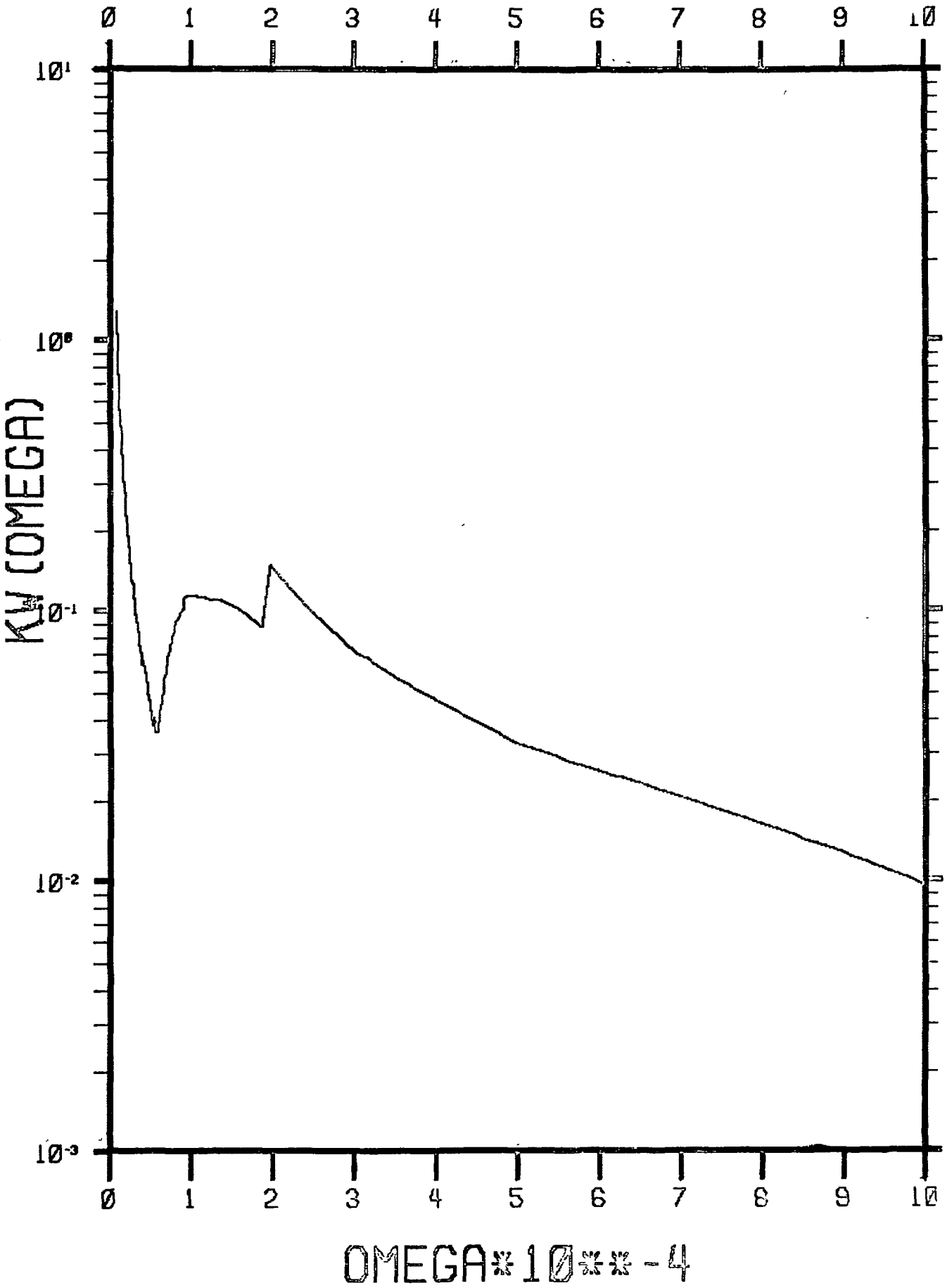

Fig. 5-2c Absorption Coefficient as a Function of Wavenumber for $H_2/H_2O/Cs$ = 0.945/0.05/0.005. T = 6000 K, p = 30 atm.

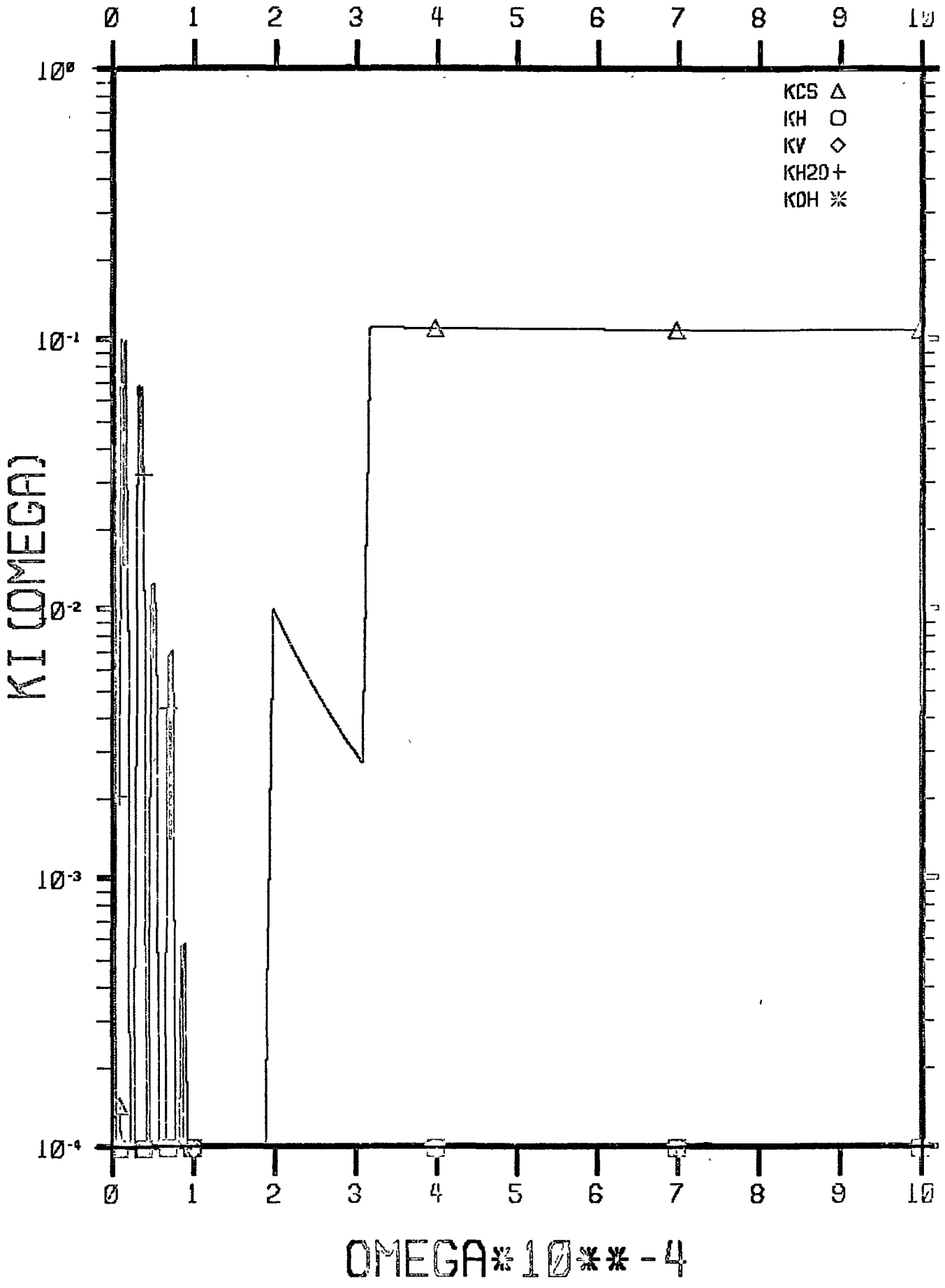

Fig. 5-3a Component Absorption Coefficients as a Function of Wavenumber for $H_2/H_2O/Cs$ = 0.945/0.05/0.005. T = 2000 K, p = 30 atm.

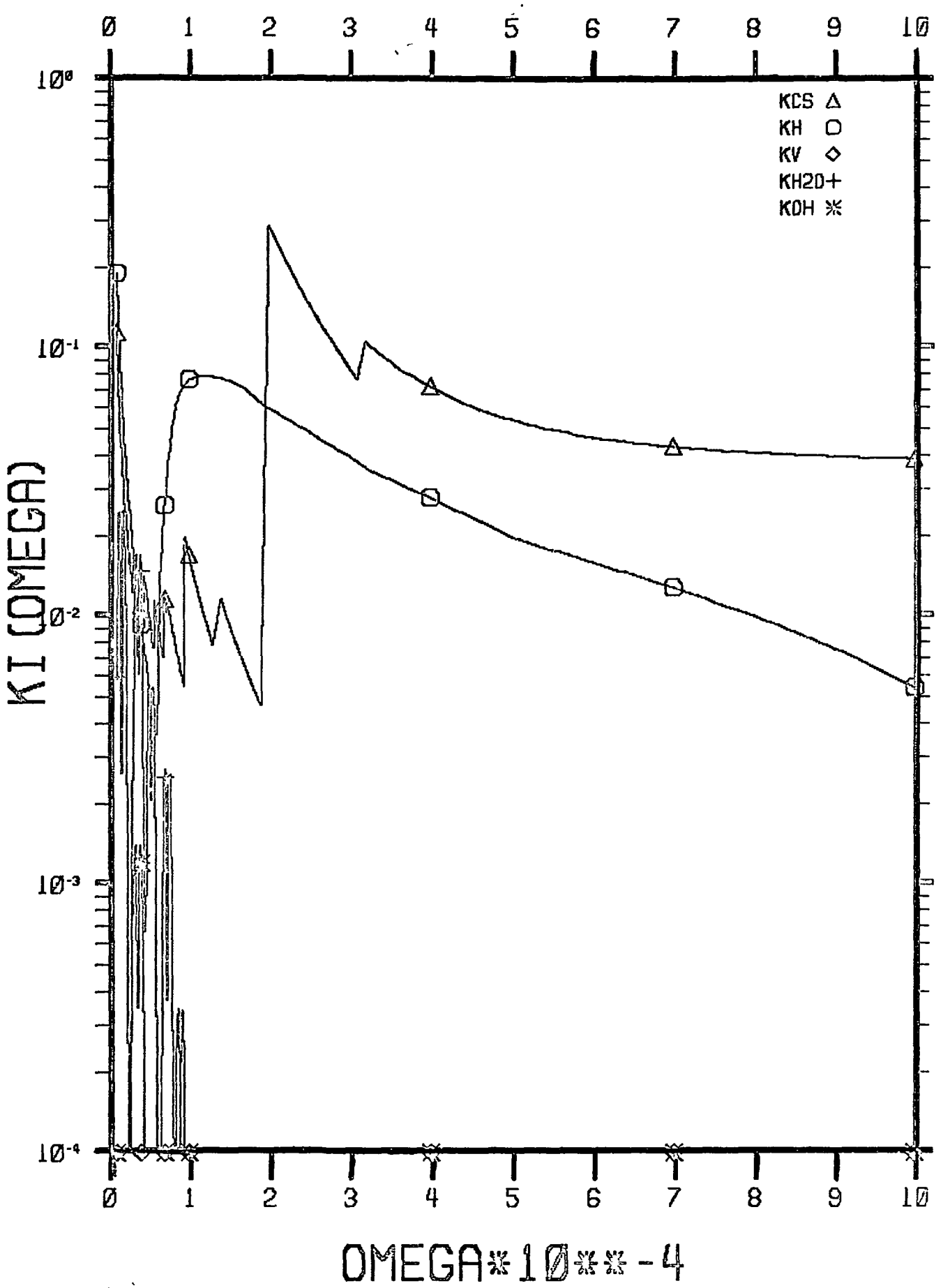

Fig. 5-3b Component Absorption Coefficients as a Function of Wavenumber for $H_2/H_2O/Cs$ = 0.945/0.05/0.005. T = 4000 K, p = 30 atm.

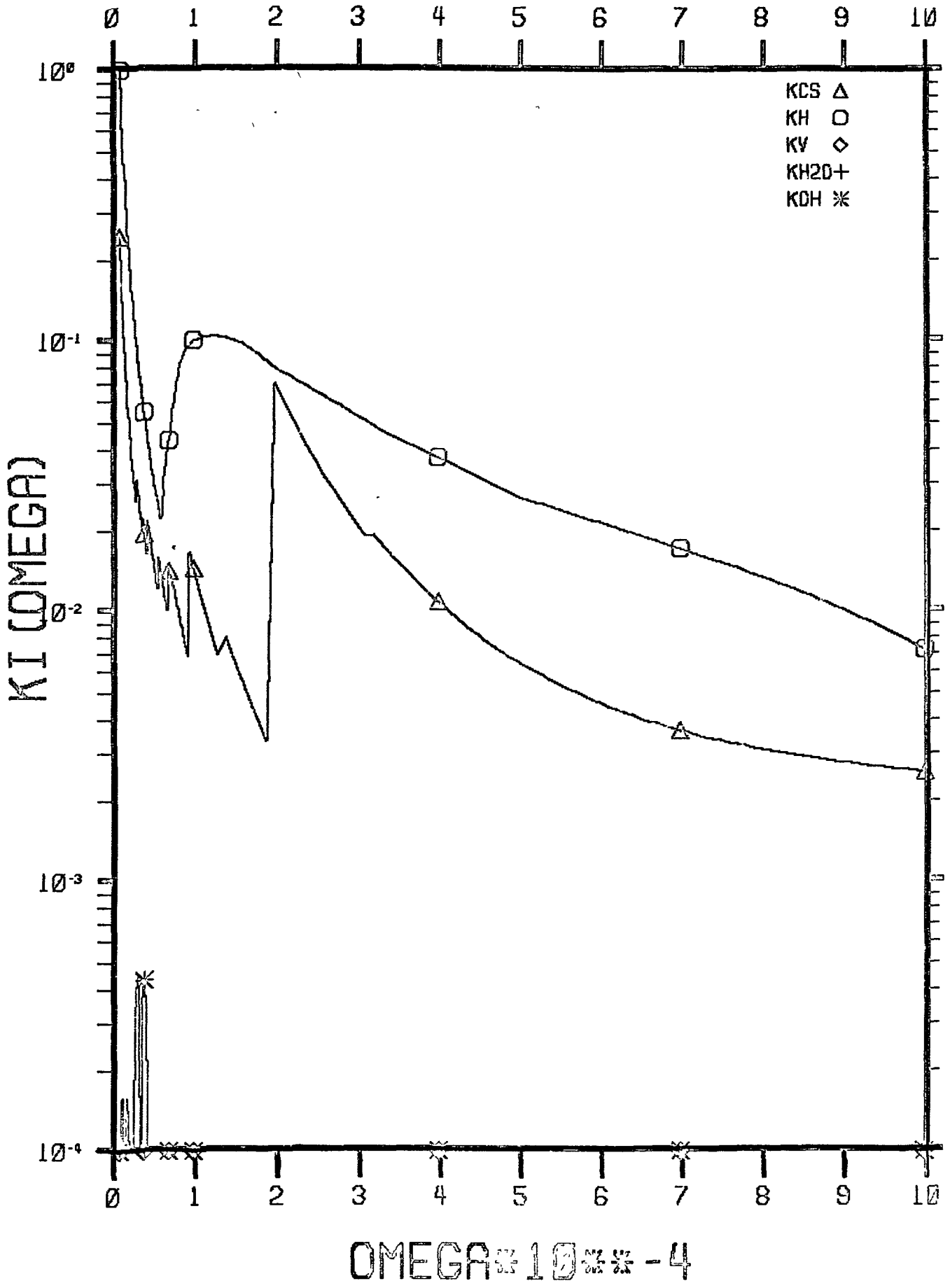

Fig. 5-3c Component Absorption Coefficients as a Function of Wavenumber for $H_2/H_2O/Cs$ = 0.945/0.05/0.005. T = 6000 K, p = 30 atm.

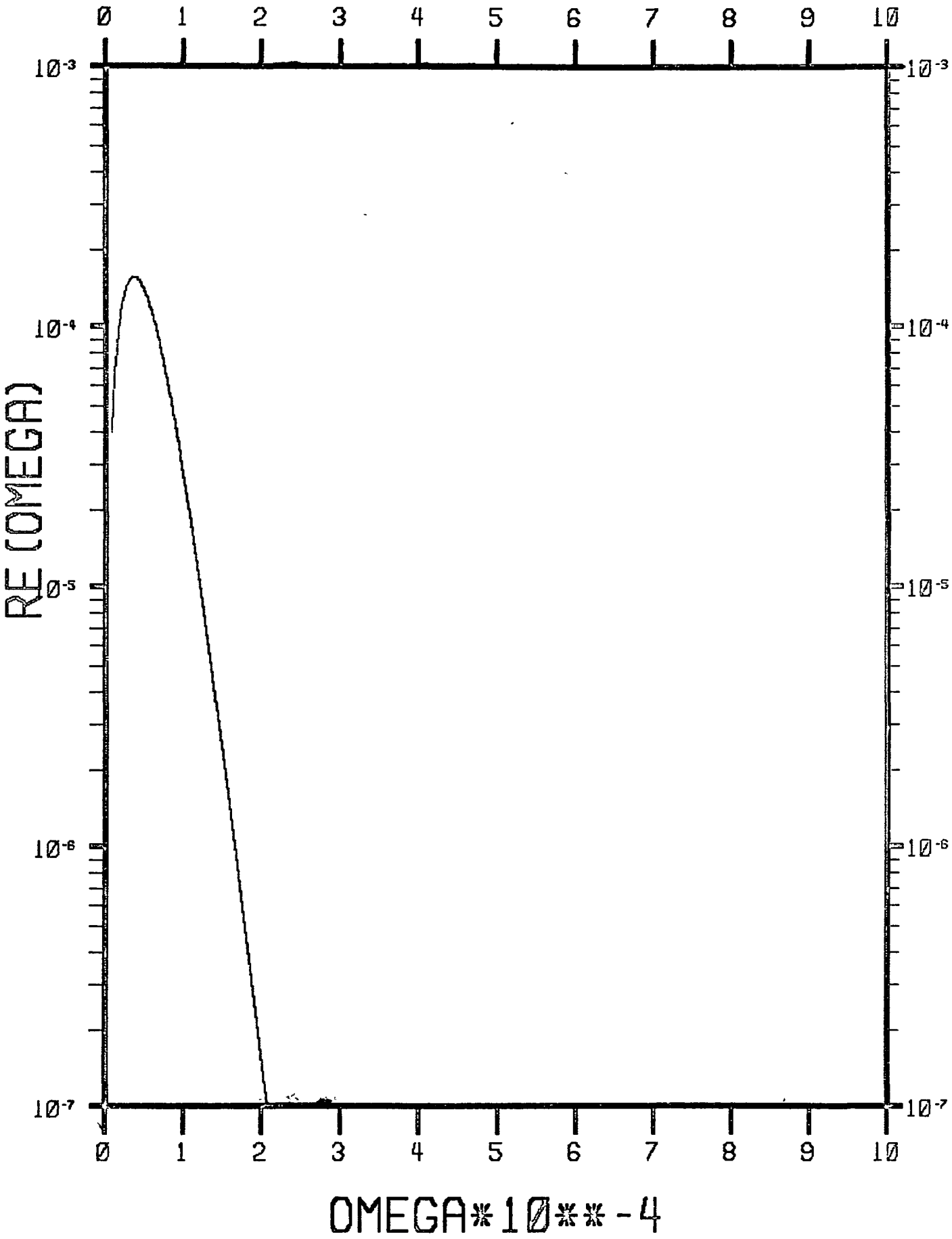

Fig. 5-4a Normalized Blackbody Function $B_\omega/\sigma T^4$. T = 2000 K.

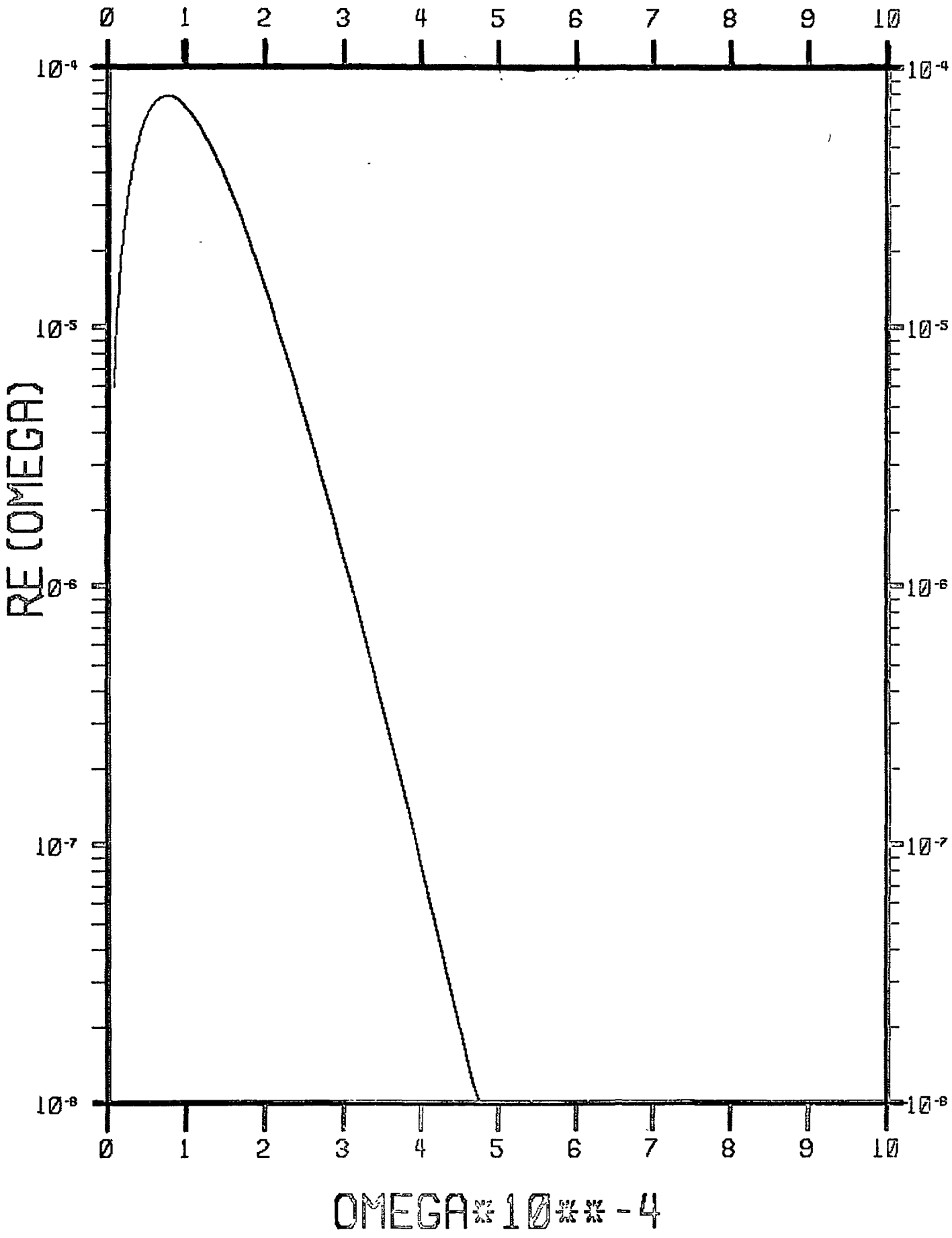

Fig. 5-4b Normalized Blackbody Function $B_\omega/\sigma T^4$. T = 4000 K.

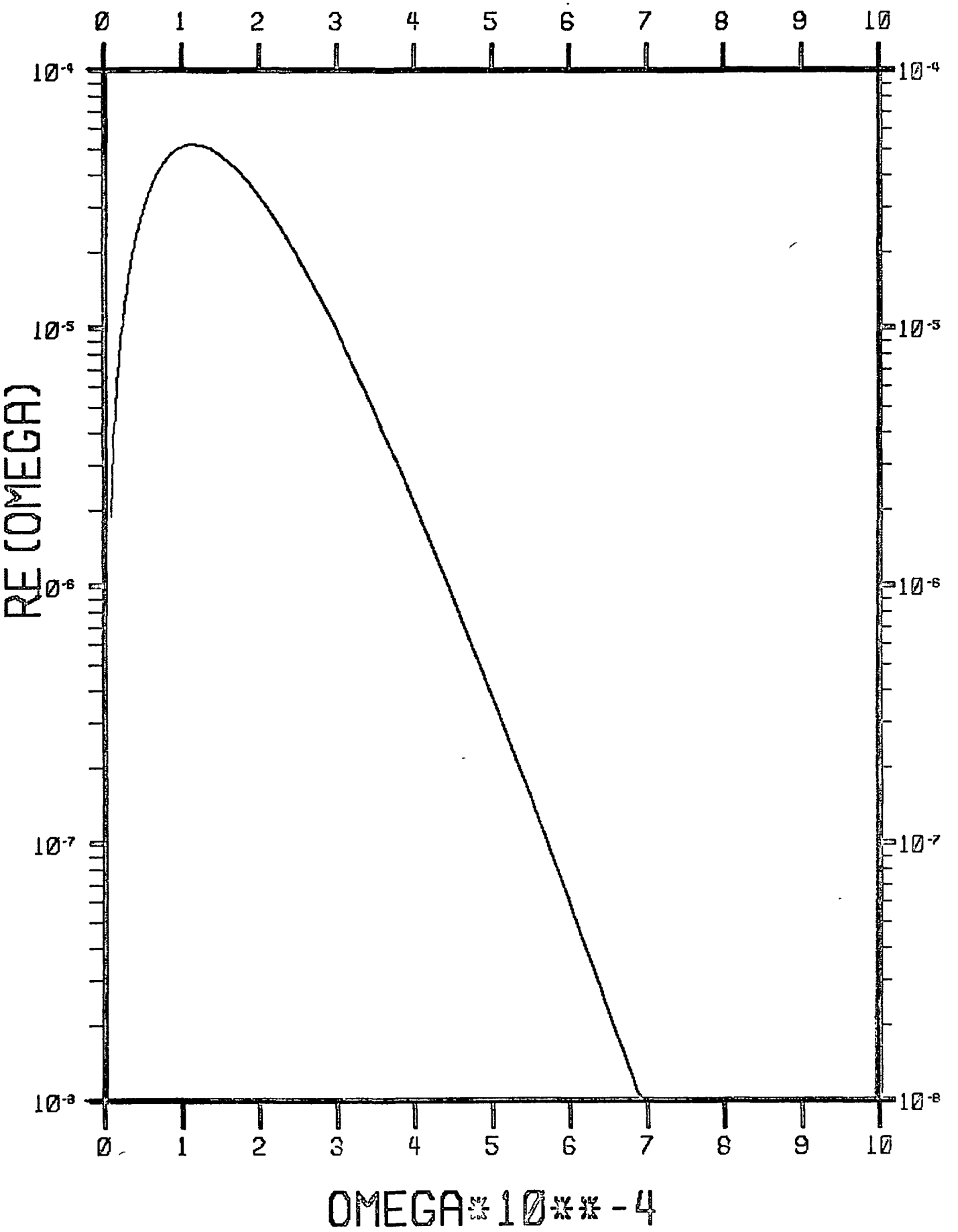

Fig. 5-4c Normalized Blackbody Function $B_\omega/\sigma T^4$. T = 6000 K.

$$k_1^* = 1.3\ \text{E-17}\ n_{Cs}^{***} + n_H n_E\ \sigma_{EH}\ (\omega = 4500) \qquad (5\text{-}21\,a)$$

$$k_2^* = 1.75\ \text{E-17}\ n_{Cs}^{**} + 4.2\ \text{E-17}\ n_{HM} \qquad (5\text{-}21b)$$

$$k_3^* = 1.0\ \text{E-17}\ n_{Cs}^{*} + 2.5\ \text{E-17}\ n_{HM}\ . \qquad (5\text{-}21c)$$

The cesium number densities are those of certain excited states, which are expressed through an approximation to the cesium partition function

$$Q_{Cs} = 2 + 6\ e^{-16616/T} + 10\ e^{-20950/T} + 20\ e^{-32540/T} + 266\ e^{-38130/T}\ . \qquad (5\text{-}22)$$

In terms of Q_{Cs} and the cesium number density n_{Cs} the excited state densities are

$$n_{Cs}^{***} = 266\ e^{-38130/T}\ n_{Cs}/\ Q_{Cs} \qquad (5\text{-}23\,a)$$

$$n_{Cs}^{**} = 20\ e^{-32540/T}\ n_{Cs}/Q_{Cs} \qquad (5\text{-}23\,b)$$

$$n_{Cs}^{*} = \left(6\ e^{-16616/T} + 10\ e^{-20950/T}\right) n_{Cs}/Q_{Cs}\ . \qquad (5\text{-}23\,c)$$

The cross-section in Eq. (5-21 a) is the E-H Bremsstrahlung cross-section from Eq. (3-18) evaluated at $\omega = 4500\ \text{cm}^{-1}$, which can be expressed as

$$\sigma_{EH}\ (\omega = 4500) = 1.08\ \text{E-43}\ T^{3/2}\ (1 + 3237/T)\ e^{-\xi} \qquad (5\text{-}24)$$

where ξ is given in Eq. (2-6). This completely defines the absorption coefficients for this band model example, which are to be used in Eqs. (5-18) and (5-19).

The contributions to the absorption coefficients defined above come from cesium, H, H^- and electrons. The spectra of Fig. 5-3 also show a contribution from water in a limited range, with considerable structure. This contribution is always thin, and only important at low temperature. Rather than treat it as an absorption coefficient, therefore, we have parametrized it directly as an added contribution to the emission for the thin case:

$$(\nabla \cdot \underline{S}^R)_{thin} = 1.85 \text{ E-21 } T^{2.9} \, n_{H_2O} \, . \qquad (5\text{-}25)$$

Thick-Thin Criteria

At any point in the flow field, a given band is taken to be thick or thin, so the radiation term is either given by Eq. (5-16) or by Eq. (5-15). We need a criteria for the transition from thick to thin. This criteria involves the product of the absorption coefficient and some typical length, r_R .

Since the absorption coefficient is of the form of Eq. (5-17), we need to evaluate the stimulated emission factor at some mean band location. Examination of the spectral absorption coefficient curves suggests that for the purpose of choosing a band to be thick or thin, we can use

$$\text{Band 1: } \omega = 4500 \text{ cm}^{-1}, \; k_1 = k_1^* \, (1 - e^{-6475/T}) \qquad (5\text{-}26a)$$

$$\text{Band 2: } \omega = 14000 \text{ cm}^{-1}, k_2 = k_2^* \, (1 - e^{-20143/T}) \qquad (5\text{-}26b)$$

$$\text{Band 3: } \omega = 23875 \text{ cm}^{-1}, k_3 = k_3^* \, (1 - e^{-34351/T}) \, . \qquad (5\text{-}26c)$$

Various methods for making the thick-thin transition were tried. In order to avoid an abrupt change from thick to thin we settled on a gradual transition, with an interpolation function.

$$k_1 r_R < 0.2 \quad \text{Thin}$$

$$k_i r_R > 5 \quad \text{Thick} \tag{5-27}$$

$$0.2 < k_i r_R < 5: \quad \text{Interpolate} .$$

The interpolation was performed using

$$\nabla \cdot \underline{S}^R = (\nabla \cdot \underline{S}^R)_{thin} + f(k_1 r_R)\left[(\nabla \cdot \underline{S}^R)_{thk} - (\nabla \cdot \underline{S}^R)_{thin}\right]$$

$$f(k_i r_R) = \frac{(k_i r_R)^2}{1 + (k_i r_R)^2} \quad . \tag{5-28}$$

The function f is 0.038 at the thin boundary and 0.96 at the thick boundary. As discussed above the details of this transition are not expected to effect the results significantly.

The choice of the length r_R was based on the radiation changing by a factor of 2, or the temperature changing by $2^{\frac{1}{4}} = 0.841$. The temperature profile near the channel centerline was fitted by a parabola centered on T ($\Psi = 0$), and passing through the nearest calculated point to the centerline at which the temperature was down below 0.841 T($\Psi = 0$), call it T*, at which r = r*. Then we chose

$$r_R = \left[\frac{0.159\ T(\Psi = 0)\ (r^*)^2}{T(\Psi = 0) - T^*}\right]^{1/2} \tag{5-29}$$

which is the point at which T = 0.841 T($\Psi = 0$) on the fitted parabola.

These relations now completely define the way to evaluate the radiative loss term $\nabla \cdot \underline{S}^R$.

5.6 Heat Flux to the Wall

The wall heating is an important parameter in the design of a laser-heated thruster, and its expression merits special mention. It is convenient to consider the wall heat flux in two parts: first the convective and diffusive part, and second the radiative part.

The convective and diffusive part has already been expressed in Eq. (5-1d) as the coefficient of r in the last term,

$$q_C = - \frac{\lambda_{C\,f}}{c_{pf}} \left[\frac{\partial h}{\partial r} + \sum (Le_i - 1)\, h_i \frac{\partial C_i}{\partial r} \right]. \tag{5-30}$$

The minus sign is introduced so that q_C is positive when heat flows into the wall (negative gradients). Use of the transformation derivative in Eq. (5-6a) enables this to be expressed as

$$q_C = - \rho u r \frac{\lambda_{C\,f}}{c_{pf}} \left[\frac{\partial h}{\partial \Psi} + \sum (Le_i - 1)\, h_i \frac{\partial C_i}{\partial \Psi} \right] . \tag{5-31}$$

The numerical evaluation of q_C at the wall is not straightforward because $u = 0$ there while $\partial/\partial\Psi$ is infinite, as already discussed in connection with the wall shape. However, if we convert the $\partial/\partial r$ to $\partial/\partial r^2$ by multiplying Eq. (5-30) by $2r$, we can then use Eq. (5-9b) to convert $\partial/\partial r^2$ to finite difference form, and get

$$q_C = \frac{2\lambda_{Cfw} r_w}{c_{pfw}} \left[h_w - h + \sum (Le_{iw} - 1)\, h_{iw}\, (C_{iw} - C_i) \right] \frac{\rho u}{4(\Psi_w - \Psi)} \tag{5-32}$$

where the quantities without the w subscript are to be evaluated at the first Ψ station away from the wall.

The radiative heating contribution has thick and thin parts, according to the model described above. Reference to Eq. (5-16a) shows the thick part to be

$$q^R_{thk} = -\frac{4\pi}{3}\lambda_R\frac{\partial T}{\partial r} = -\frac{4\pi}{3}\rho u r\lambda_R\frac{\partial T}{\partial \Psi} \quad . \tag{5-33}$$

The same conversion to $\partial/\partial r^2$ produces a finite difference form

$$q^R_{thk} = -\frac{8\pi}{3}\lambda_{Rw} r_w \frac{(T_w - T)\,\rho u}{4(\Psi_w - \Psi)} \quad . \tag{5-34}$$

The thin part of the radiative flux is expressed in terms of $\nabla \cdot \underline{S}^R$ directly by Eq. (5-15). This can be converted to a flux by intergration over r.

$$\int_0^{r_w} r(\nabla \cdot \underline{S}^R)dr = \int_0^{r_w}\left[\frac{\partial}{\partial r}(r\,S^R_r) + r\frac{\partial S^R_x}{\partial x}\right]dr$$

$$= r_w(S^R_r)_w + \int_0^{r_w} r\frac{\partial S^R_x}{\partial x}\,dr \quad .$$

We have constantly ignored the axial fluxes, and will do so here also. If we call $(S^R_r)_w = q^R_{thin}$, and recall the expression for $\nabla \cdot \underline{S}^R$ from Eq. (5-15), we have

$$q^R_{thin} = \frac{1}{r_w}\int_0^{r_w} r\left(4\int_{thin} d\omega k_\omega B_\omega\right)dr \quad . \tag{5-35}$$

This integral can be done in r space to avoid the complications of $u = 0$ at the wall.

The interpolation scheme described above requires that the interpolation function $f(k_i\ r_R)$ be included, so the final expression for the radiative heating is

$$q^R = -\frac{8\pi}{3}\lambda_{Rw} r_w \frac{(T_w - T)\ \rho u}{4(\Psi_w - \Psi)} f(k_i r_R) \qquad (5\text{-}36)$$

$$+ \frac{1}{r_w}\int_0^{r_w}\left[1 - f(k_i r_R)\right] r \left(4\int_{thin} d\omega h_\omega B_\omega\right) dr \quad .$$

The sum of Eqs. (5-32) and (5-36) gives the local wall heat flux, which can be integrated on x to give the total flux up to any station x as

$$Q_w = \int_0^x 2\pi r_w\ (q_C + q^R)\ dx \ . \qquad (5\text{-}37)$$

5.7 Numerical Method

The equations to be solved are basically the axial momentum equation (5-7a), the energy equation (5-7b), and the laser absorption equation (5-2). The equations are parabolic, since they are first order in ξ and second order in Ψ. Thus a marching scheme can be used. Knowing all conditions at a particular value of ξ, we may march forward to the next value. The process is begun with a given set of conditions at the initial station $\xi = 0$.

The dependent variables to be solved for are the axial speed u, the enthalpy h, and the laser intensity I. The pressure distribution is input. When p and h are known, the temperature and composition are found from the hypothesis of chemical equilibrium.

The non-linearity of the equations, and the coupling between u and h require an iterative solution. To advance a step in ξ, Eqs. (5-7) are solved for u and h by the finite-difference Crank-Nicholson implicit scheme. This requires the values of k_L, I and other properties at the new ξ station, which depend on the given p and an unknown T. To start the advance, a T profile is guessed, based on the profile at the present ξ station. This is used to calculate the needed fluid properties and I. Then the values of u and h are found by Crank-Nicholson at the new station. With this h and the given p, we find T and C_i from

equilibrium. If this T does not agree with the guessed profile, it is used to re-calculate the fluid properties, and the equations are again used to find new values of u and h at the new station. This process is repeated until the T profile used for the properties agrees with that found from the calculated values of u and h to a satisfactory accuracy. This then completes the calculation at the new station, and we then advance again by repeating the iterative process.

In the laser-heated flow being considered here, the properties which have the main influence on the flow are k_L and I, through the first term on the right of the energy equation (5-7b), which is the laser heat addition term. Since k_L is a strong function of T and the number densities $n_i = \rho C_i/m_i$, it is the dominant effect on the temperature profile, and controls the iteration process.

The computer code which embodies this numerical method is called LHTE.

5.8 Numerical Example

We have calculated a numerical example using the code LHTE for 10.6μm. Because the radiation model had only been developed for p = 30 atm and a mixture of $H_2/H_2O/Cs$ = 0.945/0.05/0.005, this was the case chosen. The initial profile of T was uniform at 1000 K, and the wall was held fixed at that temperature. At this pressure and temperature the initial density is 1.27E-3 g/cm^3 for this mixture, whose molecular weight is 3.47. The centerline laser intensity was taken as 10^4 W/cm^2 = 10^{11} erg/cm^2s and the power as 10^6 W. For the beam shape we took the cut-off radius to be the same as r_1, the radius to the first zero. Then Eq. (5-14) determines r_c = 11.81 cm. We chose a case which would have, if there were no losses, an I_{sp} = 2000, so the kinetic energy in the exhaust would be 1.92E-12 erg/g. Since this is also the power per unit mass flow, a power of 10^6 W (10^{13} erg/s) leads to a mass flow rate of 5.21 g/s. We took a uniform velocity profile, and set the initial wall radius r_w to r_c = 11.81 cm, so the initial area was 438.2 cm^2. Then the initial velocity for the given mass flow and density was 9.36 cm/s. Finally, we specified the pressure

gradient term as $dp/d\xi = -0.278$ dynes/cm^2, which is 2.5 times the product of the initial density and the initial velocity squared. This parameter determines the shape of the channel.

Several fluid properties also need to be specified to enable the calculation to be carried forward. The set of equations to be solved, Eqs. (5-7), contain the vescosity μ and the ratio of thermal conductivity to frozen specific heat, λ_{Cf}/c_{pf}. These can be combined to introduce the Prandtl number

$$Pr = c_{pf}\mu/\lambda_{Cf} \quad , \quad \lambda_{Cf}/c_{pf} = \mu/Pr \ .$$

Thus we can use μ and Pr to express these transport properties. Examination of our pure hydrogen calculations of μ, Section IV, indicates that a reasonable fit for 30 atm, 1000 K < T < 5000 K is

$$\mu = 7.5 \text{ E-5} + 1.24 \text{ E-7 } T \text{ (g/cm-s)}.$$

This value was used in the calculation, although it is recognized that, as pointed out at the end of Section IV, the viscosity of a mixture including cesium will be higher because of its high molecular weight. Therefore, the viscosity should be improved in the final version of the LHTE program.

The frozen specific heat c_{pf} can be found from the expressions indicated in Section IV for c_p, by ignoring the terms involving derivatives of the number densities. Likewise λ_{Cf} can be found by using the λ_{tr} and λ_{int} contributions to λ, given in Eqs. (4-55a) and 4-55b). When this is done at 30 atm, 1000 K < T < 6000 K, and the values of Pr are found, it turns out that Pr varies slowly from 0.68 to 0.67. This is in accord with the well-known fact that Prandtl number is a slowly varying function of temperature. In the sample calculation being described, a constant value of 0.65 was used, though a slightly higher value would have been preferable.

In order to reduce the complication involved in this first calculation, we used $Le_i = 1$, thus assuming that diffusion of heat and species were the same. It is known that this approximation has only a small effect on convective heat flux, compared to using more accurate values of Le_i, in reacting gasdynamics.

At the initial station, where ρ and u are constant, $\Psi = \frac{1}{2} \rho u r^2$, so the value at r_w is 0.8287. Thus Ψ goes from 0 to 0.8287. For this first calculation we used only ten intervals in Ψ, equally spaced. This is not enough to give very accurate results, especially in the high radial gradient region near the wall, but we wished only to test the calculation scheme and the nature of the results, not produce great accuracy.

The calculation was carried out to ξ = 100 cm, and some of the results are presented in the next figures. In Fig. 5-5 are presented radial profiles of the laser intensity I at a number of ξ stations.* The notable feature is the rapid absorption of laser energy near the center of the channel. By 1.5 cm, the center intensity is reduced from 10^4 to 7000 W/cm^2, and by 3.5 cm to 1500 W/cm^2. Meanwhile, there is almost no absorption outside a radius of 6 cm. The reason for this is the low temperature in the outer regions, where the laser intensity is low so the heating is low, and also the wall is constrained to stay at 1000 K.

A similar plot of the temperature profile is presented in Fig. 5-6. This starts uniform at 1000 K at ξ = 0, but heats rapidly up to 6000 K at the center by 1.33 cm. It then begins to cool by radiation, and becomes flattened at the center while the hot region spreads outward. At 7.1 cm, when Fig. 5-5 shows that most of the laser energy has been absorbed, the central temperature is down to 4000 K, and after that it continues to decrease. It appears that after the laser energy has been mostly absorbed, only energy loss prevails, and one would then want to begin the gas acceleration by sharply reducing the channel area.

* The slope discontinuities in the curves in Figs. 5-5 and 5-6 are caused by the plotting routine. The calculated curves have continuous slopes.

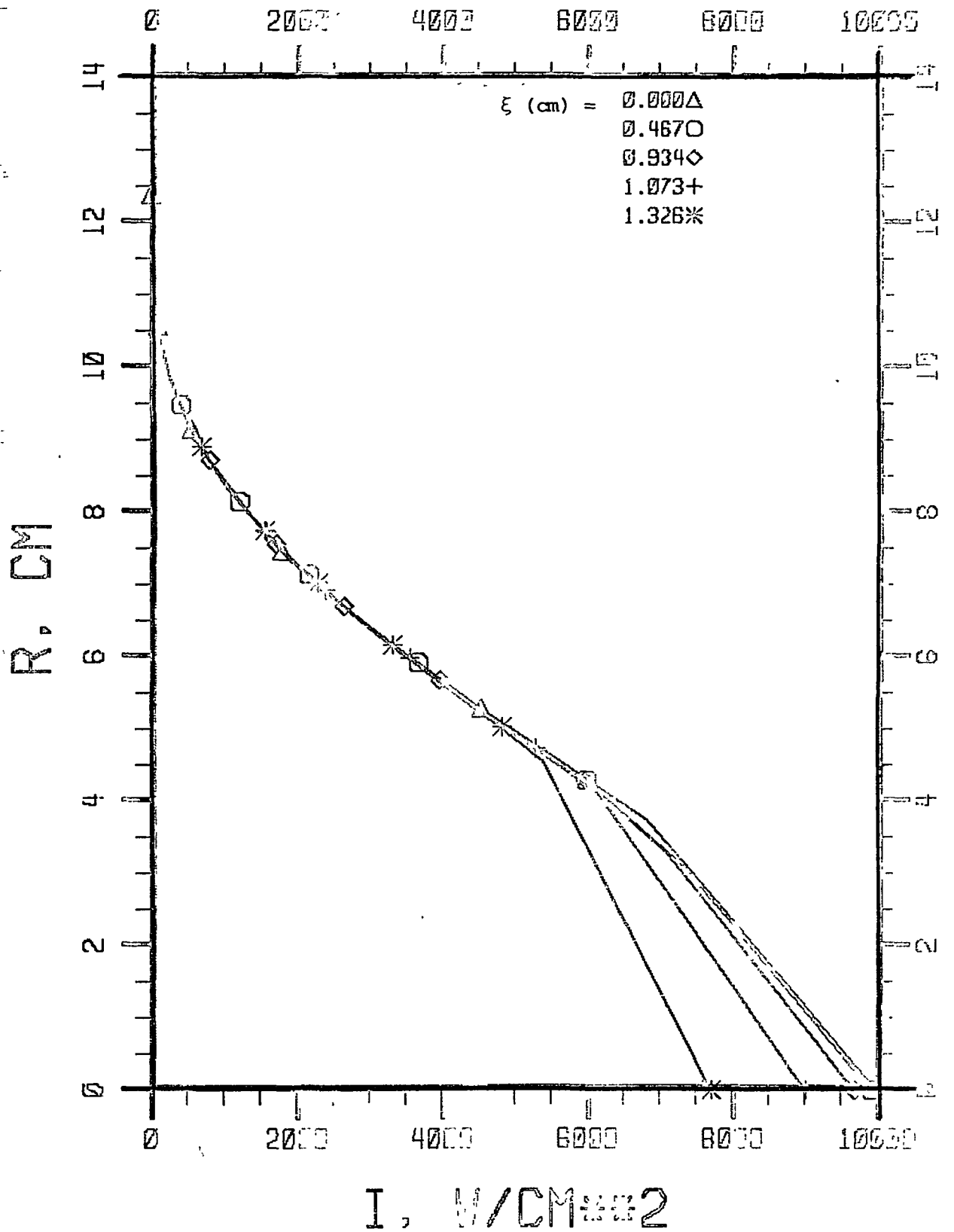

Fig. 5-5a Laser Intensity Profiles at Various Axial Stations $0 \leq \xi \leq 1.326$ cm.

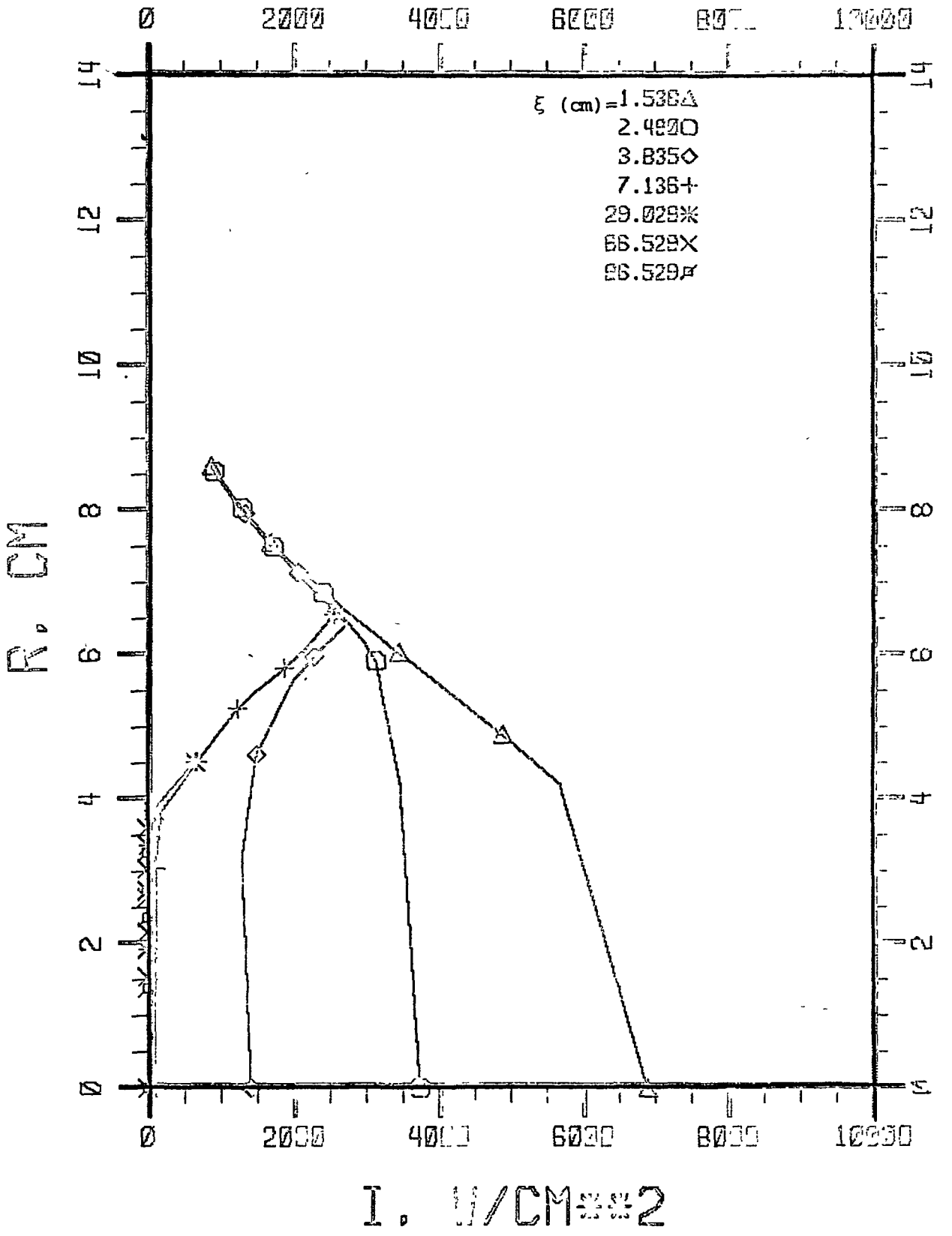

Fig. 5-5b Laser Intensity Profiles at Various Axial Stations $1.538 \leq \xi \leq 96.529$ cm.

Actually, the area is being reduced continuously in this calculation, as is clear from Fig. 5-6, where the point at 1000 K is the wall at each ξ station. To make this clearer, a plot of r_w vs ξ is given in Fig. 5-7. The choice of $dp/d\xi$ used produced the channel shape shown. By ξ = 10 cm the wall radius is down by a factor of 2, and by 100 cm it is about one quarter of its initial value. This change has produced an acceleration, since at 96.5 cm the velocity on the centerline is 362 cm/s, compared with its initial value of 9.36 cm/s. But this is only a small change in velocity, and the real acceleration of the flow will need a nozzle to expand it to supersonic speeds, of course. Back at 7.1 cm, where the laser energy is nearly fully absorbed, the centerline velocity is 142 cm/s. Most of the energy has gone into heating, not acceleration.

The absorption of laser energy can best be illustrated by calculation of the power remaining in the laser beam at any station ξ, by

$$P_L = \int_0^{r_w} 2\pi r \, I \, dr \, .$$

This quantity is plotted in Fig. 5-8 against ξ. It shows a rapid drop beginning at 1 cm. The power is reduced to 10% of its initial value by 8 cm, and to 1% by 25 cm. While some of this reduction is due to the laser beam being cut off by the shrinking channel size, most is due to absorption in the gas.

The object of the laser heating is, of course, to get the energy into the gas. The power is the gas is

$$P_G = \int_0^{r_w} 2\pi r \, (h + u^2/2) \, dr$$

although for the region calculated the kinetic energy contribution is negligible. P_G is also shown in Fig. 5-8. It rises rapidly as

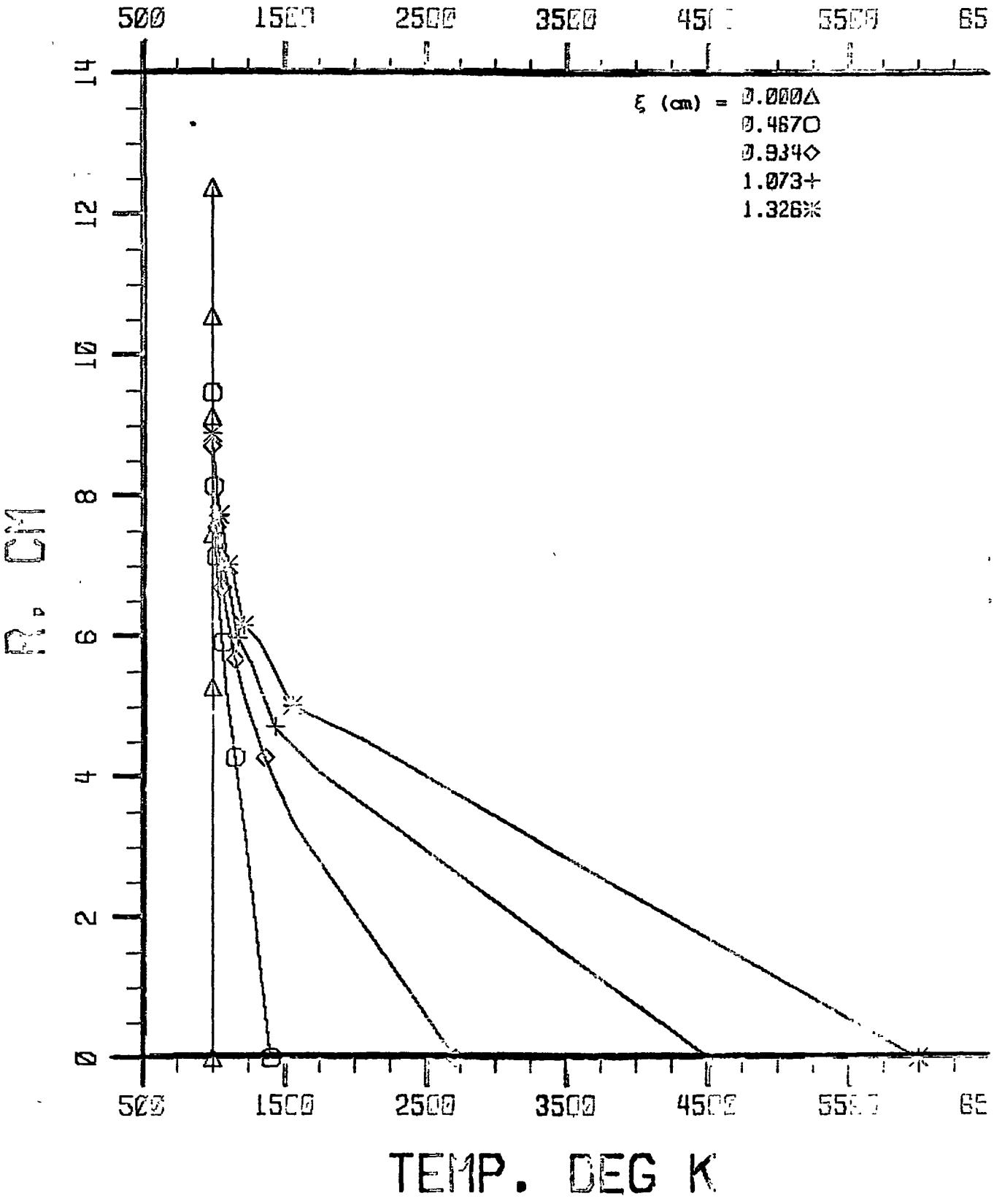

Fig. 5-6a Temperature Profiles at Various Axial Stations $0 \leq \xi \leq 1.326$ cm.

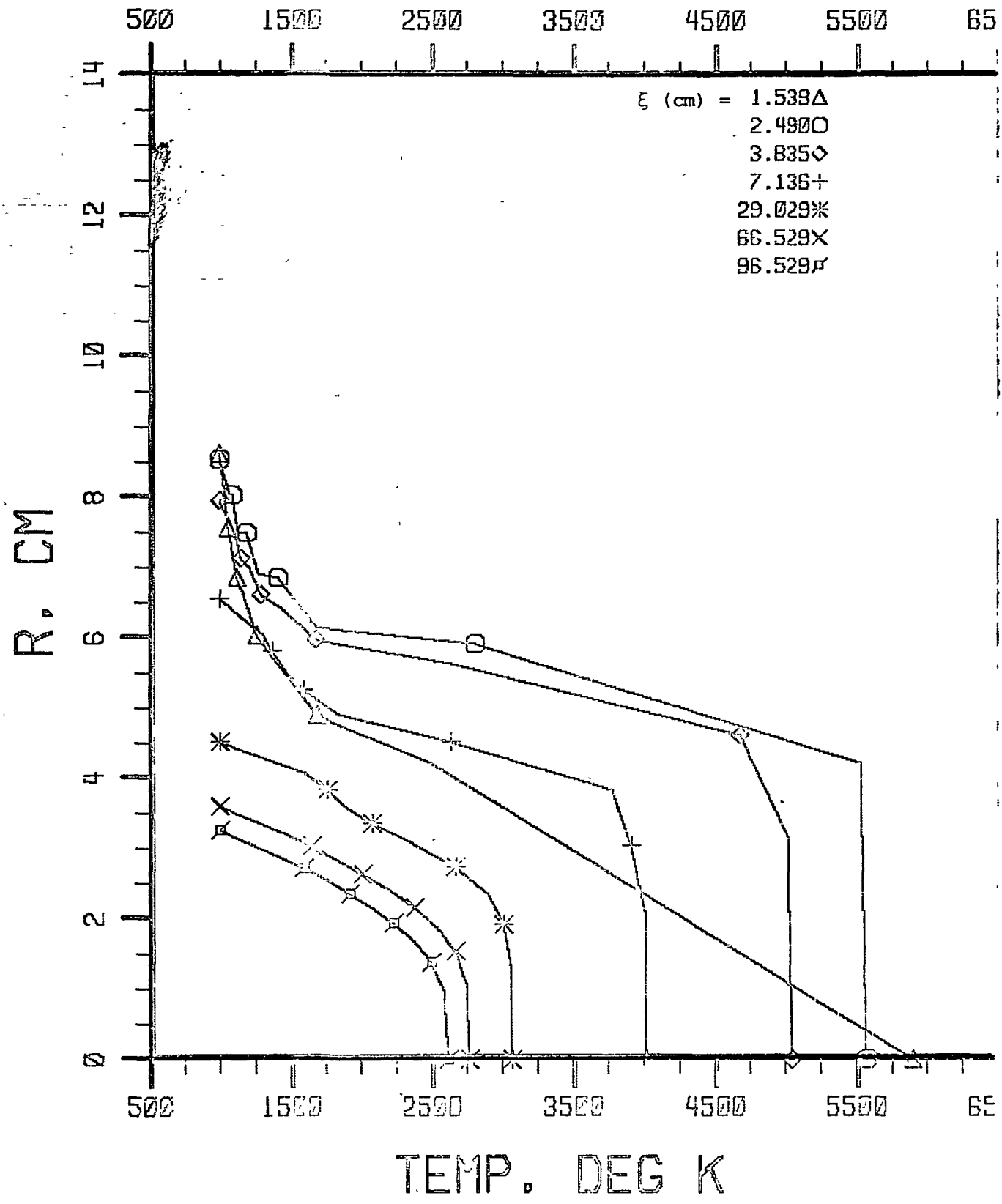

Fig. 5-6b Temperature Profiles at Various Axial Stations
$1.538 \leq \xi \leq 96.529$ cm.

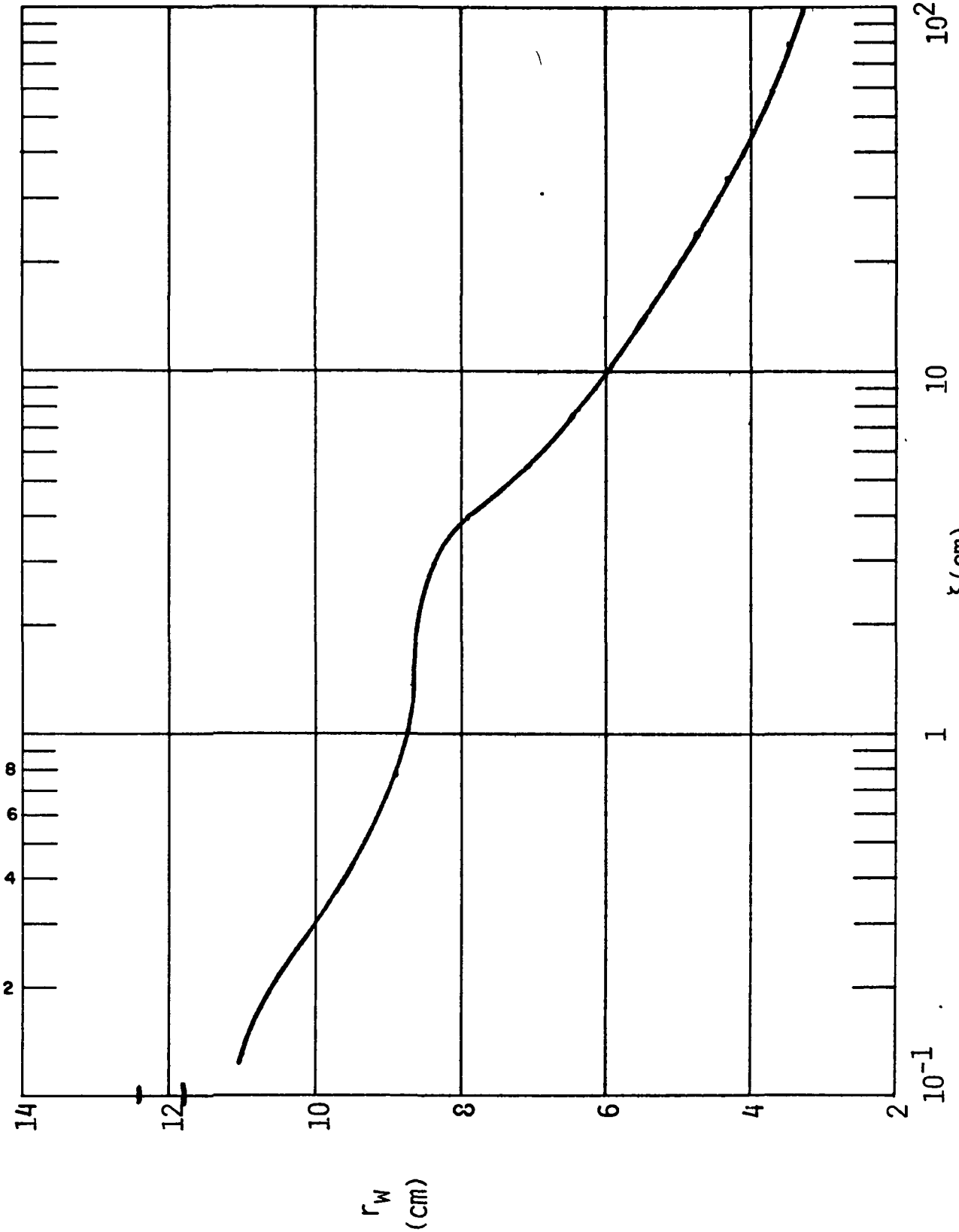

Fig. 5-7 Axial Distribution of Wall Radius.

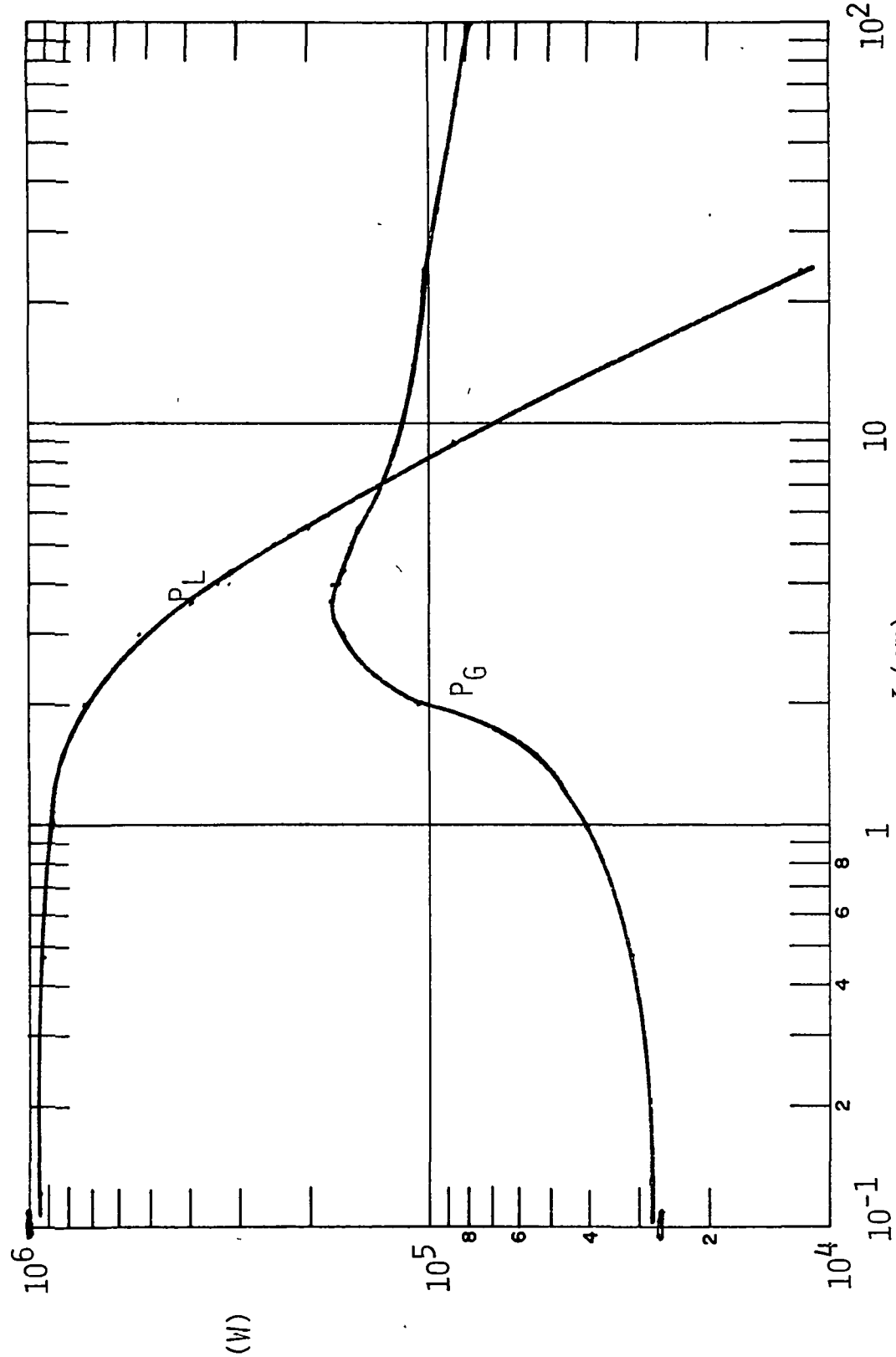

Fig. 5-8 Axial Distribution of Power in the Laser Beam P_L and Power in the Gas, P_G.

the laser energy is absorbed, but losses also rise as the temperature increases, so the power in the gas reaches a peak at about 3.6 cm and then decreases slowly. The peak power in the gas is about 0.18 MW, which is 18% of the input laser power. At this station the laser power is 0.39 MW, so 0.61 MW has been extracted from the beam. If 0.18 MW is in the gas, then the remaining 0.43 MW has been lost to the wall, either because the outer edges of the beam hit the wall as the wall radius decreased, or because of heat flux to the wall.

The amount cut off by the converging walls can be estimated by use of Fig. 5-1. The radius at 3.6 cm is 8.1 cm, down from 11.8 cm at the initial station. The P_r/P_1 curve of Fig. 5-1 shows that about 10% of the incoming beam has been cut off by that radius reduction, or 0.1 MW, leaving 0.33 MW to be accounted for by wall heat flux.

Figure 5-9 shows the distribution of convective and total local wall heat flux q_c and q_w where q_c is from Eq. (5-32) and $q_w = q_c + q^R$, with q^R from Eq. (5-36). The radiative heating is by far the dominant term as can be seen from the factor of 10^3 difference in the scales. The peak heating is about 3.3 kW/cm^2 at 2.4 cm. An estimate of the integral of q_w up to 3.6 cm is 0.25 MW, which is about 0.08 MW short of adding up to 1 MW. This 8% error can probably be accounted for by the crudeness of the Ψ-grid on which this example was calculated. Within that accuracy, we may say the energy balances, either being in the gas, in the laser beam, intercepted by the walls, or radiated to the walls.

We may note that the peak heat flux shown in Fig. 5-9, 3.3 kW/cm^2, is high, but not unreasonable, and can be handled with fairly conventional cooling methods.

This calculation was a preliminary one, meant to show that the model produces physically meaningful and reasonable results. It shows good absorption at high temperature and very little at low temperature, at least in a distance of 10 cm. It shows that at p = 30 atm a large fraction of the laser energy put into the gas is radiated to the walls, but even this heat flux can probably be handled.

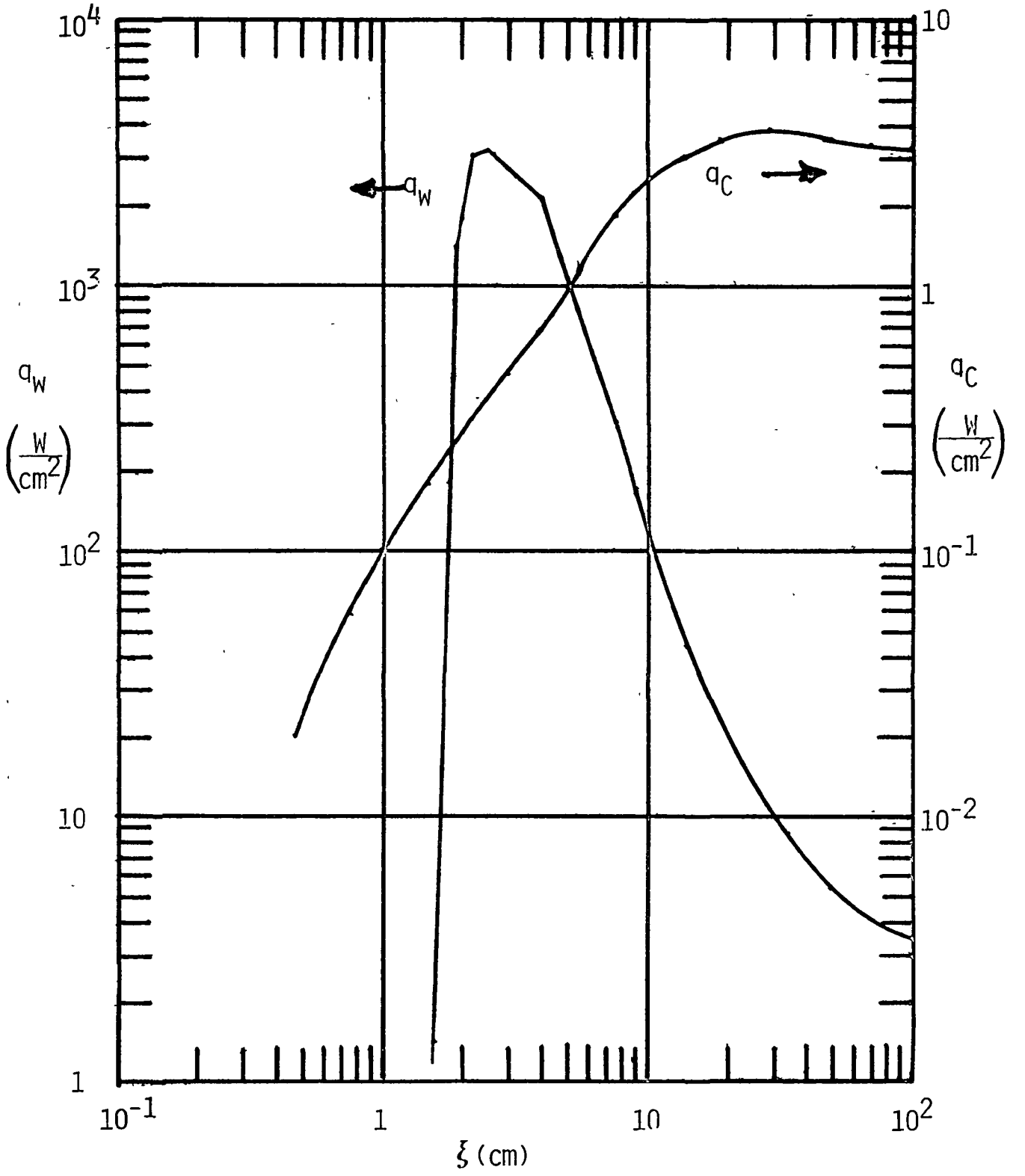

Fig. 5-9 Axial Distribution of Local Convective Wall Heat Flux q_c and Local Total Wall Heat Flux q_w.

5.9 Further Development

There are a number of further developments that are needed to make this code generally useful. Foremost is the need to generalize the radiation model to be applicable to all useful pressure levels and mixture compositions. Second, we need to get some experience with running the code to learn how to choose $dp/d\xi$ so as to maintain a desired channel shape which probably should be more nearly symmetrical than the present shape. A more refined mesh in the Ψ coordinate is also needed to fill in more points near the center. With uniform input flow and uniform spacing of Ψ points, we start with equal increments in r^2, not r. Thus in r the points get closer as r increases. This is desirable to place more points in the wall region. However, with only ten intervals in Ψ, there is inadequate definition of the central region where the large heating is taking place.

Work is proceeding to incorporate these further developments into the code to make it generally useful for parametric studies.

VI. CONCLUSIONS

This interim report describes work which has focused mainly on the physical properties of the gases which are important for modeling a CW laser-heated thruster. We have described the laser absorption properties, the radiation properties, and the thermodynamic and transport properties. We have also described a flow code to calculate the channel flow of a laser-heated gas, but only one preliminary calculation has been made so far.

The conclusions drawn, then, relate to the gas properties, and are based on calculations made with the various gas property models described.

1. For 10.6 μm radiation, a mixture of 1 part cesium to 99 parts atomic hydrogen substantially increases the absorption coefficient at low temperatures. The value of 0.1 cm is reached at 2000 K at 100 atm, 3000 K at 10 atm, and 12000 K at 1 atm.

2. For 10.6 μm radiation, water vapor has a minimum absorption coefficient at about 500 K, and appears to be quite low below 1000 K. However, the values in the vicinity of 500 K are not well-known, and the theoretical predictions have not been checked up to 1500 K by experiments. Experimental measurements between room temperature and 1500 K are needed.

3. For 5.3 μm radiation, water vapor is a good absorber from 300 to 3000 K. NO is a good low temperature absorber, and will not dissociate even though it is not an equilibrium state. CO is a good absorber above 2000 K, and remains chemically stable up to at least 6000 K.

4. For 10.6 μm radiation, a mixture of up to 5% water vapor in hydrogen does not provide good low temperature absorption.

5. For 5.3 μm radiation, both NO and water vapor up to 5% in hydrogen provide adequate absorption at low temperatures, though NO is the better absorber.

6. The continuously over-lapping line model of molecular radiation provides results in good agreement with other calculations and with experiments.

7. Cesium is a strong radiator, and its radiation will be an important contributor for thrusters of operational size (10 cm radius). It is less important for laboratory size thrusters (1 cm radius), but still strong in certain bands.

8. The thermal conductivity of cesium-seeded hydrogen is nearly the same as for pure hydrogen. The viscosity, however, increases considerably because of the high molecular weight of cesium.

9. The channel flow model of a laser-heated mixture of hydrogen, water vapor and cesium produced a preliminary calculation which seems to be physically reasonable.

REFERENCES

1. Caledonia, G.E., Wu, P.K.S., and Pirri, A.N., "Radiant Energy Absorption Studies for Laser Propulsion," NASA CR-134809 (PSI TR-20), Woburn, MA, March 1975.

2. Kemp, N.H. Root, R.G., Wu, P.K.S., Caledonia, G.E., and Pirri, A.N., "Laser-Heated Rocket Studies," NASA CR-135127 (PSI TR-53), Woburn, MA, May 1976.

3. Klosterman, E.L. and Byron, S.R., "Measurement of Subsonic Laser Absorption Wave Propagation Characteristics at 10.6μm," J. of Applied Physics, Vol. 45, Nov. 1974, pp. 4751-4759.

4. Kemp, N.H. and Root, R.G., "Analytical Studies of Laser Supported Combustion Waves in Hydrogen," NASA CR-135349 (PSI TR-97), Woburn, MA, August 1977.

5. Karzas, W.J. and Latter, R., "Electron Radiative Transitions in a Coulomb Field", The Astrophysical Journal, Supplement Series, Supplement Number 55, Vol. VI, May 1961, pp. 167-212.

6. John, T.L., "The Free-Free Transitions of Atomic and Molecular Negative Ions in the Infrared", Monthly Notices of the Royal Astronomical Society, Vol. 170, 1975, pp. 5-6.

7. Roberts, R.E., Selby, J.E.A. and Biberman, L.M., "Infrared Continuum Absorption by Atmospheric Water Vapor in the 8-12μm Window", Applied Optics, Vol. 15, 1976, pp. 2085-2090.

8. NASA, "Handbook of Infrared Radiation from Combustion Gases", SP-3080, 1973, Table A2-35, pp. 462-465.

9. Ferriso, C.C., Ludwig, C.B. and Thomson, A.L., "Empirically Determined Infrared Absorption Coefficients of H_2O from 300 to 3000°K, "J. Quant. Spec. Rad. Trans., Vol. 6, 1966, pp. 241-275.

10. United Technologies Research Center, "Coupling of CO and CO_2 Laser Radiation to the CO, H_2O, HDO, D_2O, NH_3 and DO Molecules", R77-922895-7, Contract F04611-77-C-0039, Dec. 15, 1977.

11. Tejwani, G.D.T. and Varanasi, P., "Approximate Mean Absorption Coefficients in the Spectrum of Water Vapor Between 10 and 22 Microns at Elevated Temperatures", J. Quant. Spec. Rad. Trans., Vol. 10, 1970, pp. 373-388.

12. Penner, S.S. and Varanasi, P., "Spectral Absorption Coefficients in the Pure Rotation Spectrum of Water Vapor", J. Quant. Spec. Rad. Trans., Vol. 7, 1967, pp. 687-690.

REFERENCES (Cont...)

13. Varanasi, P., Chou, S., and Penner, S.S., "Absorption Coefficients for Water Vapor in the 600-1000 cm^{-1} Region", J. Quant. Spec. Rad. Trans., Vol. 8, 1968, pp. 1537-1541.

14. Ludwig, C.B., Ferriso, C.C. and Abeyta, C.N., "Spectral Emissivities and Integrated Intensities of the 6.3μ Fundamental Band of H_2O", J. Quant. Spec. Rad. Trans., Vol. 5, 1965, pp. 281-290.

15. Weyl, G. and Shui, V., "Condensation and Laser Attenuation in Water Plumes from a Laser-Propelled Rocket", AIAA Journal, Vol. 15, December 1977, pp. 1770-1777.

16. Slack, M. and Ludwig, C.B., "Plume Data Analysis of Advanced Propellants", AFRPL-TR-78-4, Sept. 1978, Vol. II, Appendix.

17. Young, L.A., "CO Infrared Spectra", J. Quant. Spec. Rad. Trans., Vol. 8, 1968, pp. 693-716.

18. Penner, S.S., "Quantitative Molecular Spectroscopy and Gas Emissivities", Addison-Wesley, 1959, Chapter 11 and Appendix.

19. Penner, S.S. and Olfe, D.B., "Radiation and Re-entry". Academic Press, 1968, Chapter 1.

20. Hottel, H.C., in McAdams, W.H., "Heat Transmission," 3rd Edition, McGraw-Hill, New York, 1954, Chapter IV.

21. Olfe, D.B., "Equilibrium Emissivity Calculations for a Hydrogen Plasma at Temperatures up to 10,000°K", J. Quant. Spec. Rad. Trans.,Vol. 1, 1961, pp. 104-133.

22. Young, L.A., "CO Infrared Spectra", J. Quant. Spec. Rad. Trans., Vol. 8, 1968, pp. 693-716.

23. Penner, S.S. and Varanasi, P., "Approximate Band Absorption and Total Emissivity Calculations for CO_2", J. Quant. Spec. Rad. Trans., Vol. 4, 1964, pp. 799-806.

24. Penner, S.S. and Varanasi, P., "Approximate Band Absorption and Total Emissivity Calculations for H_2O", J. Quant. Spec. Rad. Trans., Vol. 5, 1965, pp. 391-401.

25. Ludwig, C.B. and Ferriso, C.C., "Prediction of Total Emissivity of Nitrogen-Broadened and Self-Broadened Hot Water Vapor", J. Quant. Spec. Rad. Trans., Vol. 7, 1967, pp. 7-26.

26. Ferriso, C.C., Ludwig, C.G. and Boynton, F.P., Int. J. Heat and Mass Trans., Vol. 9, 1966, p. 853.

27. NASA, "Handbook of Infrared Radiation from Combustion Gases", SP-3080, 1973, pp. 284 and 281.

28. Stallcop, J.R., "Absorption of Infrared Radiation by Electrons in the Field of a Neutral Hydrogen Atom", Astrophysical J., Vol. 187, 1974, pp. 179-183.

29. Condon, E.U. and Shortley, G.H., "The Theory of Atomic Spectra", Cambridge University Press, 1951, p. 143, Fig. 5.

30. Allen, C.W., "Astrophysical Quantities", 2nd Edition, University of London, 1964, p. 93.

31. Ambartsumyan, "Theoretical Astrophysics", Pergamon Press, 1958, p.54, Fig. 15a.

32. Patch, R.W., "Thermodynamic Properties and Theoretical Rocket Performance of Hydrogen to 100,000K and 1.01325 x 10^8 N/m^2 ", NASA SP-3069, 1971.

33. Yos, J.M., "Transport Properties of Nitrogen, Hydrogen, Oxygen and Air to 30,000K". RAD-TM-63-7, Avco Corporation, Wilmington, MA., March, 1963.

34. Mayer, J.E. and Mayer, M.G., "Statistical Mechanics", John Wiley and Sons, Inc., New York, 1940, pp. 160-164.

35. Nicolet, W.E., et al, Appendix B of "Analytical Design Study for a High-Pressure, High-Enthalpy Constructed Arc Heater", AEDC TR-75-47 (Aerotherm Final Report 74-125), Aerotherm Division/ Acurex Corporation, Mountain View, CA., December, 1974.

36. Hirshfelder, J.O., Curtiss, C.F., and Bird, R.B., "Molecular Theory of Gases and Liquids", John Wiley and Sons, Inc., New York, Corrected Printing with Notes added, 1964.

37. Vincenti, W.G. and Kruger, C.H. Jr., "Introduction to Physical Gas Dynamics," John Wiley and Sons, 1965, Chapter XI, Sec. 9.

☆U S GOVERNMENT PRINTING OFFICE 1981—740-066/378 REGION NO. 4